TECHNICAL RESEARCH REPORT

COLD CATHODES FOR SEALED OFF CO_2 LASERS

Final Report for
NASA Grant NGR-21-002-216
and Progress Report for
NASA Grant NGR-21-002-345

January 1973

U. Hochuli

DEPARTMENT OF
ELECTRICAL ENGINEERING

UNIVERSITY OF MARYLAND

COLLEGE PARK, MARYLAND 20742

COLD CATHODES FOR SEALED OFF CO_2 LASERS

BY

U. HOCHULI, UNIVERSITY OF MARYLAND
COLLEGE PARK, MARYLAND

ABSTRACT

Experimental results of a group of theoretically selected cold cathode materials are presented. These tests indicate Ag-CuO, Cu and Pt-Cu as three new cold cathode materials for sealed off CO_2 lasers. The power output of a test laser with an Ag-CuO cathode and a gas volume of only 50 cm^3 varied from 0.72 W to 1.1 W at 3000 hours and yields still 0.88 W after 8000 hours. Gas discharge tubes with Cu cathodes and a volume of 25 cm^3 yield life times in excess of 10,000 hours. Gas analysis results, obtained from a similar tube over a period of 3000 hours, look most promising. A Pt-Cu alloy cathode shows an extremely promising V-I characteristic over a period of 2800 hours.

CONTENTS

COLD CATHODES FOR SEALED-OFF CO_2 LASERS[+]

by

U. Hochuli [*]

INTRODUCTION

Most of the gas discharge tubes used for CO_2 lasers are high impedance devices requiring only small currents; cold cathodes are suitable electron emitting sources to furnish these currents. Gas removal due to cathode sputtering usually limits the life of discharge tubes filled with noble gases. Moreover, dissociation of CO_2 into CO and O_2 with successive oxygen removal due to oxide layer formation is a consideration for the CO_2 laser. The degree of dissociation is very much influenced by the cathode surface chosen. It is a difficult problem to find the proper cathode materials that do not remove gas by sputtering and avoid consumption of any gas mixture constituent through scale formation.

Background

The CO_2 laser was discovered in 1964 [1]. Its high efficiency and power capability make it ideal for communication purposes as well as for energy sources. Despite the recognition of its importance we have so far had no entirely satisfactory cold cathode for the CO_2 laser. It is true that the state of the art has been much advanced in the last two years but we are still looking for a cathode that is noise free, does not produce sputtering deposits and lasts

---

[+]Work initiated by ONR, ARPA and supported by NASA.

[*]University of Maryland, College Park, Md. 20742

for 10000 hours or more with small gas volumes. The nickel cathode invented by Dr. Carbone [2], the platinum cathode discovered by Dr. Whittemann [3] and the N_iO cathode developed by Honeywell depend on a relatively large gas volume and can yield life times of several thousand hours under this condition. Used in a 1W CO_2 laser with a typical gas volume of the order of 50 to 100 cm^3 they usually last less than 1000 hours. The demand for a space qualified laser tube with a life expectancy of at least 2000 hours has justified the need for CO_2 laser cold cathode research. These facts also indicate that we are dealing with a difficult and important unsolved problem.

CATHODE PARAMETERS INVOLVED

Sealed-off CO_2 lasers are relatively tolerant of the composition of the gas mixture used. One of the most efficient mixtures uses He CO_2N_2 and X_e. It has been shown by several researchers [4] that CO can be substituted for N_2. We have optimized one of our own 1W lasers with respect to gas composition and the results are shown by Figures 1 to 22. From these measurements we must conclude that the substitution of CO for N_2 has little effect on power output. E. g., we measure a power output of 1.3W at 6 mA and 5100 V across the laser tube for a gas mixture containing 9.1 Torr He, 4.25 Torr CO_2, 5.45 Torr CO and 1.2 Torr Xe. This result must be compared with a power output of 1.2W obtained at 6 mA and 4980 V across the laser tube for a mixture consisting of 10 Torr He 4.65 Torr CO_2 4.65 Torr N_2 and 0.7 Torr Xe. For these two cases the substitution of CO for N_2 gave a slightly larger power output and also a slightly higher efficiency. We have to mention that our results have been measured during the first 10 minutes the laser was turned on and do not reflect long term changes in the composition of the gas mixture. The laser tube for

our measurements originally gave an output of 1.7W and successive cathode tests produced a slight, visible layer of deposits on the internal gold coated mirror. These deposits reduced the power output from 1.7 to 1.3 W under otherwise identical conditions.

It has also been shown that a small amount of H_2 or H_2O can be added and this may further increase power output and efficiency [5]. Our own incomplete measurements for H_2 addition are shown in Figures 23 to 25. These variations in the gas composition are not only important for the achievement of maximum power output or efficiency, they also profoundly affect the cathode chemistry and therefore the life of the laser tube. The other parameters of the cathode are the current density, the temperature and the composition of the cathode surface. The current density can, to a certain extent, be controlled by the choice of the cathode geometry. We have normalized the cathodes, designed for a current of 6 mA, to 4 diameters to conform to available or easily modified ceramic sputter shields. These normalized cathode configurations are shown in Fig. 27.

The operating temperature of these cathodes depends, of course, on the current and it can be raised by using thermal insulation outside of the cathode sleeve. Typical temperatures for one cathode configuration are shown in Fig. 28. The last parameter, the composition of the cathode surface, is dealt with in the next paragraph:

Choice of cathode materials

We would like to find cathode materials that are chemically inert in the presence of the particular gas mixture used. The second requirement is a very low sputtering rate of the materials used for the cold cathode surface

and the last requirement asks for a minimum of negative ion formation in the sputtering products. This is necessary to prevent material deposits at the anode end due to the attraction of such negative ions by the positive anode.

Of particular interest are the metal-oxides with a larger oxygen dissociation pressure than the one of the reaction

$$2\,CO + O_2 \rightleftharpoons 2\,CO_2,$$

Some of these oxides are shown in the standard free-energy diagram in Fig. 29 located above the reaction mentioned. The dissociation O_2 pressure can be read from this diagram or from Fig. 30. In the presence of a mixture of equal parts CO and CO_2 these oxides are reduced to their lower oxidation state under condition of thermal equilibrium and in the absence of the electrical discharge current. (It is noteworthy that most of these metals and oxides also act as catalysts for the CO oxidation reaction. The fact that the degree of CO_2 dissociation is indeed affected by the cathode surface chosen is also documented in the literature [6].) The use of one of these materials as a cold cathode exposes it to additional processes such as ion bombardment, photo-, field- and thermal emission with the result that the surface has a tendency to stay in the higher oxidation state. Oxidation at the cathode end of discharge tube is unexpected but has been observed and described [7].

The discharge conditions of most of the small CO_2 lasers result in cathode current densities above 2 mA/cm^2. Experience shows that insulating oxide layers can usually not support such current densities over prolonged periods of time. This difficulty can be avoided by using semiconducting oxide layers. Most of the oxides under consideration are of this type and their electrical

conductivity as well as their catalytic activity increase with temperature. Unfortunately, reliable data of electrical conductivity of oxides vs. temperature is rather scarce in the recent literature.

EXPERIMENTAL APPROACH

It was obvious from the beginning of the research that a large number of different cathode materials had to be tested. To build a laser for each different cathode would have been prohibitively expensive in terms of manpower, material expenses and testing facilities. A faster and far cheaper approach was to test gas discharge tubes alone. This was done and the standard geometry chosen for the discharge tubes is shown in Fig. 31. Discharge voltage measured at constant current and color of the discharge vs. time are coarse and not always sufficient indicators of the condition of the tubes. We felt that at least a partial gas analysis was necessary to verify the composition of the gas mixture over the life span of the moxt promising discharge tubes. This can be achieved either by periodically analyzing gas samples in the mass-spectrometer or by infrared absorption spectroscopy. We have chosen infrared absorption spectroscopy to obtain an indication of the CO_2 and CO content of the tubes. This required the attachment of an absorption cell with infrared transmitting windows to each discharge tube. The cell geometry chosen increased the gas volume of the discharge tube from roughtly 25 cm^3 to 50 cm^3. The most successful cathodes are tested in actual lasers.

Gas Analysis

As previously mentioned, the CO and CO_2 content was monitored with infrared absorption spectroscopy. The absorption cells had a path length of 7.8 cm, 1 mm thick Irtran 2 windows and their geometry is shown in Fig. 32.

The absorption spectrum between 2000 and 2500 cm^{-1} was measured with a DigiLab model FTS 14 double beam spectrometer. The resolution of this instrument is insufficient to display the true line shape of a single rotational CO_2 or CO line. For this reason we chose an equivalent slit width that would enable us to sample over two or more rotational lines. A slit width of 8 cm^{-1} achieves this objectively, saves time and was chosen for all measurements. Fig. 33 shows a sample spectrum of the reference mixture of 20 Torr He CO_2 CO X_e in the pressure ratios 15:7:7:1 and indicates maximum absorption of roughly 10% for CO_2 and 1.2% for CO. Further measurements were made with expanded scales, Fig. 34 and the results for other gas compositions are shown in Figs. 35 to 40.

Experimental Techniques

All the discharge tubes and lasers were made from Pyrex and had tungsten electrode feed-throughs. Gallium arsenide and Irtran 2 windows as well as the internal gold coated quartz mirrors were attached with indium film seals developed for this purpose in our laboratory [8]. All these seals are of the ultrahigh vacuum type and no Epoxy resin was used anywhere. The tubes were evacuated with an oil diffusion pump and the electrodes outgassed with RF generator and torch. The first discharge was usually in pure oxygen followed by a burn-in period of 1 to 2 days in the final mixture. Subsequently, the tubes were refilled, sealed off and run on the test stand. Practically all the cathode alloys were fabricated in our own laboratory and then cast and machined or rolled and formed into the final shape. Internal oxidation of the silver alloys were performed in a temperature-controlled furnace with a quartz tube flushed with O_2 as a working chamber.

EXPERIMENTAL RESULTS

From the oxygen dissociation curves in Fig. 30 we see that gold forms the most unstable oxides, followed by silver, MnO_2, Pt O, PdO and CuO.

Gold Cathodes

We would expect that gold, the most noble metal with respect to oxidation would be a rather inert cathode surface. Unfortunately, gold sputters very badly and we have so far not been able to get reasonable life with such cathodes in He CO_2CO Xe and HeCO_2N_2Xe mixtures.

Silver Cathodes

The next noble metal, silver, does not work successfully in the He$CO_2N_2X_e$ mixtures probably because the volatile Ag NO_3 can be formed. In He CO_2COX$_e$ mixtures we see an entirely different picture. Here we can nicely observe how the discharge oxidizes the spot of impact at the cathode. This area becomes dark due to silver oxide formation, with a resulting local decrease in the electrical conductivity. This lowered electrical conductivity then forces the cathode spot to move to an unoxidized area. If the cathode has a temperature of 200 to 300^{o}C we can later observe how the original, oxidized area returns again to pure silver by dissociation. Such cathodes can have quite a long life and some of them are surprisingly sputterfree. Their drawback is the electrical instability caused by the moving cathode spot. Typical characteristics are shown in Figure 41.

We have also tried to reduce the surface resistivity of the oxide layer by increasing the temperature. This attempt was unsuccessful and usually resulted in increased sputtering. Another method is to alloy the silver with a metal that forms oxides with a higher electrical conductivity. The additional

metal in the alloy has to be oxidized in order to prevent oxygen depletion in the final gas mixture. This process then leads to:

Silver Matrix Cathodes

Silver at high temperatures is quite transparent to oxygen and for this reason silver alloys can be internally oxidized. The best known example are probably the AgCdO alloys used for electrical contacts. This compound can be formed by sintering compressed Ag-CdO powder slugs or by exposing the AgCd alloy to an oxidizing atmosphere at high temperatures for extended periods of time. We have formed AgCdO, AgCuO, $AgMnO_2$ and AgZnO cathodes and used sintered AgCdO and AgNiO cathodes. These cathodes consist essentially of a silver matrix holding the oxide particles. Curves from reference [9] for the AgCuO internal oxidation process are shown in Fig. 42. Silver matrix cathodes should be relatively inert to surface damage and free of electrical instabilities once sufficiently low surface resistivity has been achieved.

AgCdO Cathodes

Results for these cathodes are shown in Figs. 43 to 46. The main sputtering deposits stay close to the cathode; slight anode deposits do occur.

AgCuO Cathodes

These cathodes work quite well, Fig. 47 to 49, but still show moving cathode spots. Anodes stay very clean and surprisingly low cathode deposits occur with the 2L 4.5 type cathodes. Notice the CO decrease and the CO_2 increase with time for cathodes with 10% or more Cu. In these cathodes sputtered Cu O is reduced to Cu_2 O giving off oxygen. The partial pressures of CO and CO_2 stayed fairly well balanced for the cathode with 5% Cu while pure

Ag cathodes show an excess of CO in Fig. 41. Ag Cu/O cathodes are not successful in the presence of N_2.

Ag MnO_2 Cathodes

The cathodes were first oxidized at 750°C and then at 500°C to achieve conversion to MnO_2, known to be an excellent catalyst [10]. Results are shown in Fig. 50. Anode deposits do occur with these discharge tubes but the cathode spots are relatively quiet. The cathodes are unsuccessful in the presence of N_2.

Ag Ni O Cathodes

Results are shown in Fig. 51. The anodes stay relatively clean and the cathodes are quiet in these discharge tubes.

Ag Zn O Cathodes

Results are shown in Fig. 52. Quiet cathode spot, very light anode deposits. The cathode with 10% Zn shows some cathode deposits. These cathodes are unsuccessful in the presence of N_2.

Cu Cathodes

Oxide layers can be formed in an oxygen discharge and such cathodes live surprisingly long with quite large current densities. It is a known fact that thin oxide layers on Cu grow very slowly at room temperature [11]. Anodes stay very clean; cathodes are unsuccessful in the presence of N_2. Cathode spots move when large current densities are used, but practically no sputtering occurs. Cathode spots are quiet with lower current densities but the sputtering rate is higher. Results are shown in Fig. 53.

Oxide Layer Cathodes

Such cathodes can be formed by oxidizing alloys in an oxygen atmosphere

for a prolonged period of time at elevated temperatures. The scaling layers so formed usually contain the oxide of the less noble component of the alloy. Suitable layers have to adhere very well, e.g., Cu O on Au [12], and are only allowed to continue growing at an infinitesimal rate at the operating temperature of the cathode. Such cathodes are of course much more delicate than matrix cathodes formed by internal oxidation. For this reason we have not stressed their development and only a few were tried.

Platinum Cathodes

Pure platinum cathodes dissociate very little CO_2 [6] but sputter badly and are not successful. We have tried to reduce the sputtering by alloying Pt with Ag, Au, Cu and Ni. The results show that sputtering can indeed be reduced drastically but the life of the discharge tubes tested was generally less than 1000 hours. The addition of hydrogen or water vapor does, however, change the situation. It is well known that platinum oxides can be reduced by atomic hydrogen at room temperature in a cycle similar to the water vapor cycle in incandescent lamps [13]. Langmuir described this cycle as follows:

"A lamp made up with a side tube containing a little water which is kept cooled by a freezing mixture of solid carbon dioxide and acetone (-78.5°C) will blacken very rapidly when running at normal efficiency, although the vapor pressure of water at this temperature is only about $4 \cdot 10^{-4}$ mm.

The explanation [Langmuir states] of the behavior of water vapor seems to be as follows:

The water vapor coming into contact with the filament is decomposed, the oxygen combining with the tungsten and the hydrogen being evolved. The oxide distils to the bulb, where it is subsequently reduced to metallic tungsten

by atomic hydrogen given off by the filament, water vapor being simultaneously produced. The action can thus repeat itself indefinitely with a limited quantity of water vapor.

Several experiments indicated that the amount of tungsten that was carried from the filament to the bulb was often many times greater than the chemical equivalent of the hydrogen produced, so the deposit on the bulb could not well be formed by the simple attack of the filament by water vapor.

Another experiment demonstrated that even the yellow oxide, WO_3, could be reduced at room temperature by atomic hydrogen. A filament was heated in a well-exhausted bulb containing a low pressure of oxygen; this gave an invisible deposit of the yellow oxide on the bulb. The remaining oxygen was pumped out and dry hydrogen was admitted. The filament was now lighted to a temperature (2000°K) so low that it could not possibly produced blackening under ordinary conditions. In a short time the bulb became distinctly dark, thus indicating a reduction of the oxide by the active hydrogen. Further treatment in hydrogen failed to produce any further darkening, showing that the oxide could only be reduced superficially."

Platinum alloy cathodes working with gas mixtures containing hydrogen or water vapor are essentially mass transport cathodes with transport rates controlled by the impurity used. In this case we need far larger impurity concentrations to reduce sputtering and preliminary results are seen in Figs. 54 and 55.

Pd Cathodes

Just as with Pt these cathodes seem to be good catalysts but sputter far too much. We have not yet had time to check their behavior with gas mixtures

containing H_2 or H_2O.

Ni Cathodes

The life of discharge tubes using nickel with oxidized or unoxidized surfaces has always been restricted to less than 10000 hours by our test conditions. The substitution of CO for N_2 in the gas mixture did not improve this result.

CATHODE ALLOYS TESTED

These are shown in the following tables I and II.

Table I

Cathode alloys tested in $HeCO_2N_2Xe$

15/7/7/1 gas mixtures

Main-element / Impurity	Ag	Au	Co	Cu	Mn	Ni	Pd	Pt	Re
Ag	100			3			1, 3, 10	1, 3	
Au		100					10	3, 10	
Cd	0.8, 2 5, 10, 20								
Co									
Cu	20			100	38		3, 7 10, 14	0.3, 1, 3, 10, 30	
Mn	0.5, 3 5, 10		0.5, 2 10						
Ni	15						3	0.2, 0.5, 1, 1.5, 2, 2.5, 3, 6, 10	
Pd							100		
Pt	3, 10					10		100	
Re									100
Zn	10								

The numbers represent impurity % by weight.

Table II

Cathode alloys tested in $HeCO_2COXe$

15/7/7/1 gas mixtures

Main-element / Impurity	Ag	Au	Co	Cu	Mn	Ni	Pd	Pt	Re
Ag	100	10						1, 3	
Au	18	100						1, 10	
Cd	1, 10								
Co			100						
Cu	5, 10, 20	5		100	38				
Mn	1.25 3, 10			2, 10		10			
Ni	15		40			100		0.5 1, 2	
Pd	10, 18								
Pt	3, 26							100	
Re									100
Zn	1, 3, 10								

The numbers represent impurity % by weight.

LASERS

A typical result for a laser with a nickel cathode is shown in Fig. 56. Far more encouraging is the power output vs time of the laser with a 1 L4. 5 Ag 20 Cu/O cathode shown in Fig. 57. This cathode is actually somewhat too small and has worked with a larger than optimum current density. As a result of this sputtering has taken place but the deposits are nicely confined to the cathode area. The most impressive fact is the lack of visible deposits in the bore, on the anode, or on the gold coated internal mirror at the anode end after 8000 hours of continuous service. The sputtering in the cathode area is almost completely eliminated with the next larger 2 L 4. 5 type cathode. Comparison of the last two results shows that indeed much progress has been made during the past year.

CONCLUSION

From the many test results available we see that careful selection of gas mixture composition, cathode material, and geometry promise CO_2 laser life of 10, 000 hours or more. So far Ag-Cu and pure Cu cathodes are the most successful ones in combination with the He CO_2 CO Xe mixture. Both of these cathodes show a minimum of sputtering deposits in the bore and on the anode. To date we have not been able to completely suppress the flickering of the cathode spot in the Ag-Cu cathodes. Pure Cu cathodes show the same effect for current densities above 18 mA/cm^2. Lowering the current density to 12 mA/cm^2 stabilizes these cathodes at the expense of increased sputtering. The sputtering products are still confined to the cathode area and if the results of the gas analysis continue to confirm the excellent appearance of the 10, 000 hour-old discharge tubes we may very well have the best overall results with the pure Cu cathode. This solution would also be very attractive from the

point of view of simplicity: namely a simple cathode working with the least complicated efficient gas mixture available.

Surprisingly good discharge characteristics are shown in Fig. 55 for a Pt cathode alloy containing 30% Cu in combination with a $HeCO_2\ N_2X_eH_2$ gas mixture. This result has to be reproduced and confirmed by gas analysis. The cathode itself seems to be electrically quiet but produces anode deposits. Much more experience is needed with this cathode type and we are exploring the influence of the composition of the Pt-Cu alloy. However, from an engineering point of view we have some reservations. The addition of a small amount of H_2 or H_2O very much increases the complexity of the cathode problem. New chemical compounds can be formed and it is of course very well known that the control of the hydrogen pressure depends to a certain extent on the surface properties of the materials used for the fabrication of the laser tube.

APPENDIX

I. Laser V-I characteristics for different gas mixtures

These characteristics are shown in Figs. 1a to 26a. The voltages shown represent the values directly across the laser tube and do not include series resistance drop. Fig. 27a shows the design of the laser tube.

II. Laser power output for mixtures with low CO and CO_2 content

This information is shown in Figs. 28a to 29a and is useful to determine the laser output near the end of the life when the CO_2 and CO concentrations have fallen off from their initial values.

References

[1] C. K. N. Patel, W. L. Faust, and R. A. McFarlane, "CW Laser Action on Rotational Transistions of the $\Sigma_u^+ - \Sigma_g^+$ vibrational band of CO_2," Bull. Am. Phys. Soc., Vol. 9, p. 500, April 27, 1964.

[2] R. J. Carbone, "Long-term Operation of a Sealed CO_2 Laser," IEEE J. Q. E. Vol. QE-3, pp. 373-375, September 1967.

[3] W. J. Witteman, "Increasing Continuous Laser Action on CO_2 Rotational Vibrational Transistions through Selective Depopulation of the lower Laser Level by Means of Water Vapor," Phys. Letters, Vol. 18, p. 125, August 15, 1965.

[4] Norio Karube and Eiso Hamaka, "Decomposition of CO_2 Molecules in a Sealed CO_2 Laser," J. Appl. Phys., Vol. 9, p. 3883, 1969.

[5] W. J. Witteman and H. W. Werner, "The Effect of Water Vapor and Hydrogen on the Gas Composition of a Sealed Off CO_2 Laser," Phys. Letters, Vol. 26A, p. 454, April 1968.

[6] E. N. Lotkova, V. N. Ochkin, and N. N. Sobolev, "Dissociation of Carbon Dioxide and Inversion in CO_2 Laser," J. Q. E., 7, 396, 1971.

[7] D. V. Ignatove, "Recherches Electronographiques sur les Pellicules d' Oxydes Apparaissant sur l' Aluminium et le nickel dans une décharge Electrique en Millieun Gaeux d' Oxygene," J. Chim. Phys. 54, 96, 1957.

[8] U. Hochuli and P. Haldemann, "Indium Sealing Techniques," Rev. Sci. Instr. 43, 1088, 1972.

[9] Ernst Raub and Max Engel, "Zundern Kupferhaltiger Legierungen der Edelmetalle," Z. f. Metallkunde 38, 83, 1938.

[10] M. Katz, "Advances in Catalysis," Academic Press, Inc., New York 1953.

[11] Jacques Benárd, "L' oxidation des metaux," 1, 126, Gauthier-Villars and Co., Paris, 1962.

[12] O. Kubachewski, "Das Verhalten von Platin-und Goldlegierungen mit Kupter," Z. Elektrochem. 49, 451, 1943.

[13] S. Dushman and J. M. Lafferty, "Scientific Foundations of Vacuum Technique, 2nd ed., p. 647, John Wiley and Sons, Inc., New York, 1967.

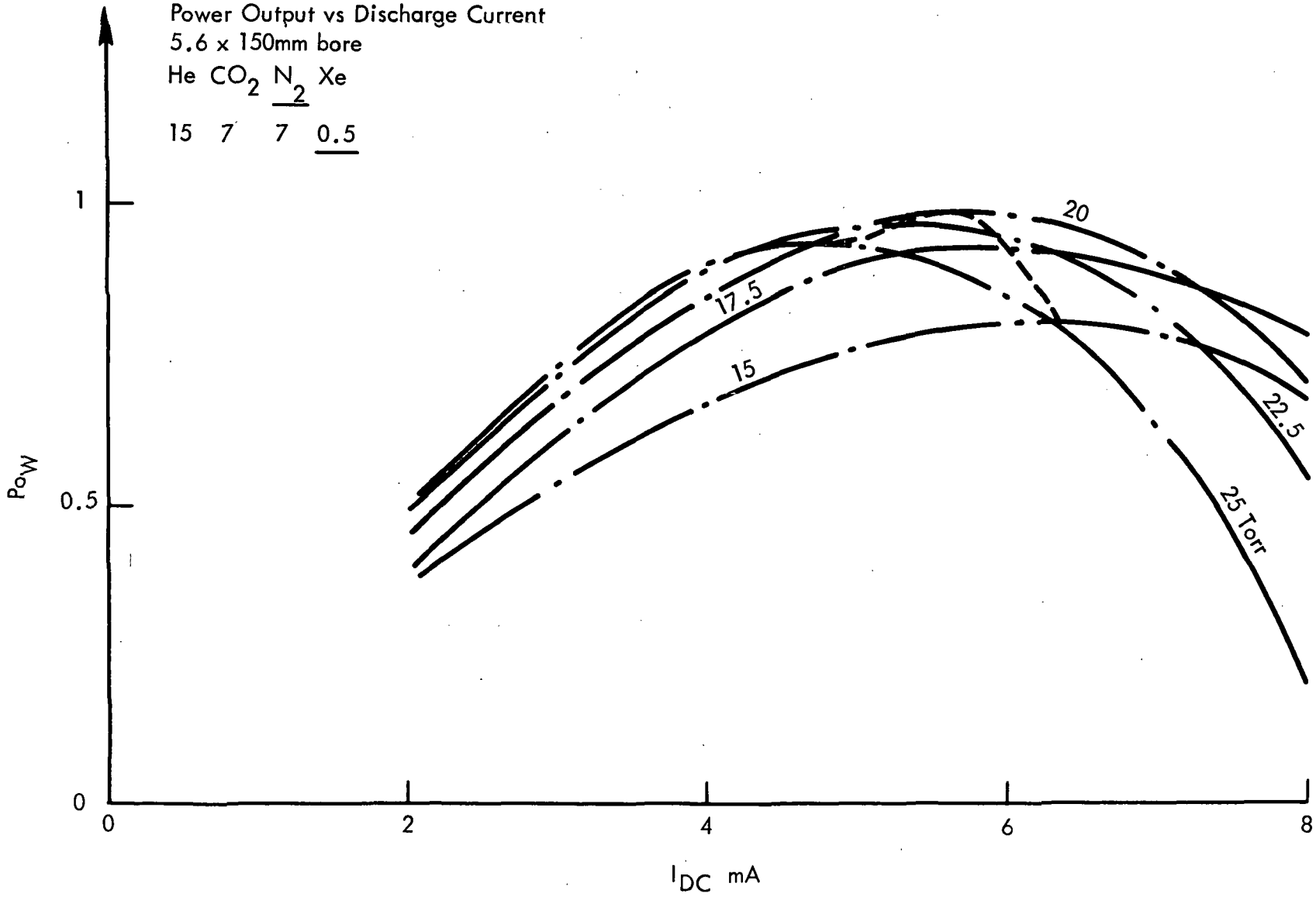

Figure 1. Power output as a function of discharge current [Po (Watts vs I_{DC} (mA)] for a 150 mm length laser tube with a 5.6 mm bore.

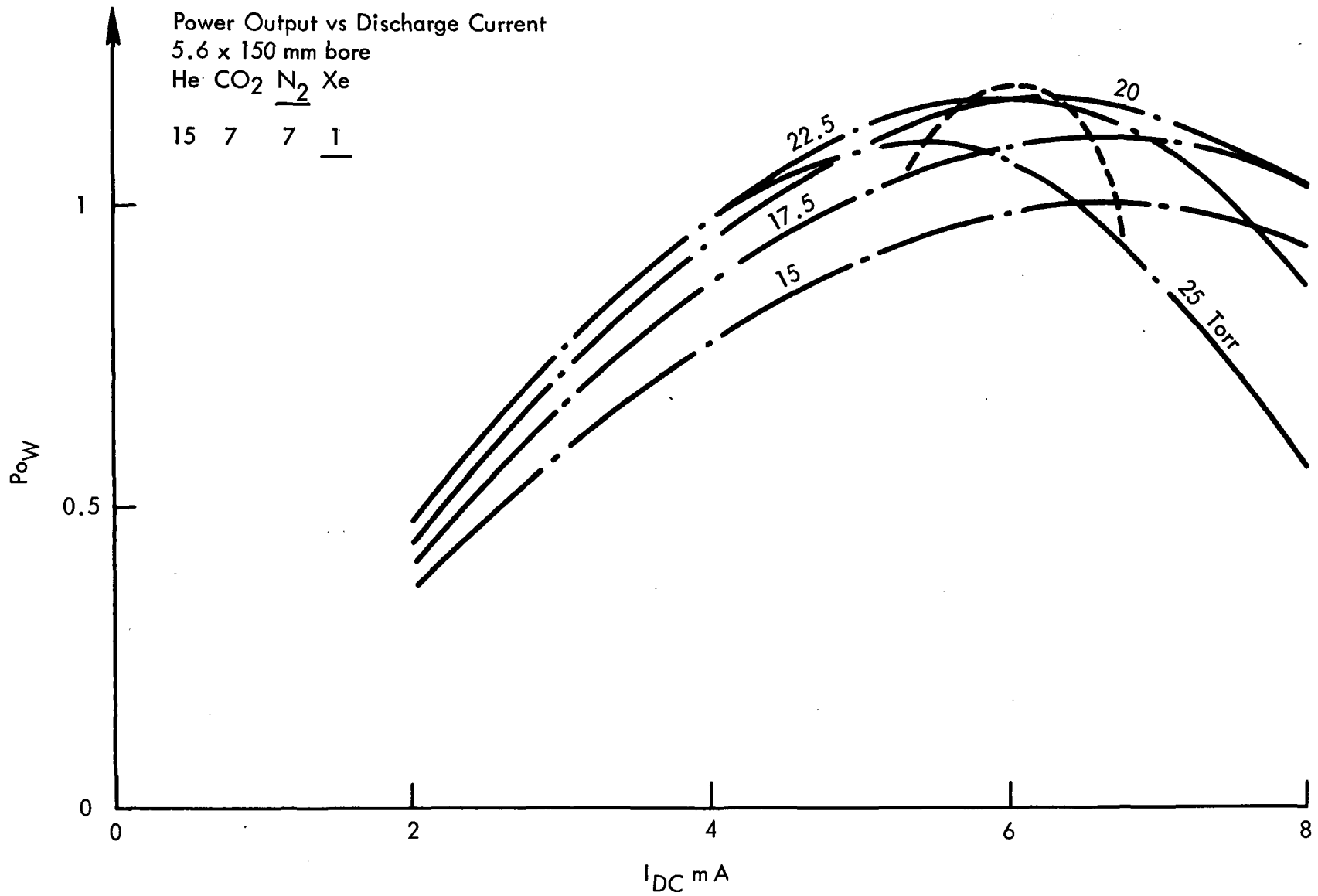

Figure 2. Power output as a function of discharge current [Po (Watts) vs I_{DC} (mA)] for a 150 mm length laser tube with a 5.6 mm bore.

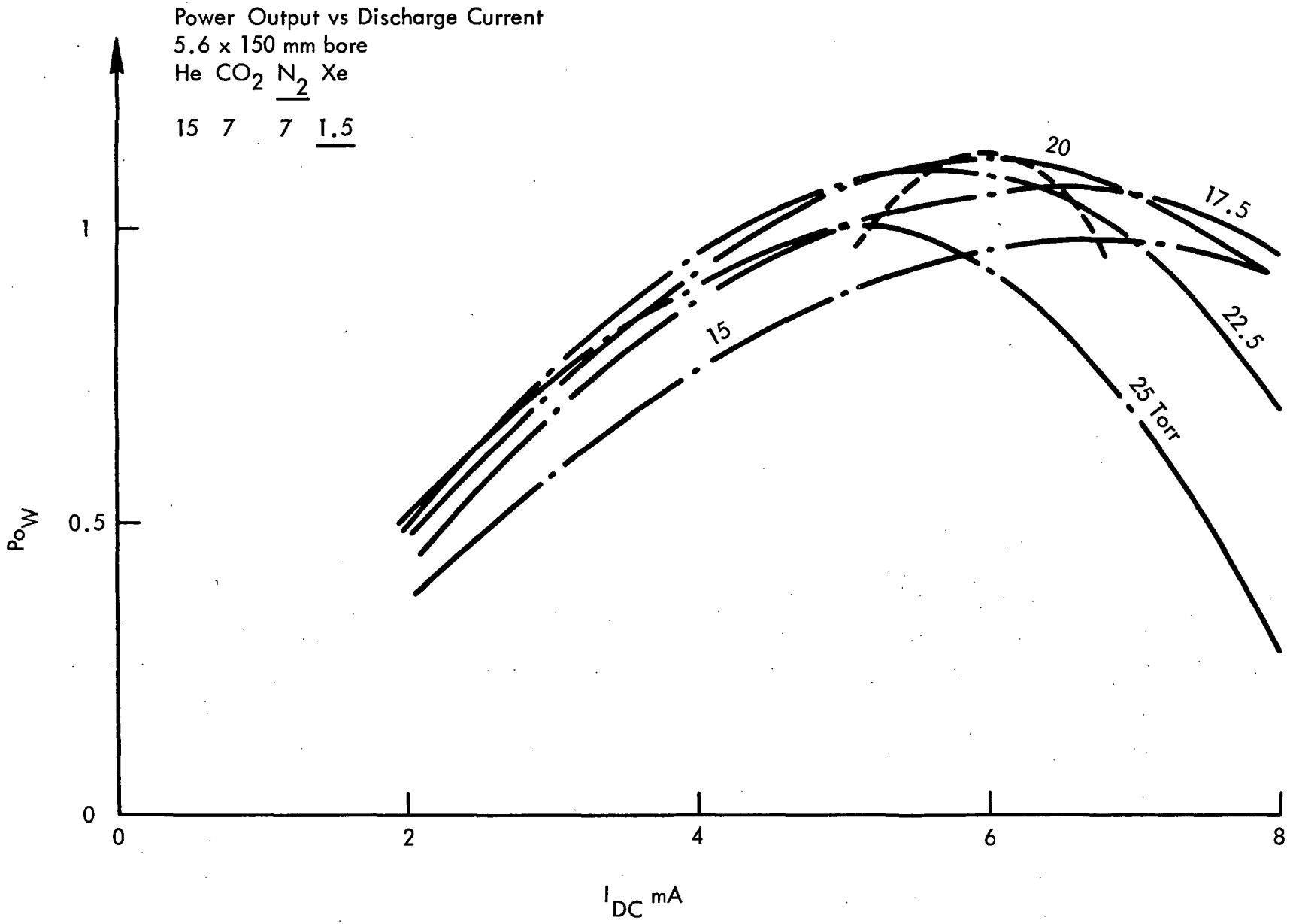

Figure 3. Power output as a function of discharge current [Po (Watts) vs. I_{DC} (mA)] for a 150 mm length laser tube with a 5.6 mm bore.

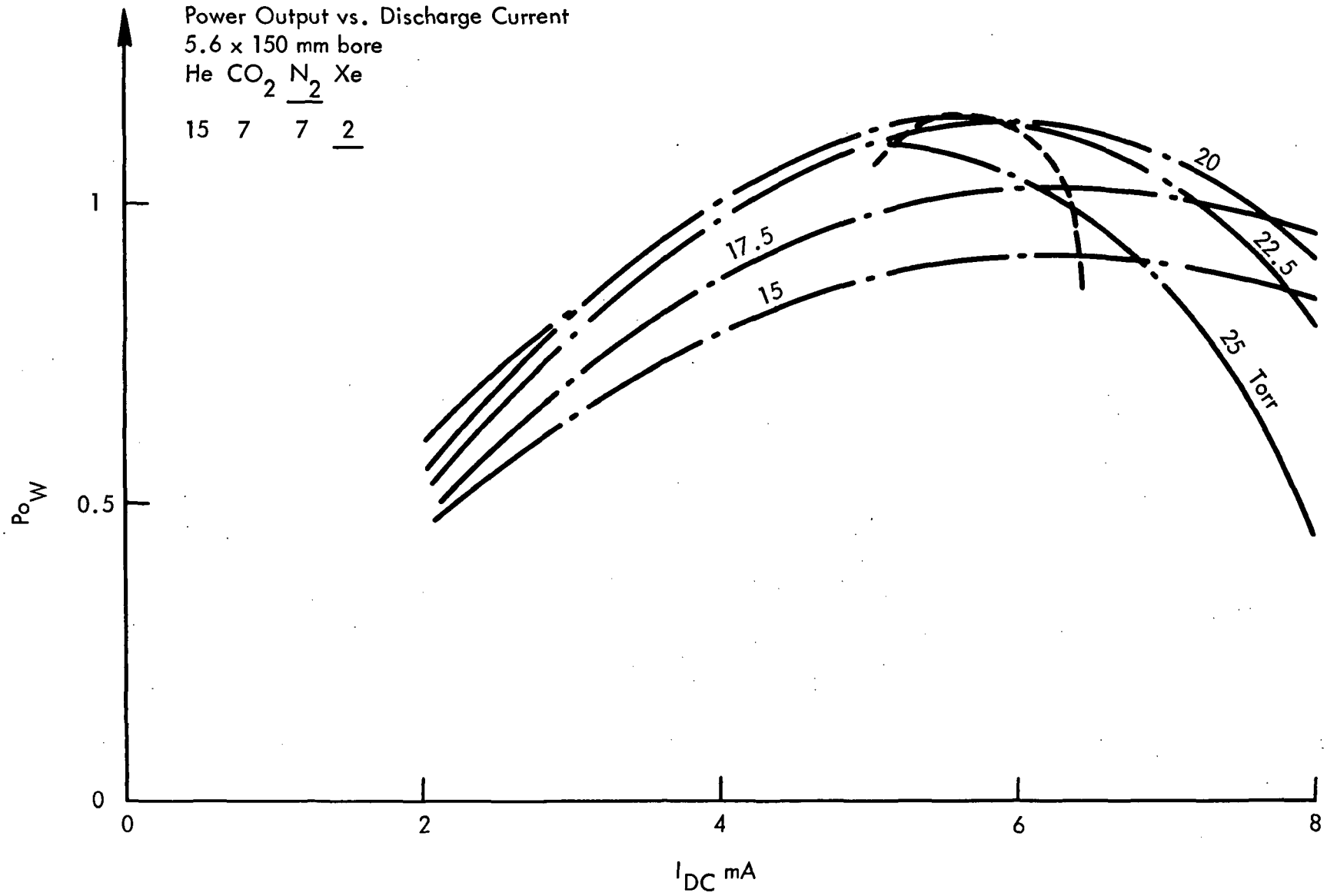

Figure 4. Power output as a function of discharge current [Po (Watts) vs. I_{DC} (mA)]for a 150 mm length laser tube with a 5.6 mm bore.

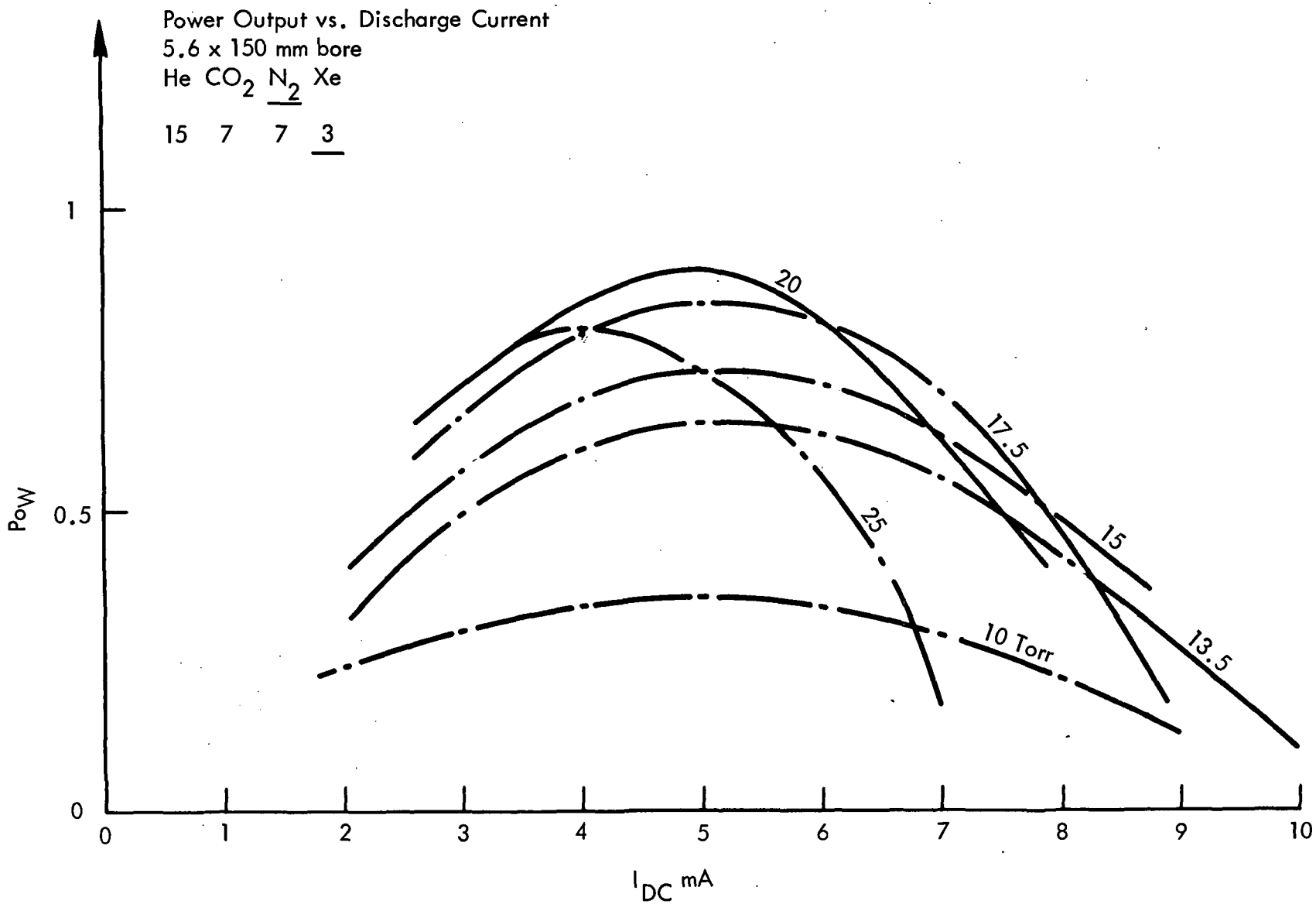

Figure 5. Power output as a function of discharge current [Po (Watts) vs. I_{DC} (mA)]for a 150 mm length laser tube with a 5.6 mm bore.

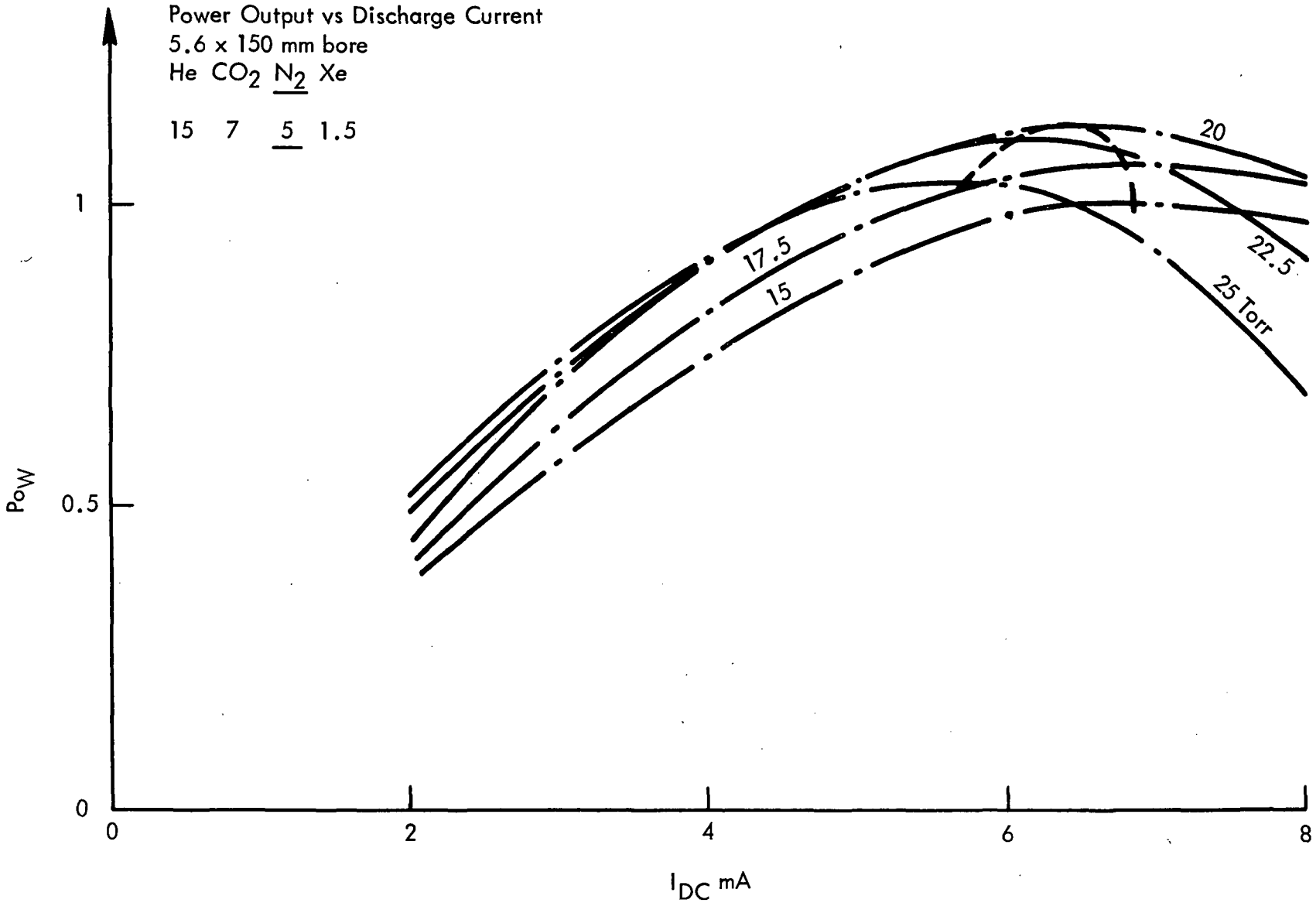

Figure 6. Power output as a function of discharge current [Po (Watts) vs I_{DC} (mA)] for a 150 mm length laser tube with a 5.6 mm bore.

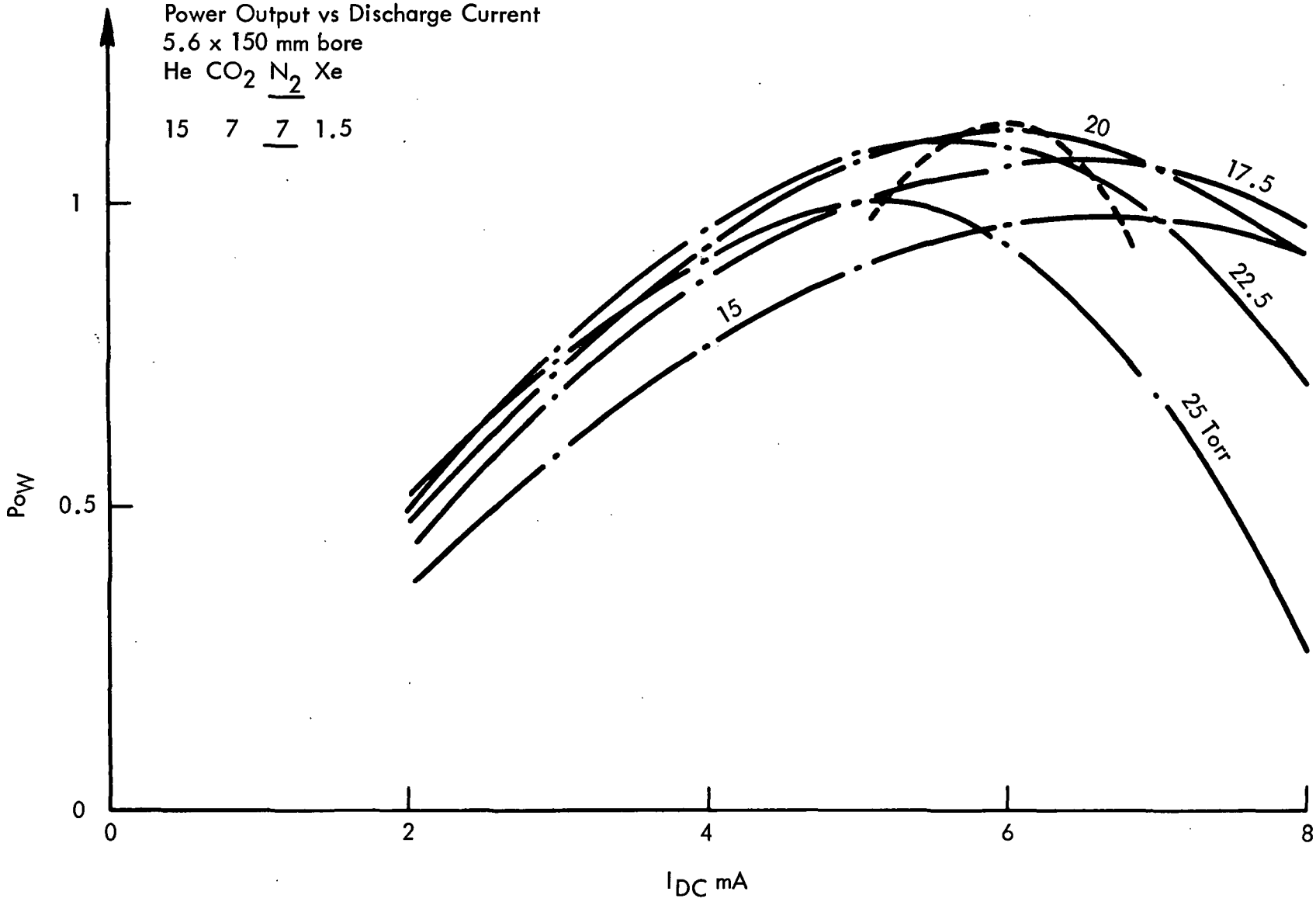

Figure 7. Power output as a function of discharge current [Po (Watts) vs I_{DC} (mA)] for a 150 mm length laser tube with a 5.6 mm bore.

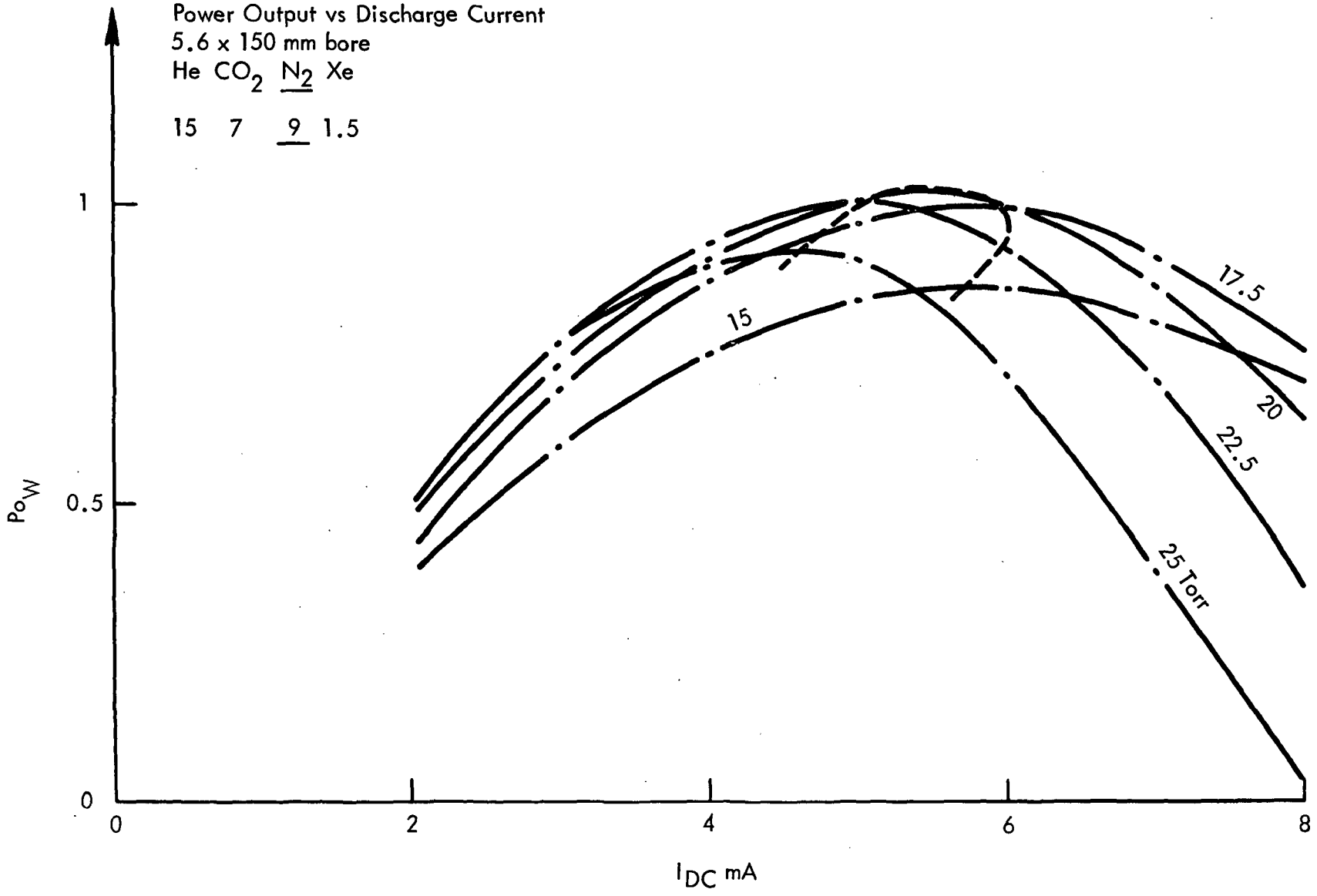

Figure 8. Power output as a function of discharge current [Po (Watts) vs I_{DC} (mA)] for a 150 mm length laser tube with a 5.6 mm bore.

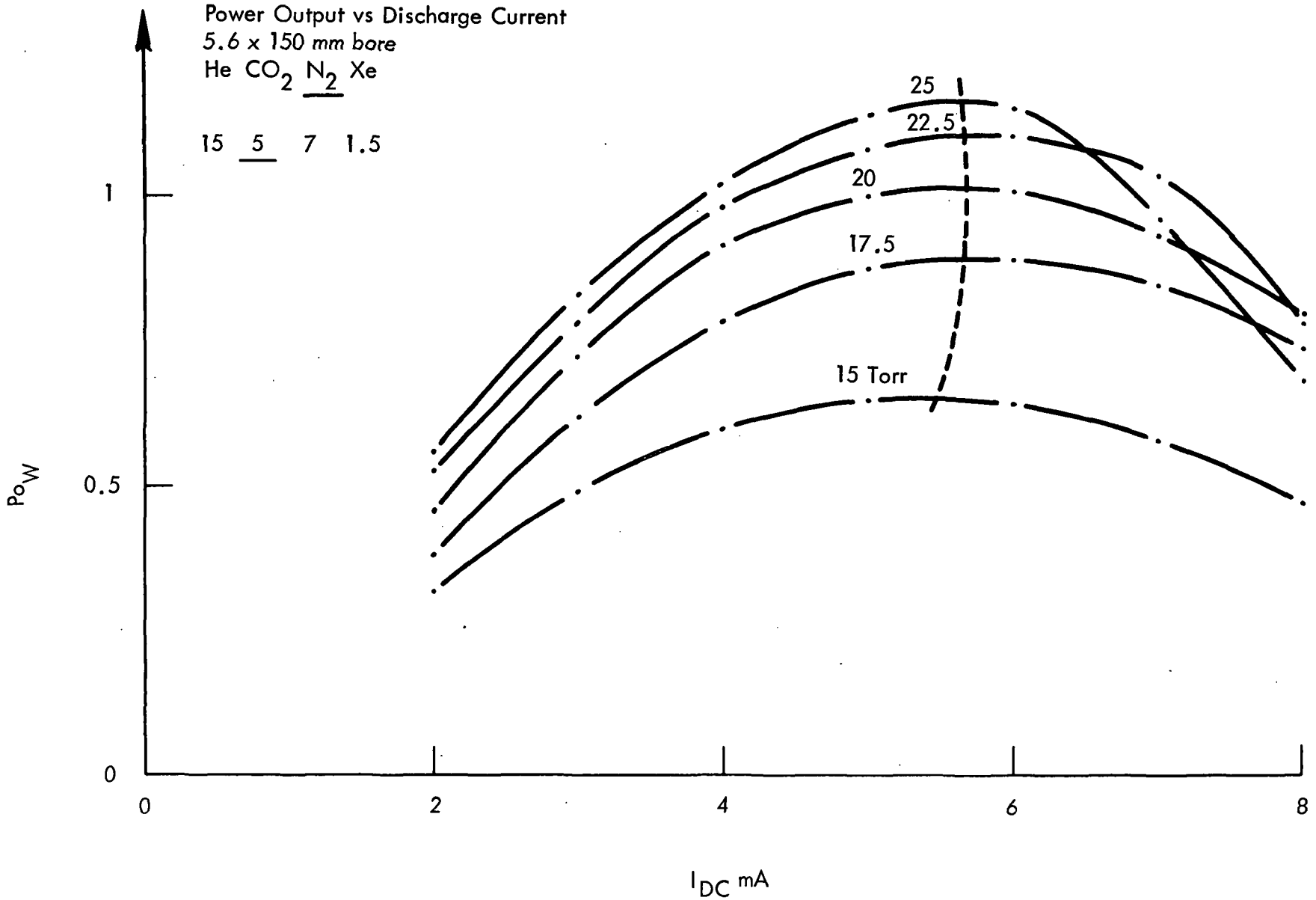

Figure 9. Power output as a function of discharge current [Po (Watts) vs I_{DC} (mA)] for a 150 mm length laser tube with a 5.6 mm bore.

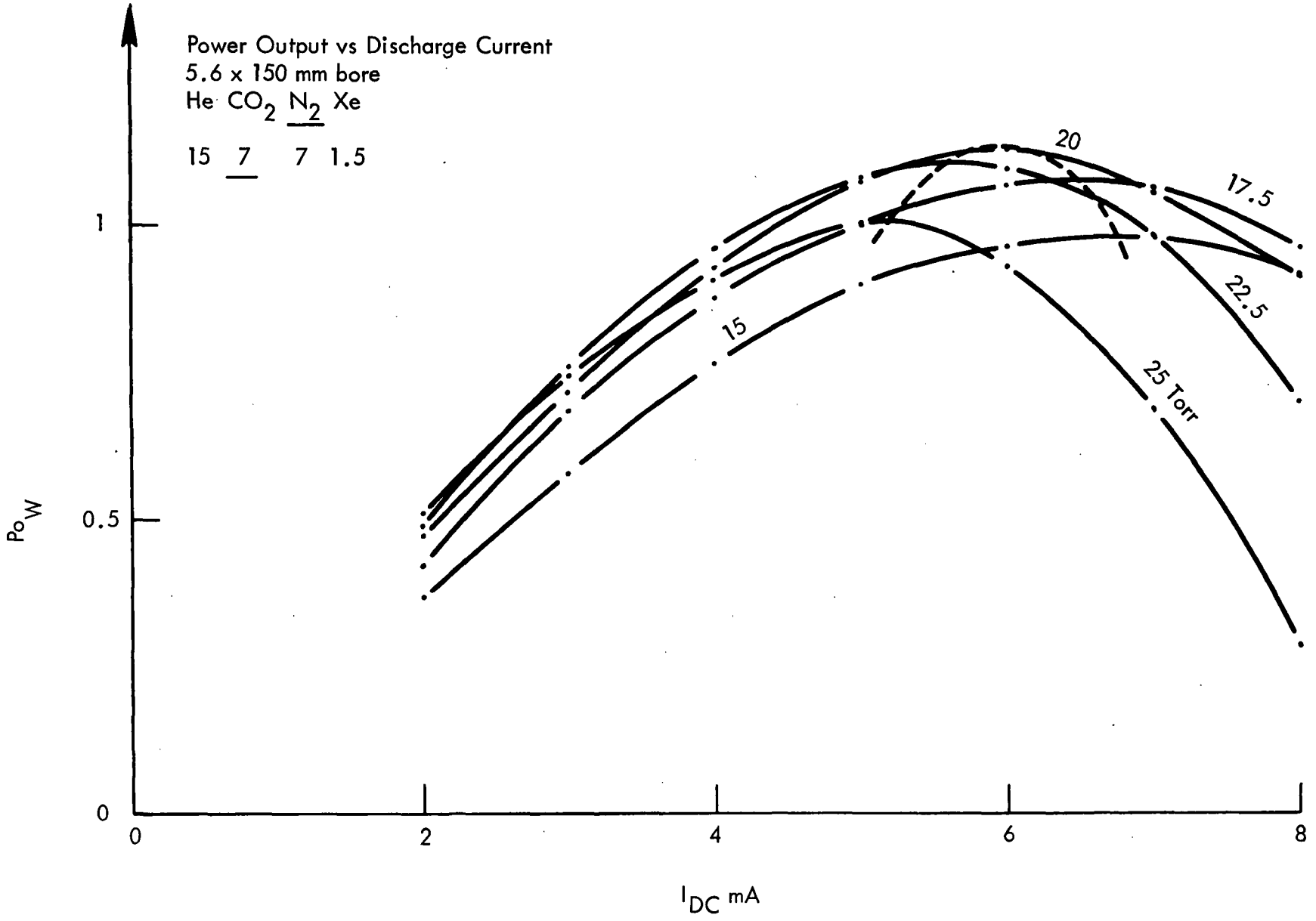

Figure 10. Power output as a function of discharge current [Po (Watts) vs I_{DC} (mA)] for a 150 mm length laser tube with a 5.6 mm bore

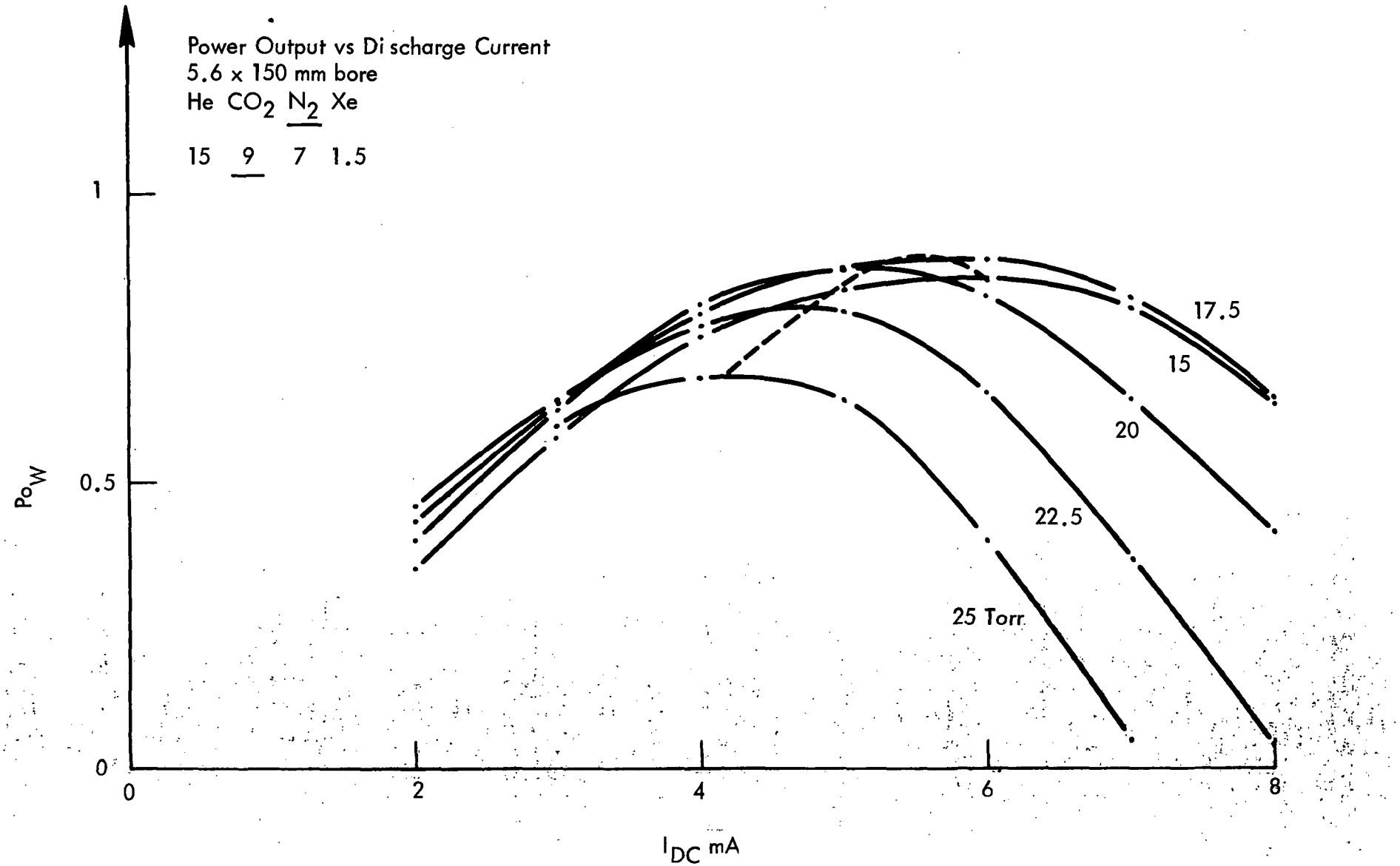

Figure 11. Power output as a function of discharge current [Po (Watts) vs I_{DC} (mA)] for a 150 mm length laser tube with a 5.6 mm bore.

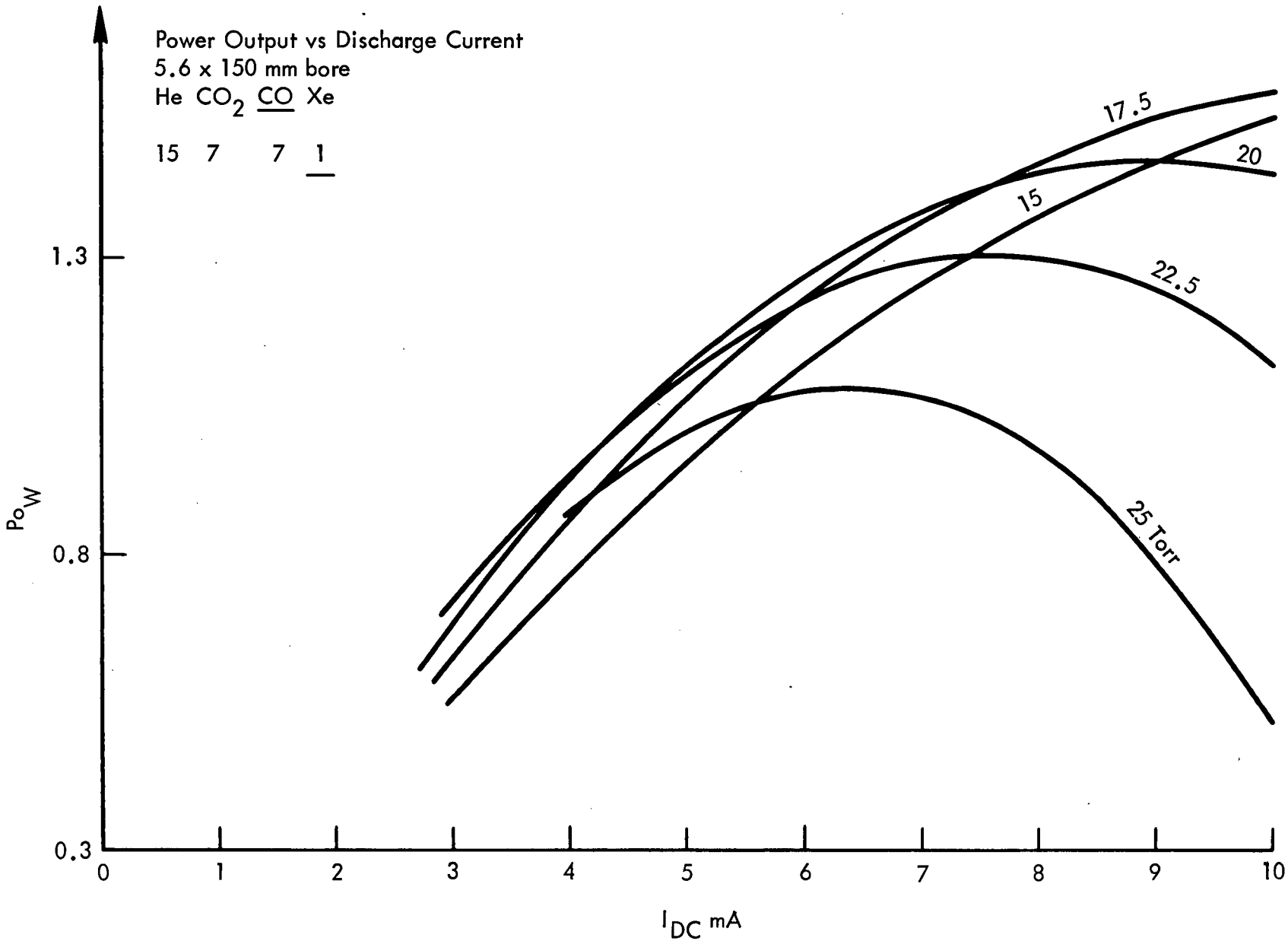

Figure 12. Power output as a function of discharge current [Po (Watts) vs I_{DC} (mA)] for a 150 mm length laser tube with a 5.6 mm bore.

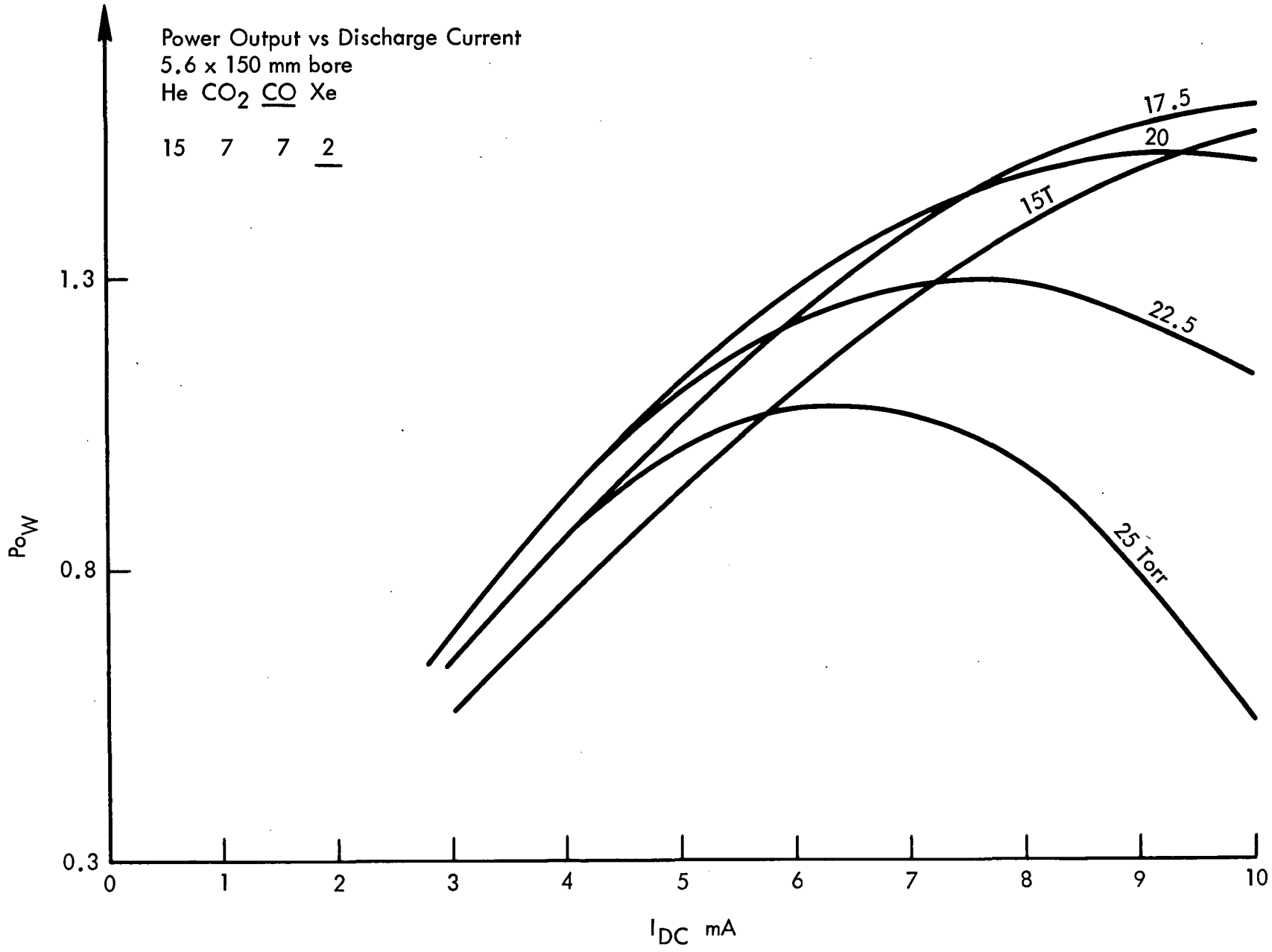

Figure 13. Power output as a function of discharge current [Po (Watts) vs I_{DC} (mA)] for a 150 mm length laser tube with a 5.6 mm bore.

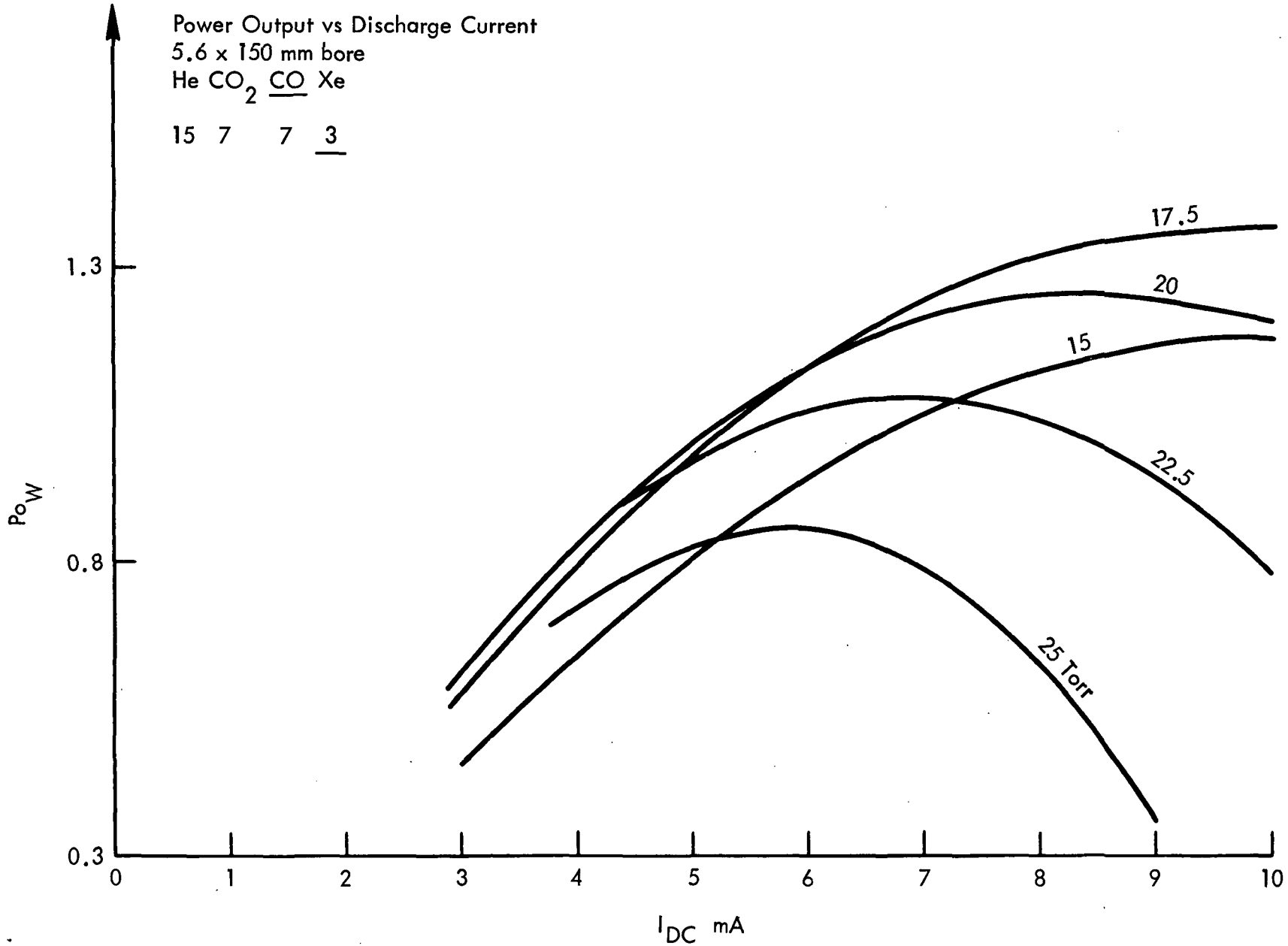

Figure 14. Power output as a function of discharge current [Po (Watts) vs I_{DC} (mA)] for a 150 mm length laser tube with a 5.6 mm bore.

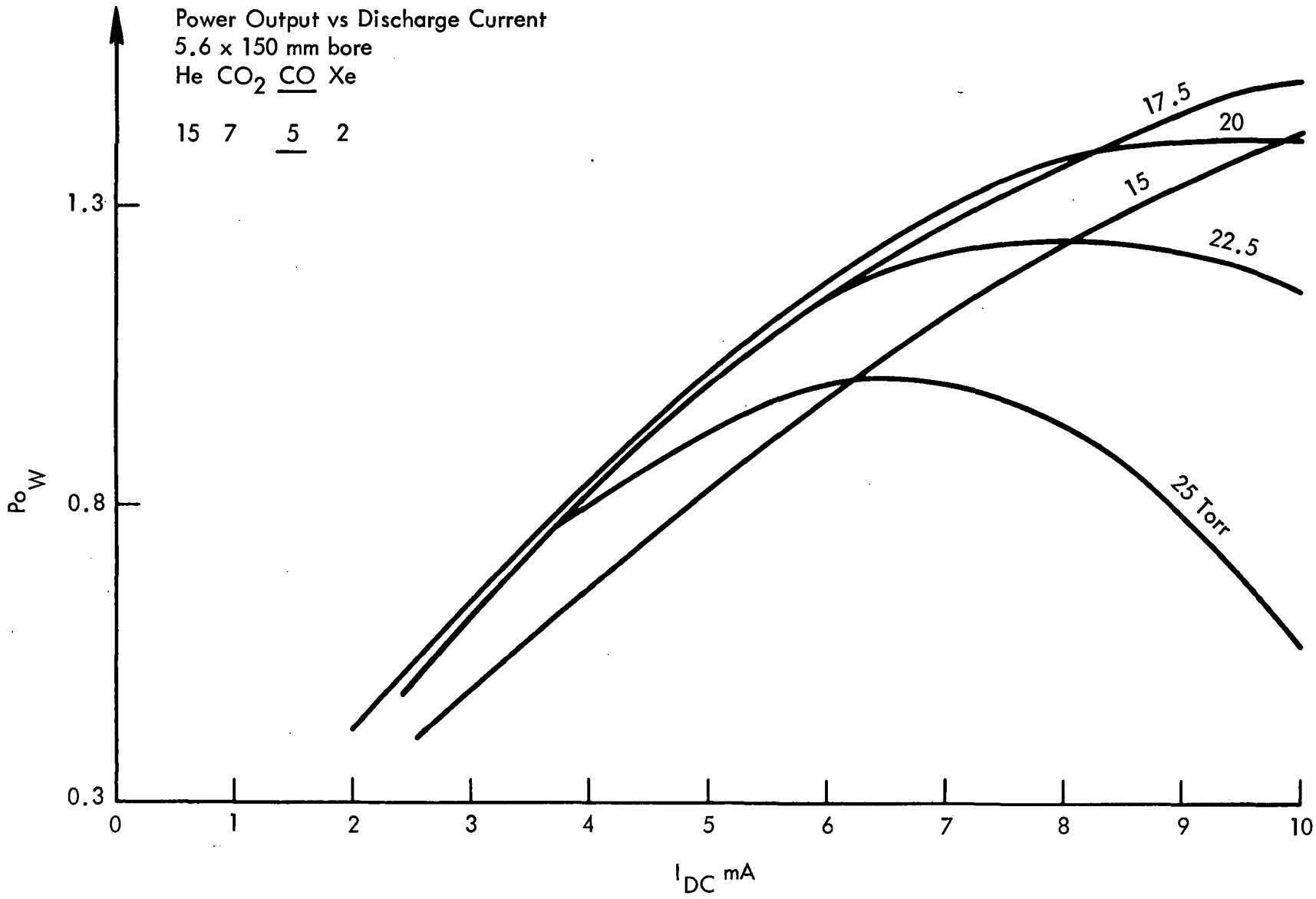

Figure 15. Power output as a function of discharge current [Po (Watts) vs I_{DC} (mA)] for a 150 mm length laser tube with a 5.6 mm bore.

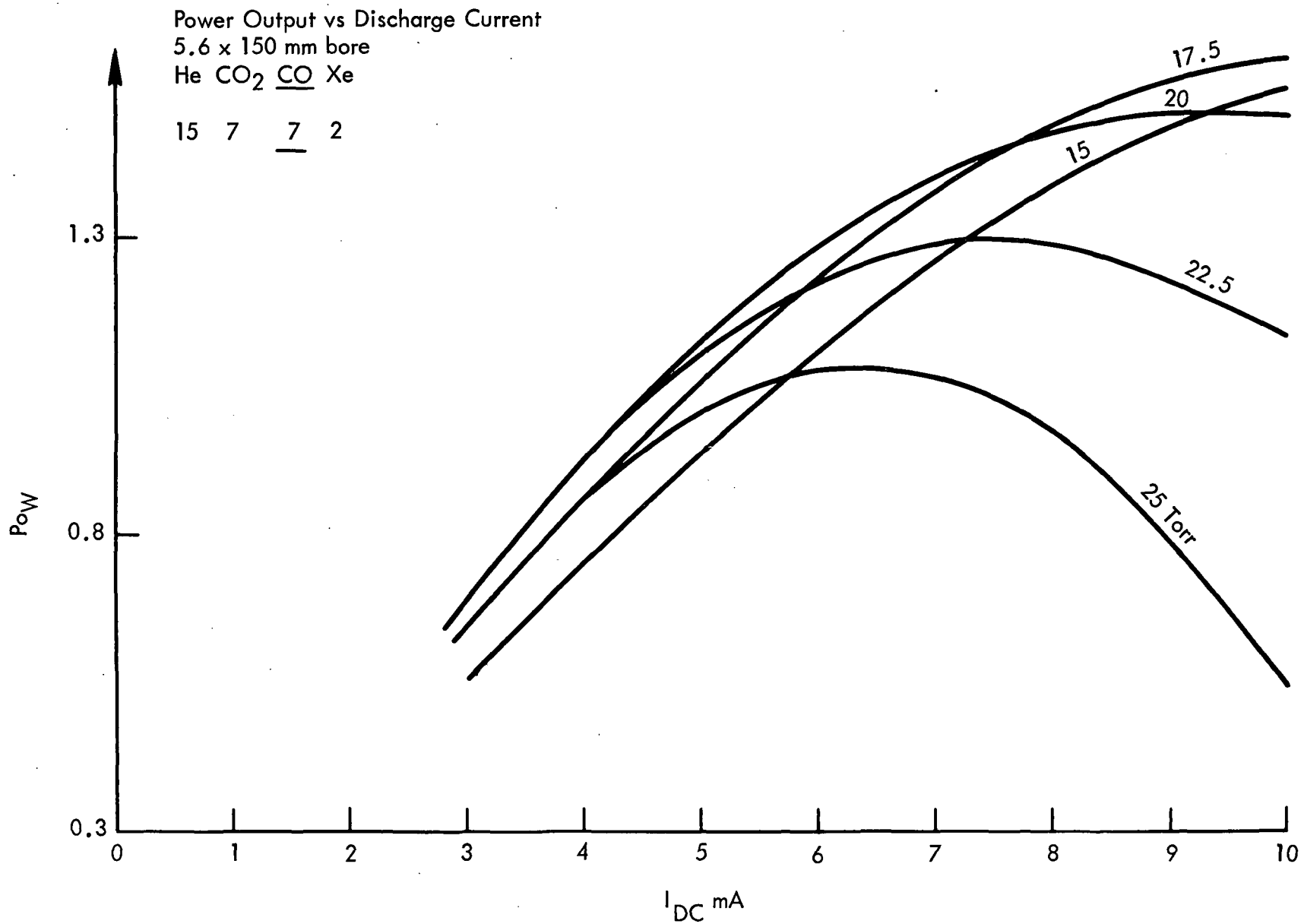

Figure 16. Power output as a function of discharge current [Po (Watts) vs I_{DC} (mA)] for a 150 mm length laser tube with a 5.6 mm bore.

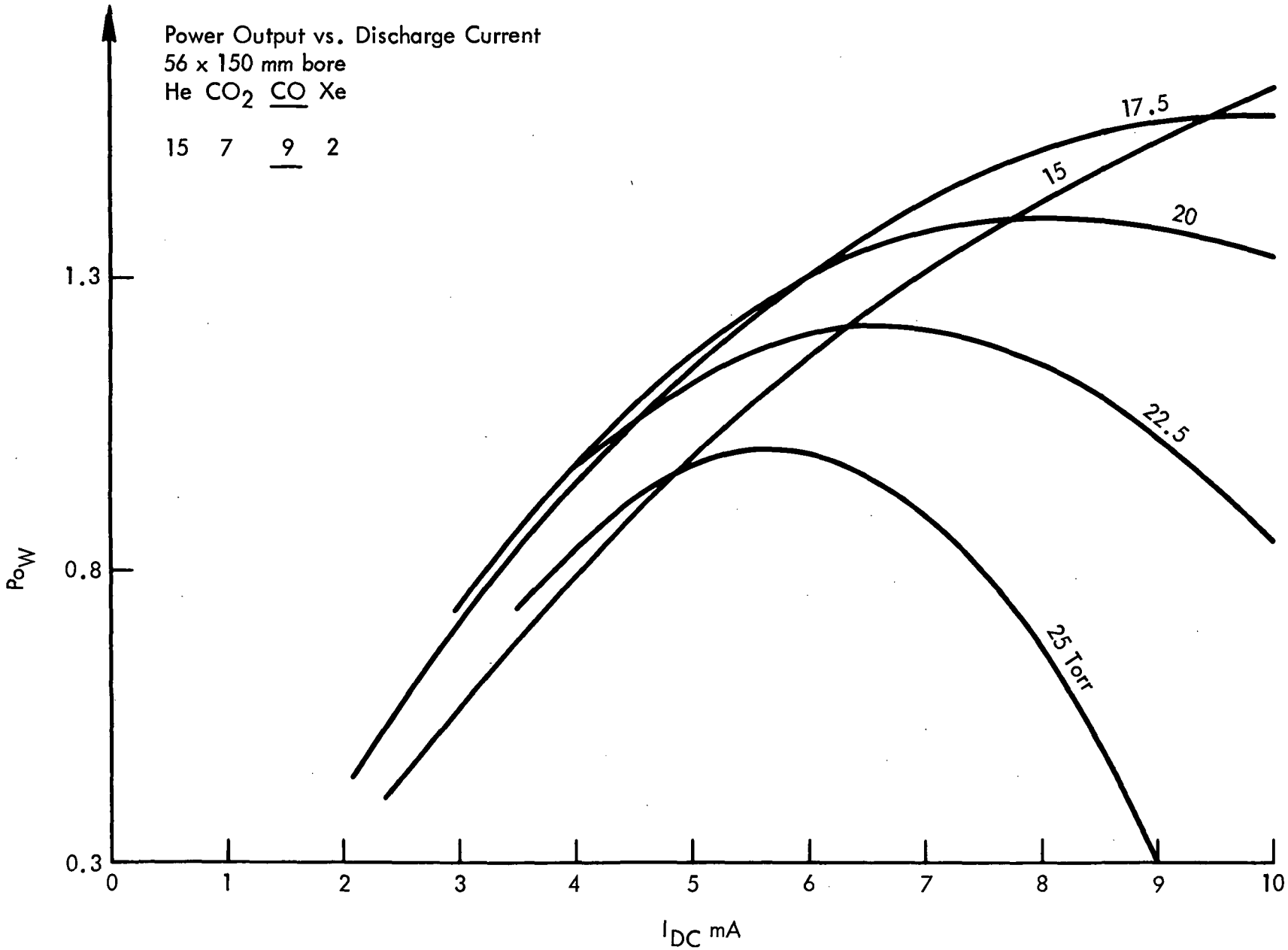

Figure 17. Power output as a function of discharge current [Po (Watts) vs I_{DC} (mA)] for a 150 mm length laser tube with a 5.6 mm bore.

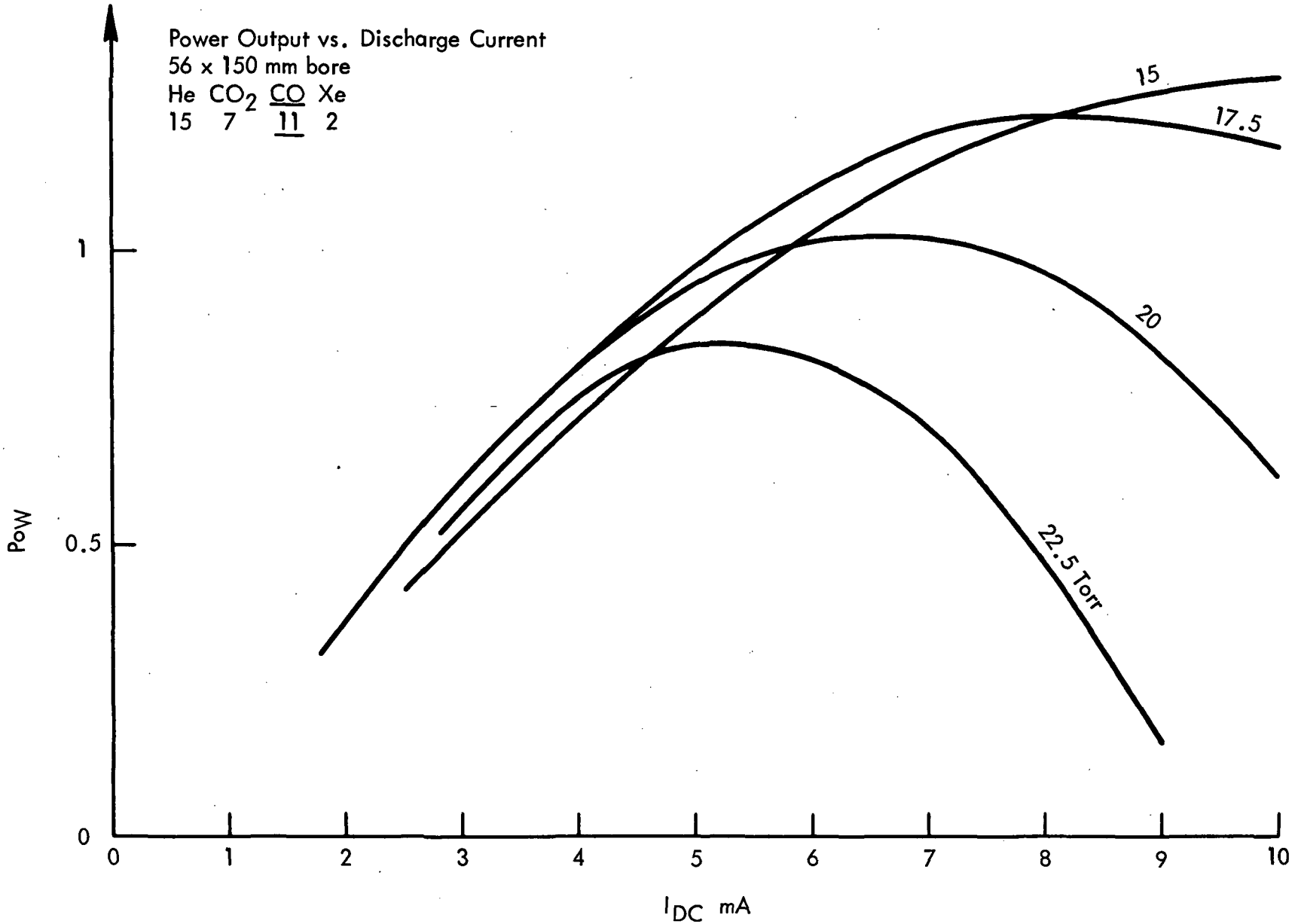

Figure 18. Power output as a function of discharge current [Po (Watts) vs I_{DC} (mA)] for 150 mm length laser tube with a 5.6 mm bore.

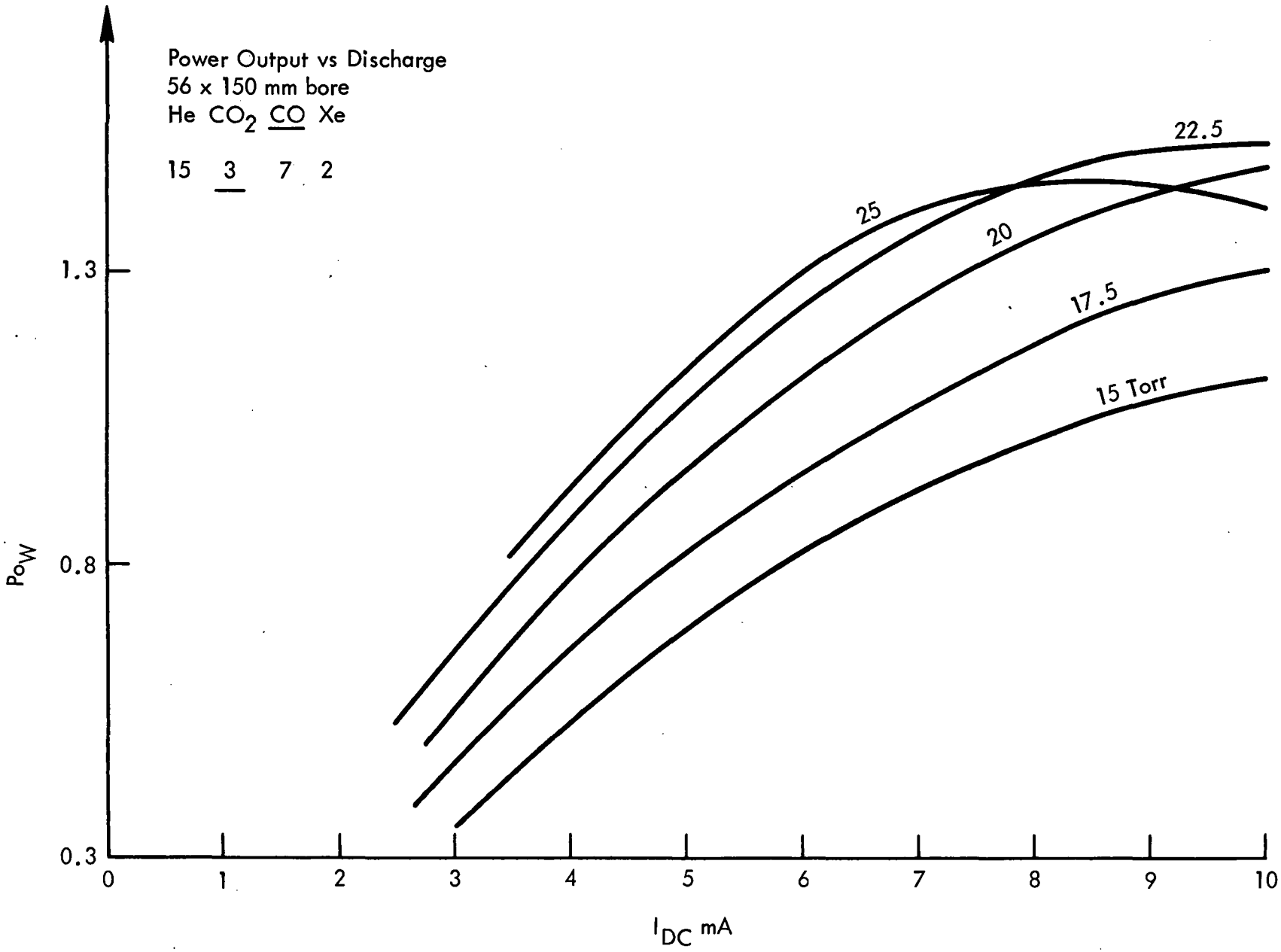

Figure 19. Power output as a function of discharge current [Po (Watts) vs I_{DC} (mA)]for 150 mm length laser tube with a 5.6 mm bore.

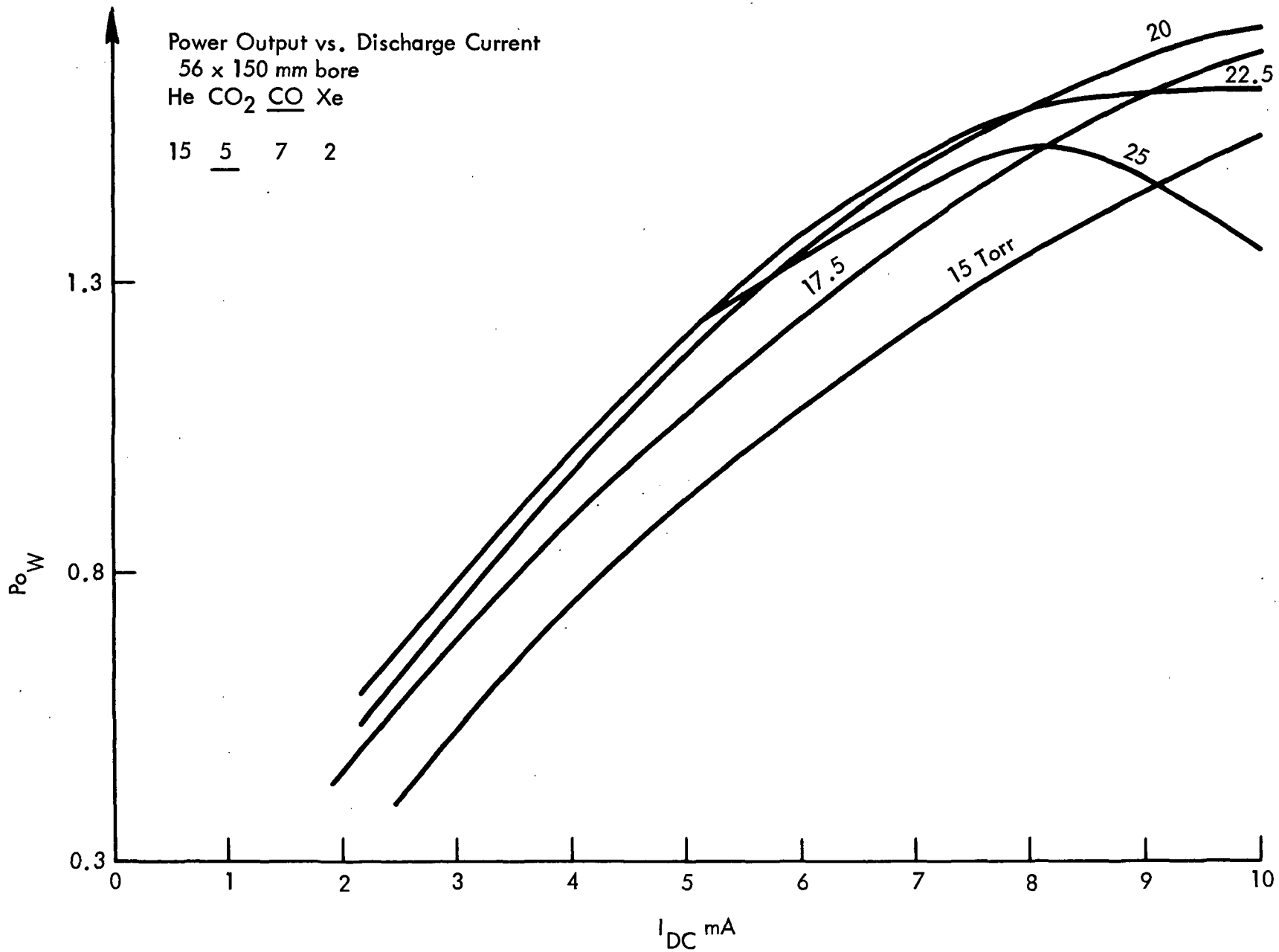

Figure 20. Power output as a function of discharge current [Po (Watts) vs I_{DC} (mA)]for 150 mm length laser tube with a 5.6 mm bore.

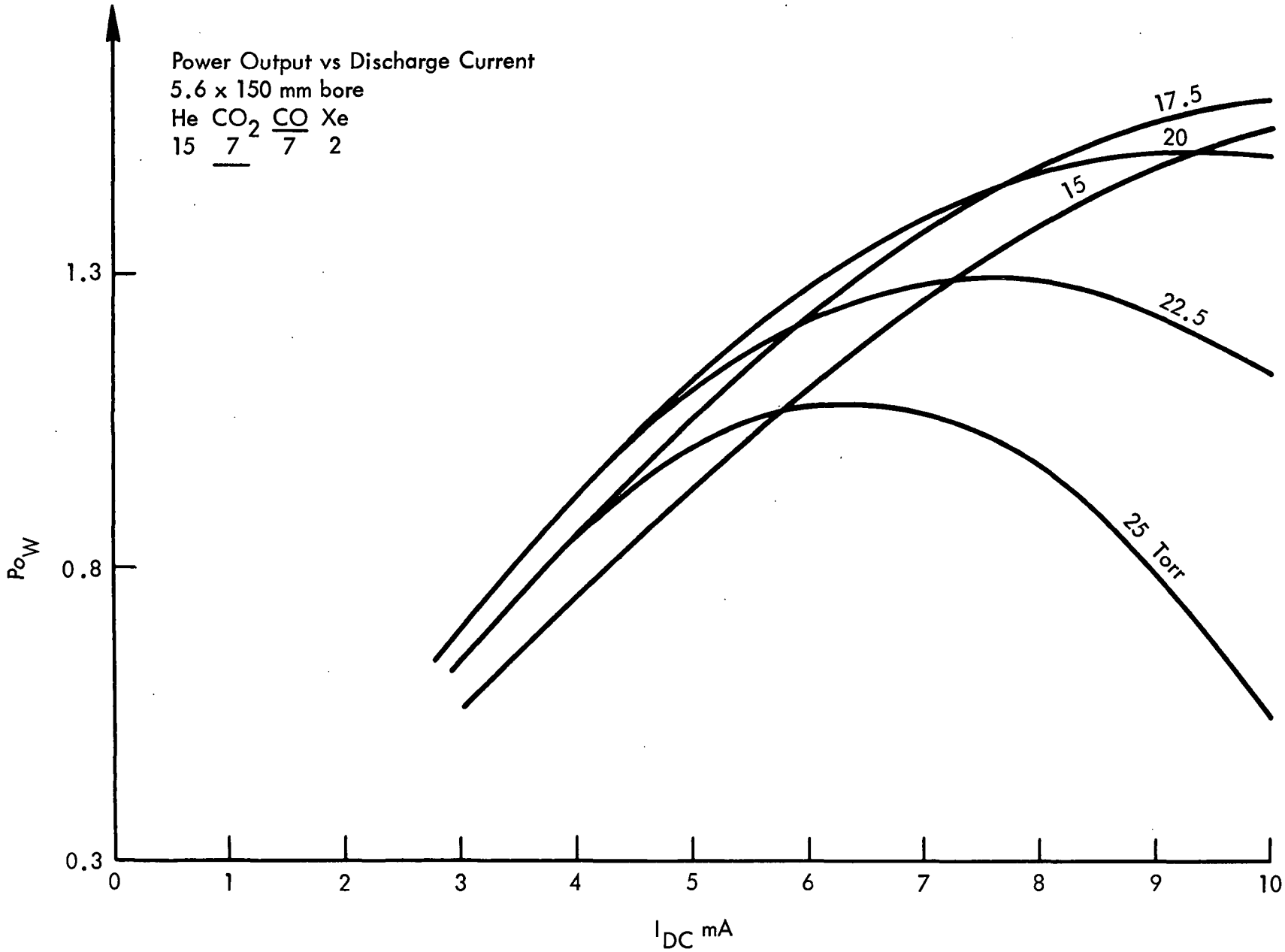

Figure 21. Power output as a function of discharge current [Po (Watts) vs I_{DC} (mA)] for a 150 mm length laser tube with a 5.6 mm bore.

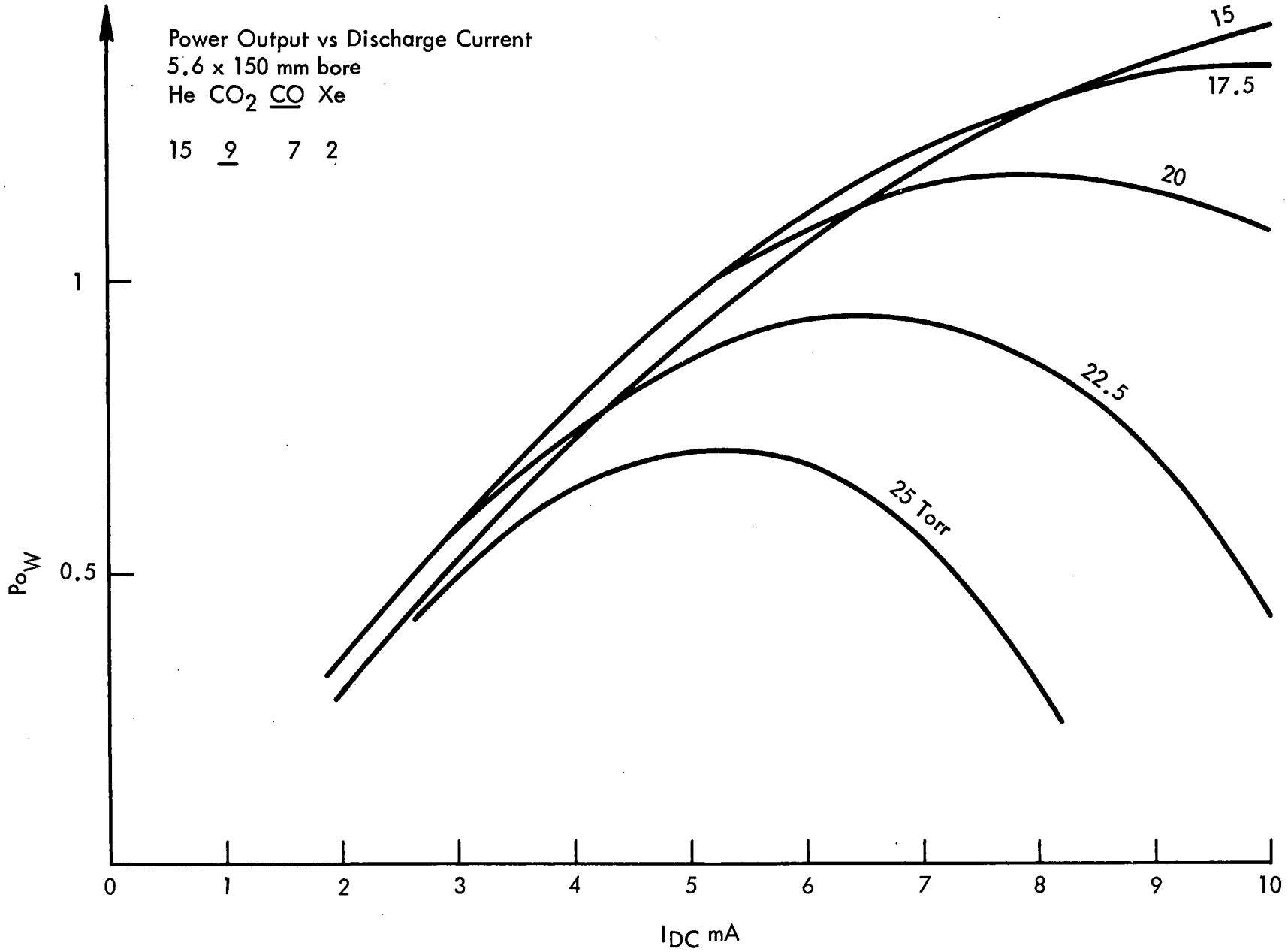

Figure 22. Power output as a function of discharge current [Po (Watts) vs I_{DC} (mA)] for a 150 mm length laser tube with a 5.6 mm bore.

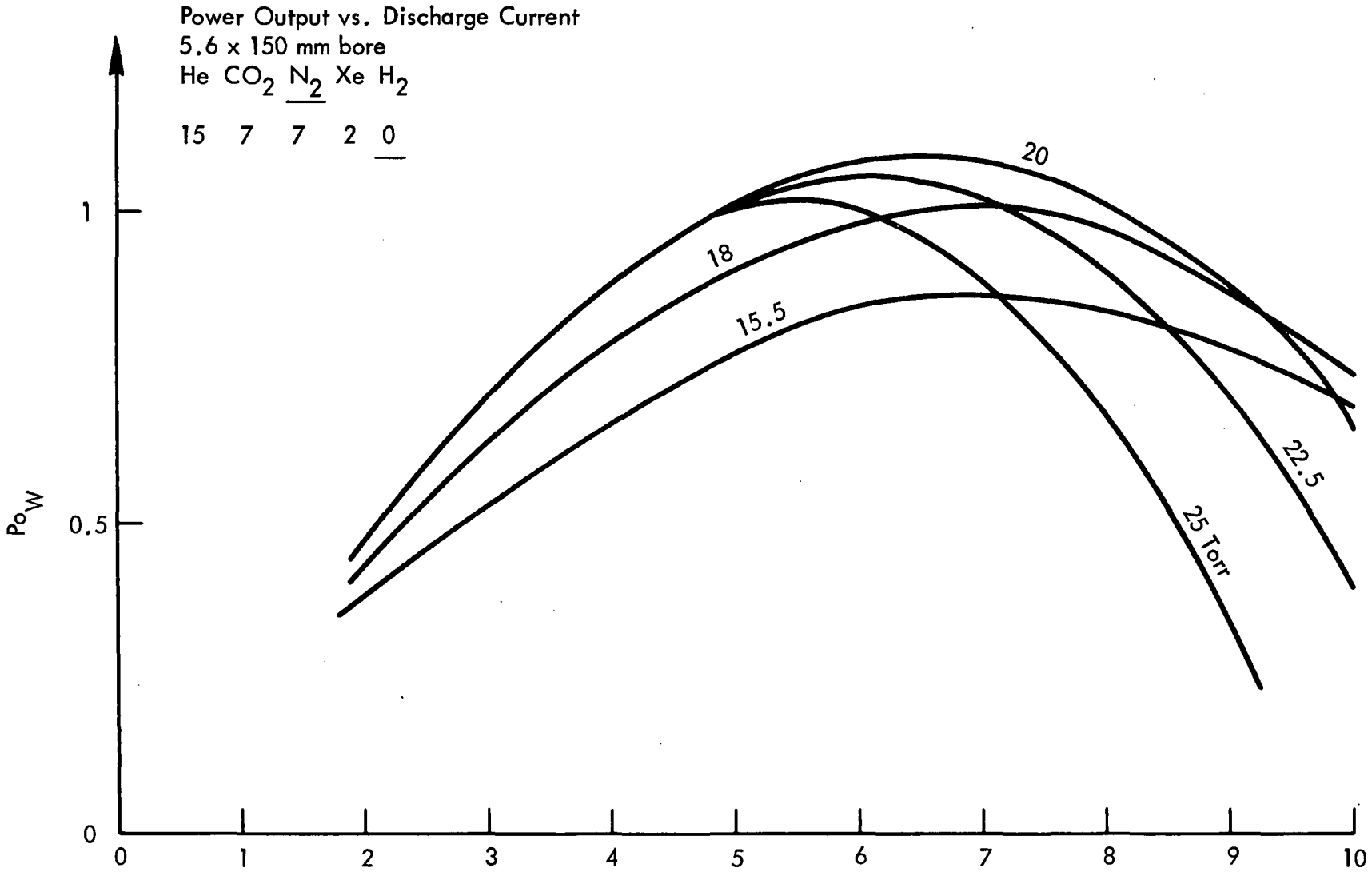

Figure 23. Power output as a function of discharge current [Po (Watts) vs I_{DC} (mA)] for a 150 mm length laser tube with a 5.6 mm bore.

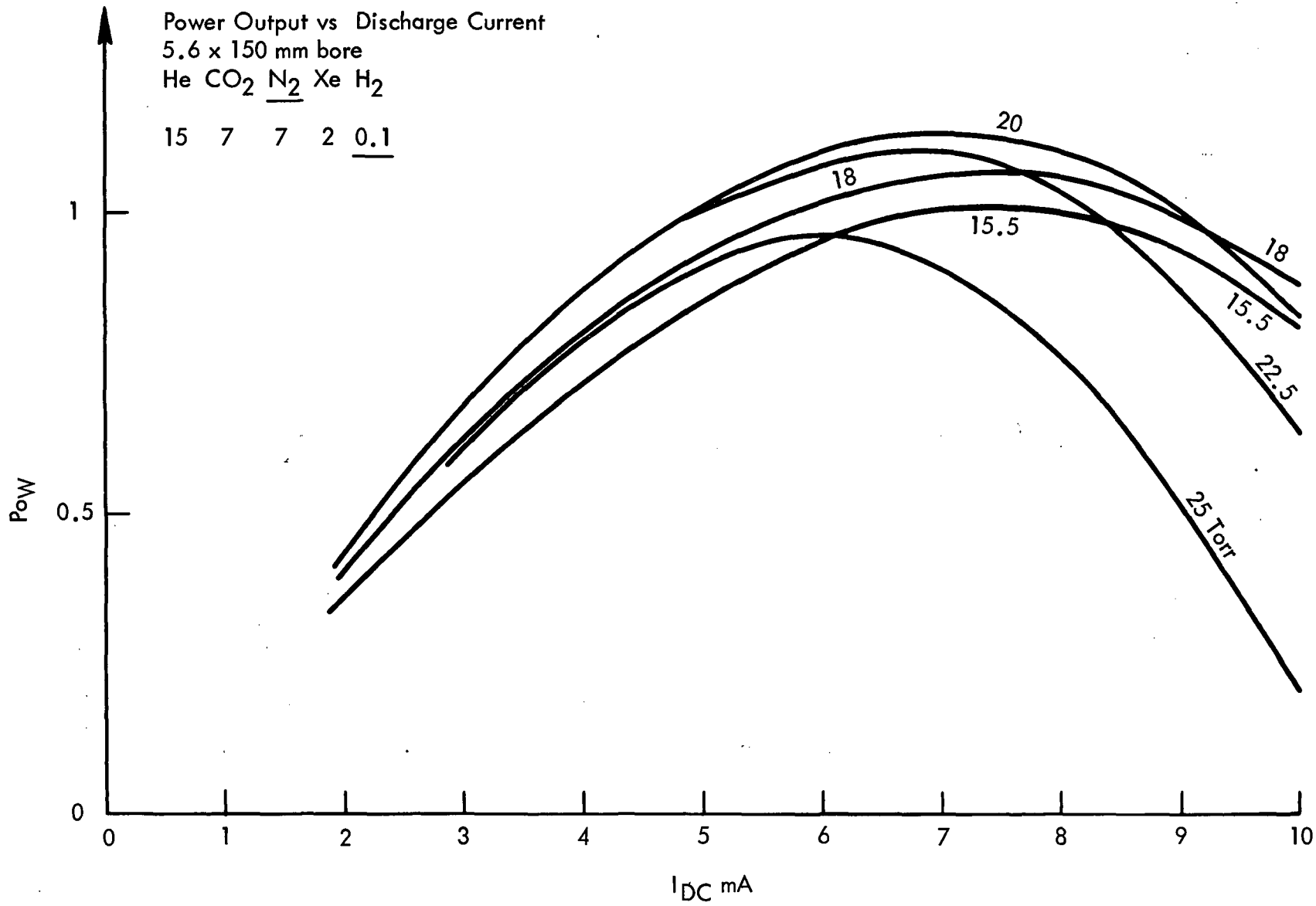

Figure 24. Power output as a function of discharge current [Po (Watts) vs I_{DC} (mA)] for a 150 mm length laser tube with a 5.6 mm bore.

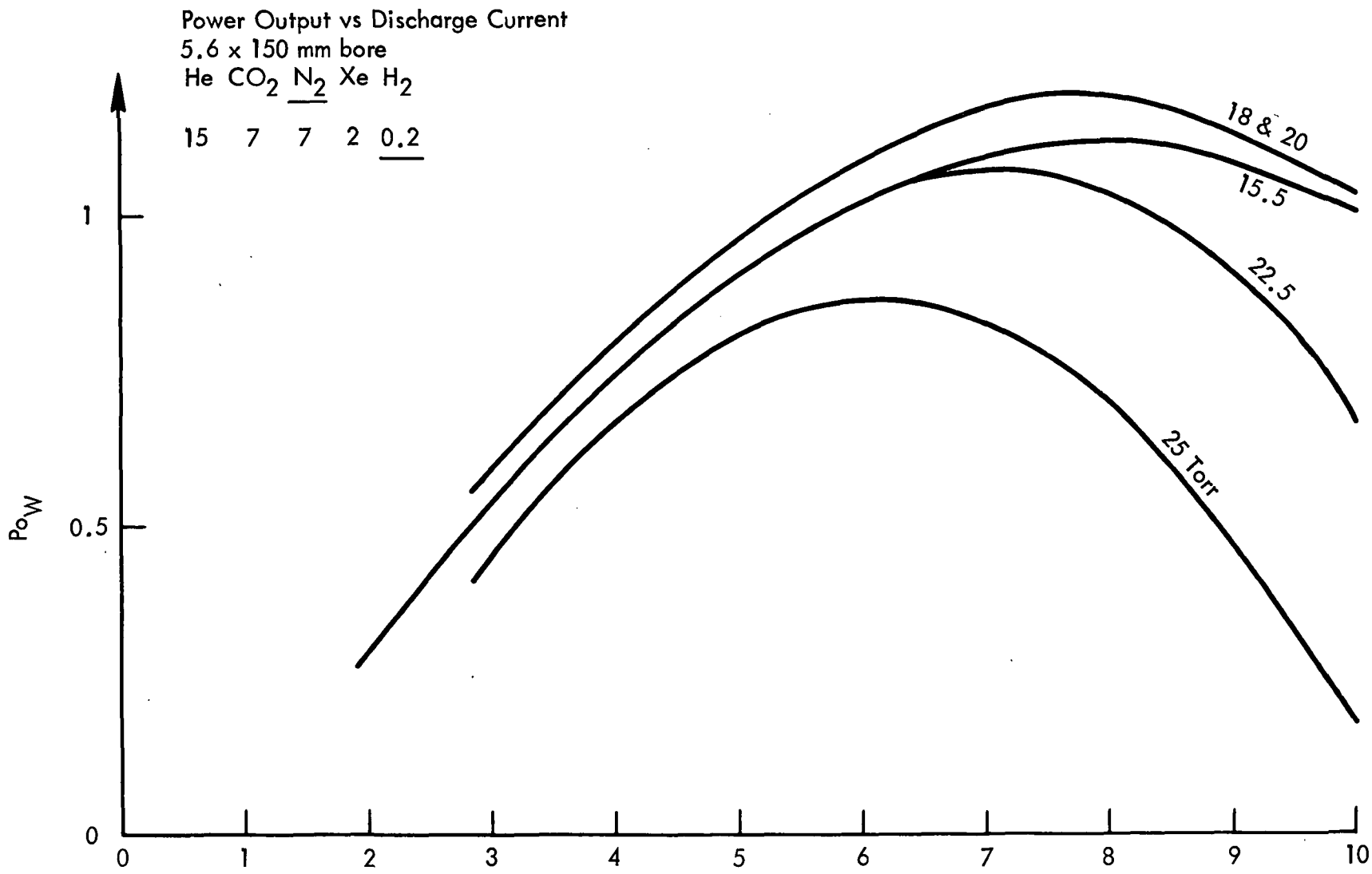

Figure 25. Power output as a function of discharge current [Po (Watts) vs I_{DC} (mA)] for a 150 mm length laser tube with a 5.6 mm bore.

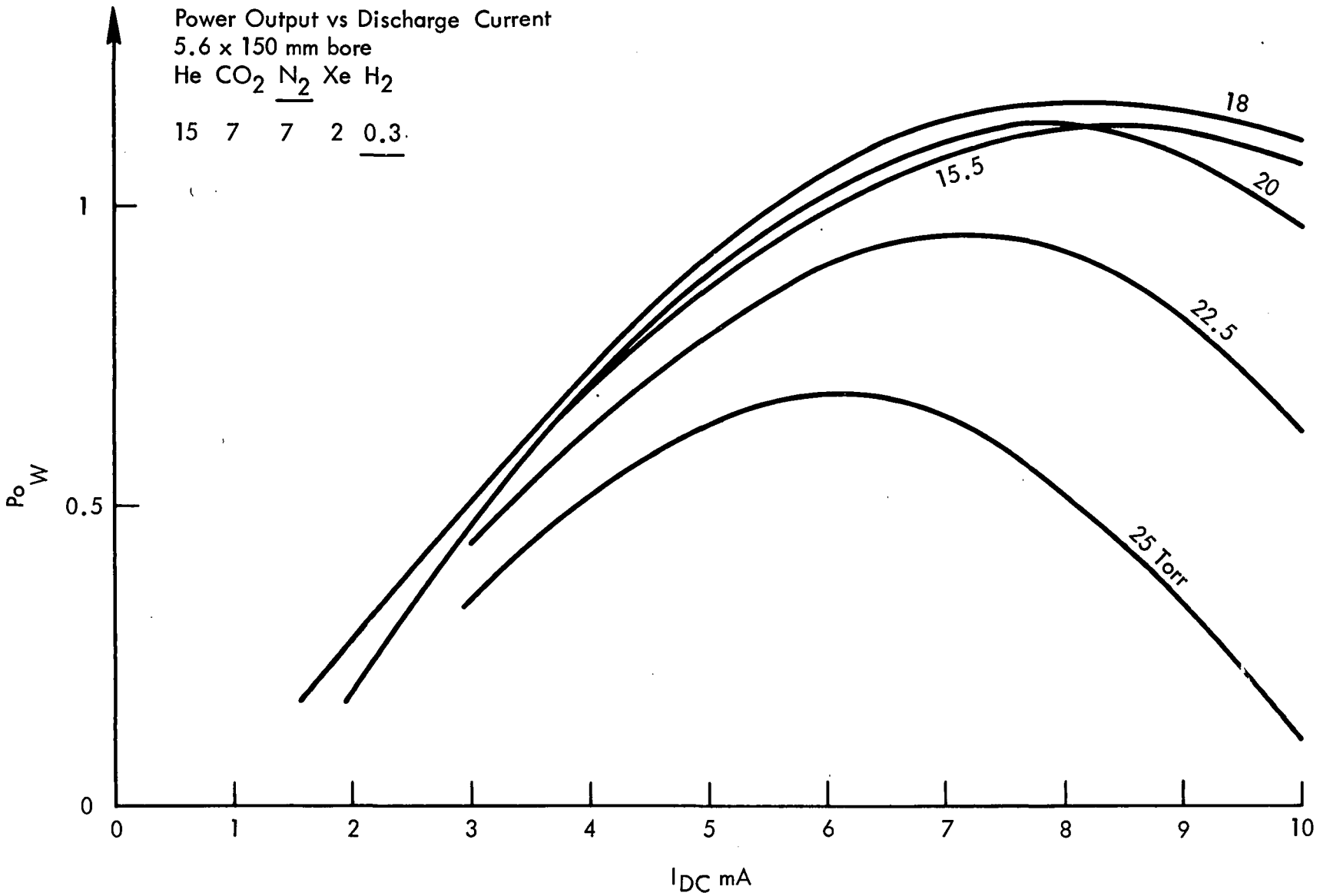

Figure 26. Power output as a function of discharge current [Po (Watts) vs I_{DC} (mA)] for a 150 mm length laser tube with a 5.6 mm bore.

TYPE 1 LX 3.5 mm ID
x mm MAX. DEPTH

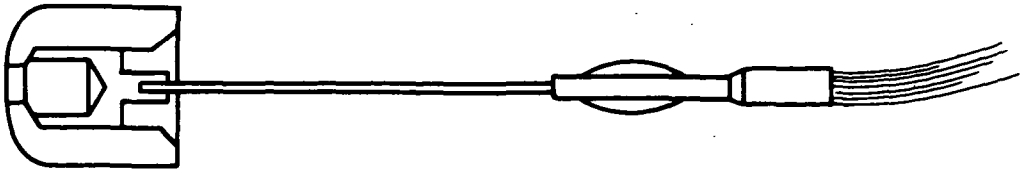

TYPE 2 LX 5 mm ID
x mm MAX. DEPTH

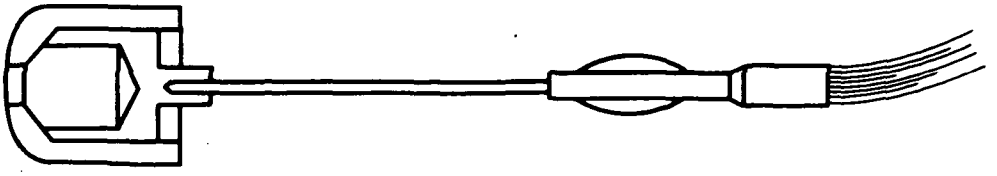

TYPE 3 LX 8.5 mm ID
x mm MAX. DEPTH

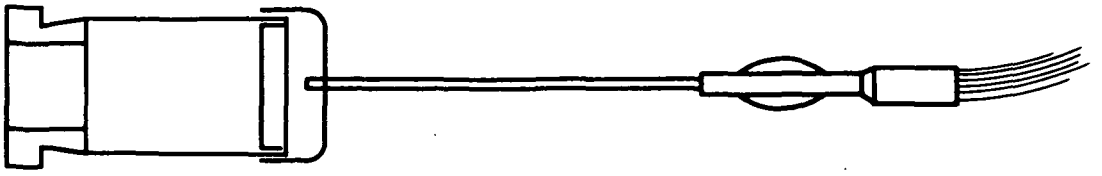

TYPE 4 LX
x mm MAX. DEPTH

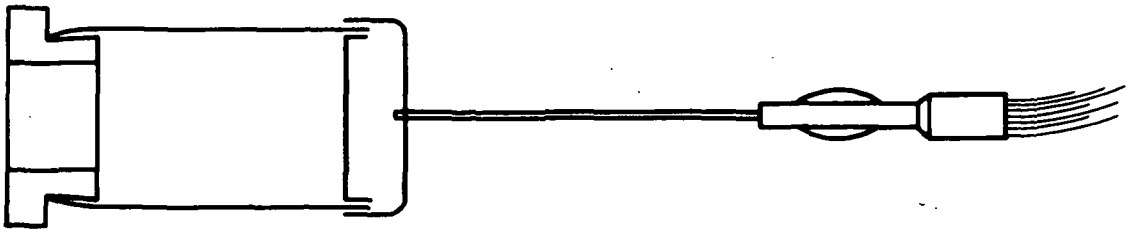

Figure 27. Cathode types.

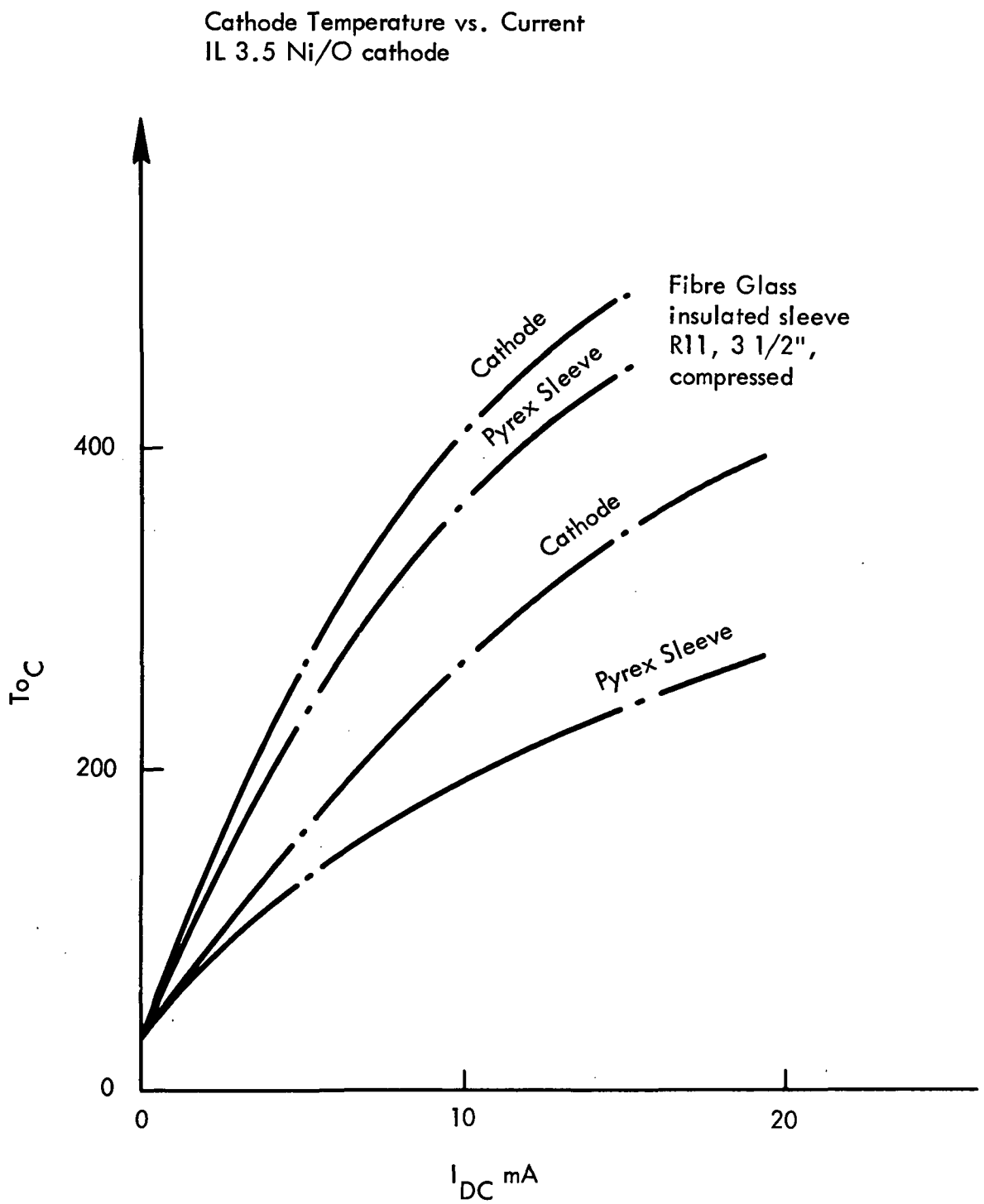

Figure 28. Cathode temperature [T(°C)] vs Current (I_{DC}).

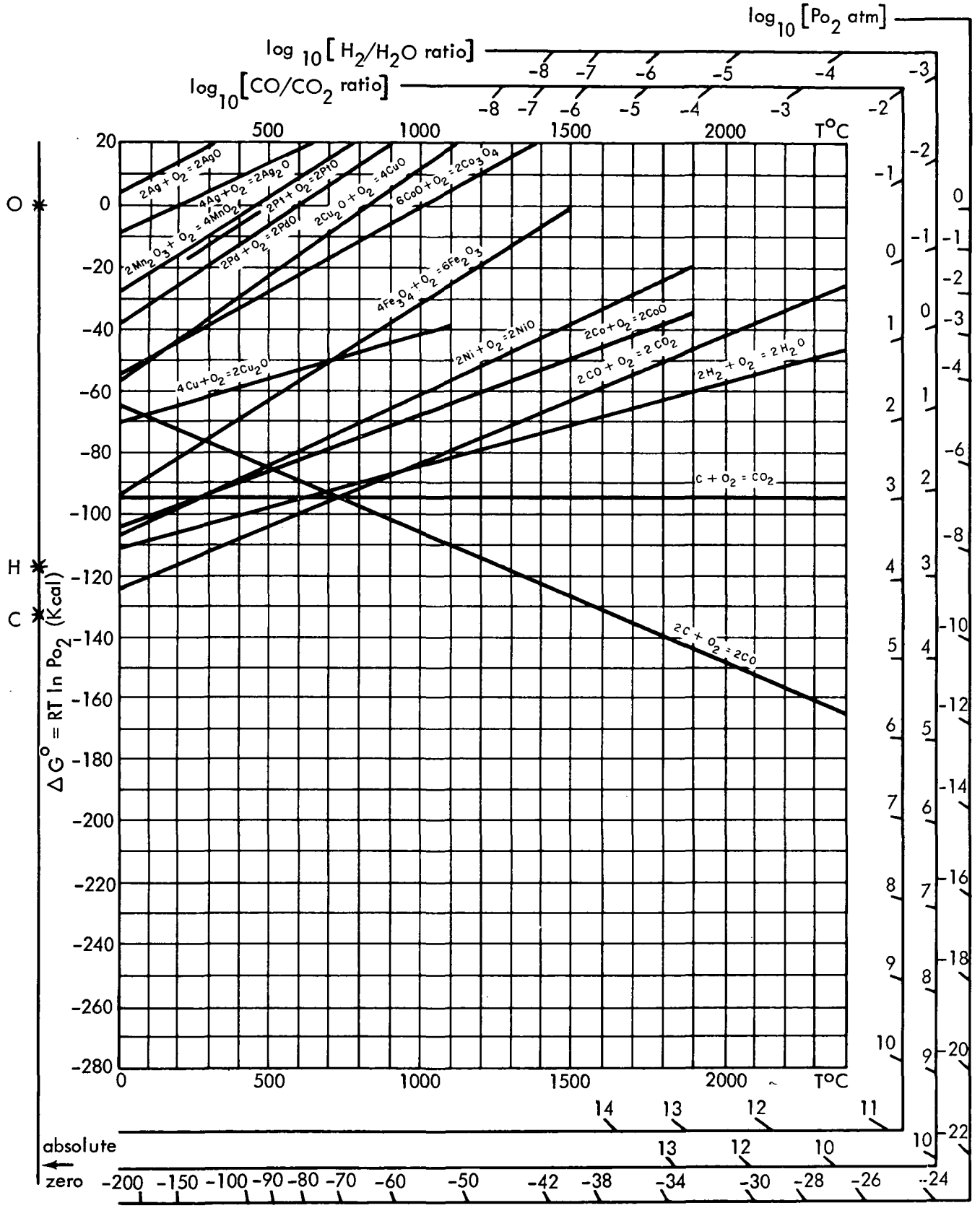

Standard free energy of formation of oxides as a function of temperature.

Figure 29. Standard free energy of formation of oxides as a function of temperature.

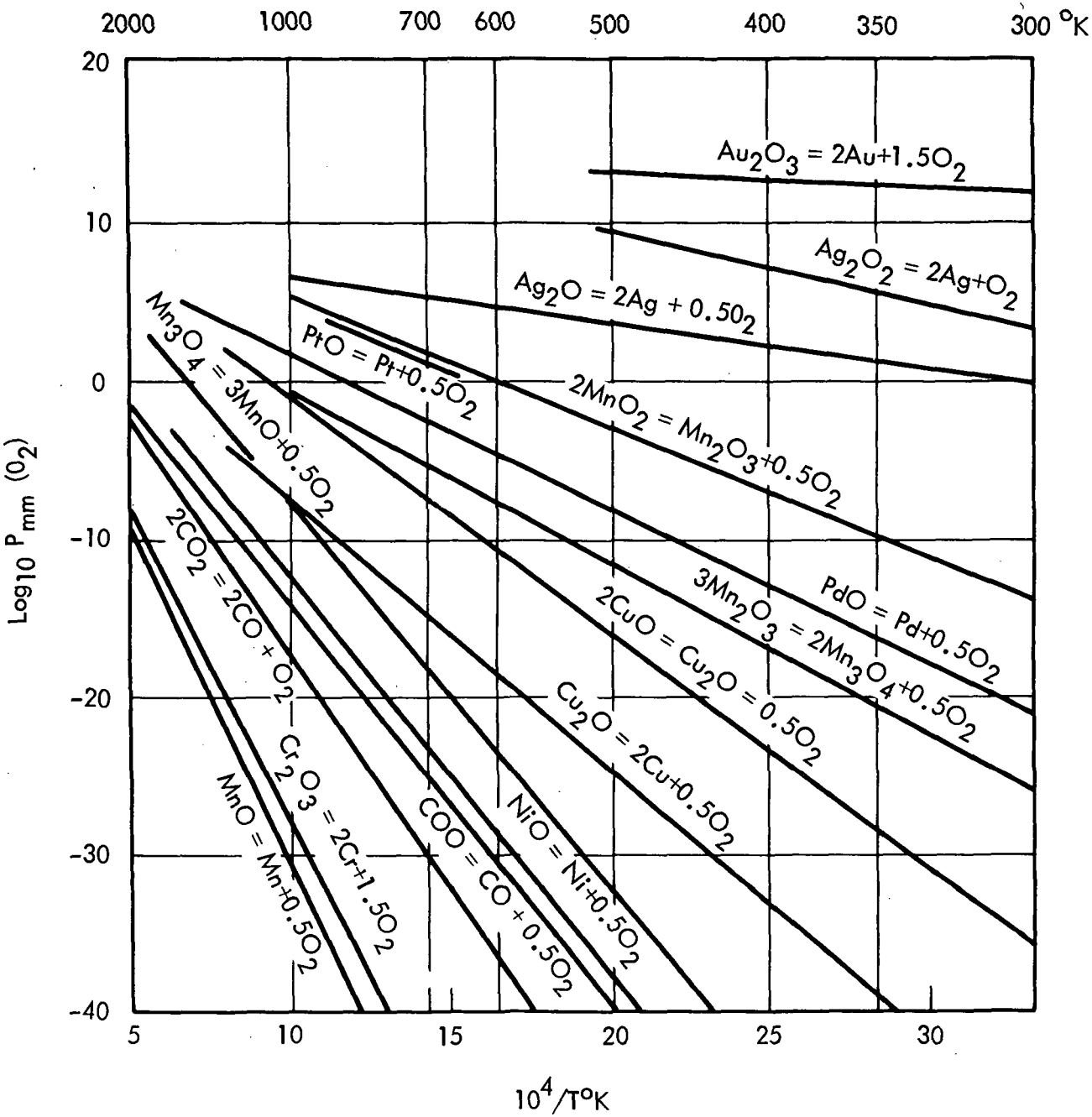

Figure 30. Dissociation pressure of oxides as a function of temperature.

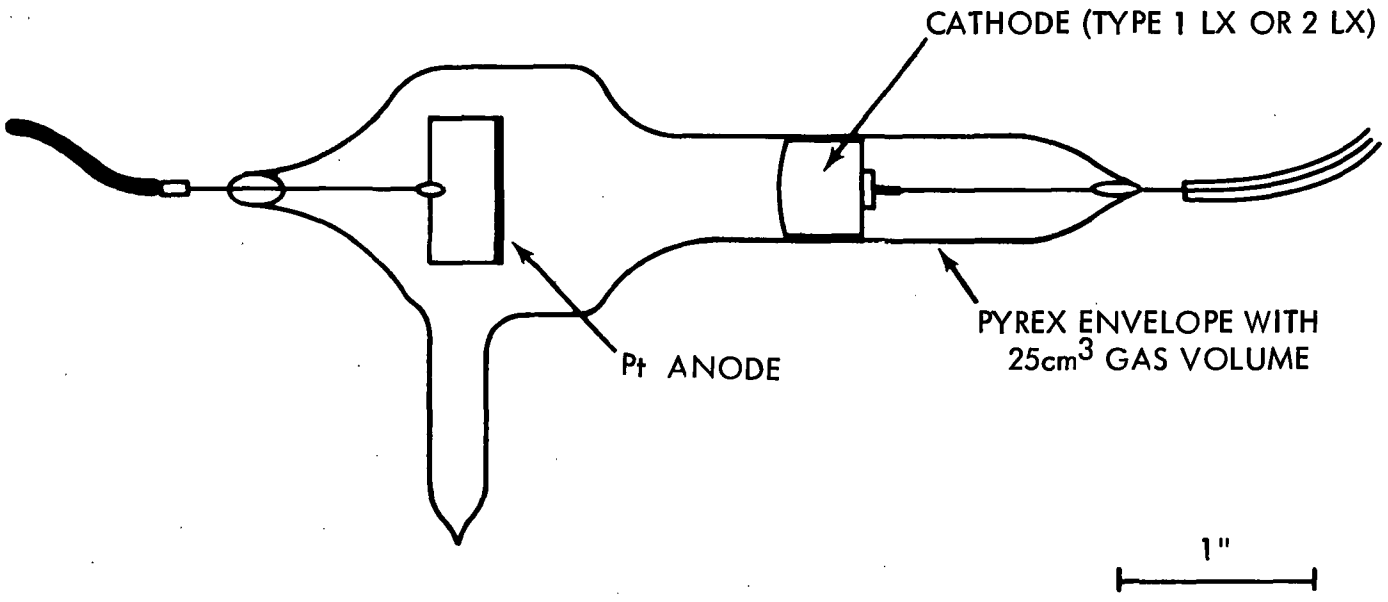

Figure 31. Discharge tube.

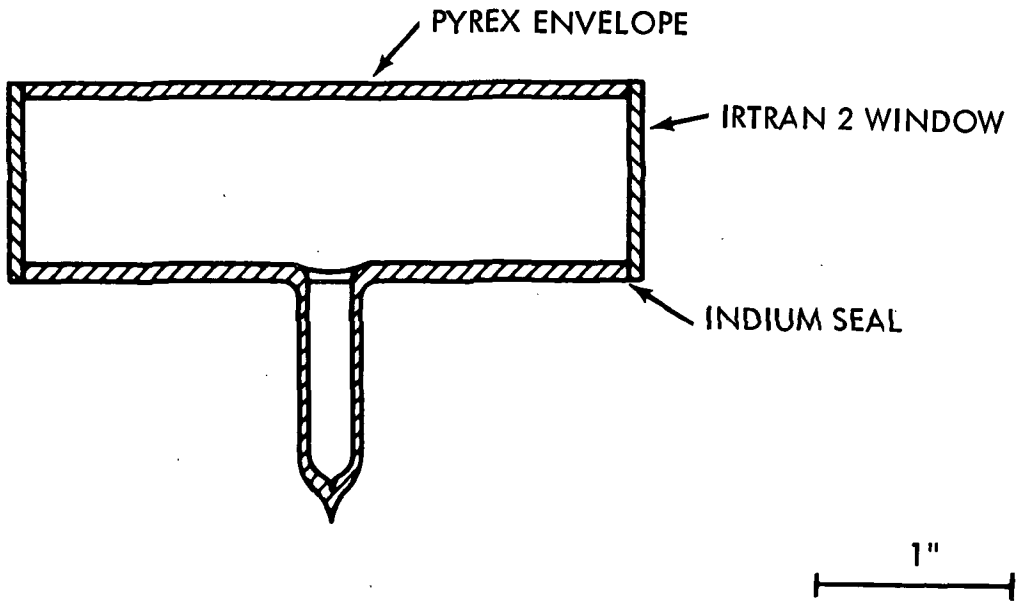

Figure 32. Infrared absorption cell.

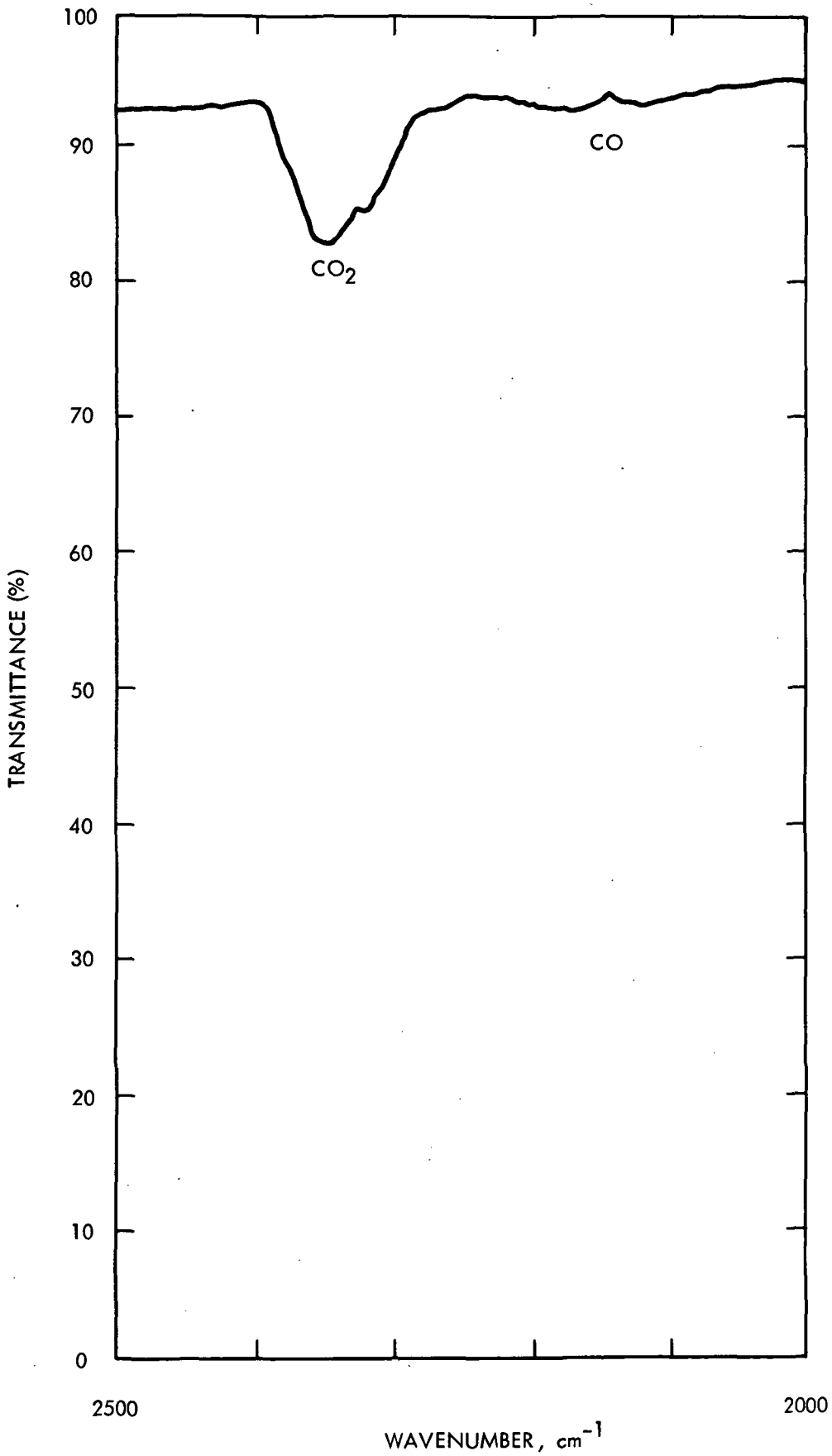

Figure 33. Infrared spectrum of CO_2 and CO in a gas mix of 20.1 torr total pressure (4.7 CO_2; 4.7 CO; 0.7 Xe and 10 torr He) in a 7.8 cm path length cell employing a Digilab FTS-14 with equivalent slit width of 8 cm^{-1}.

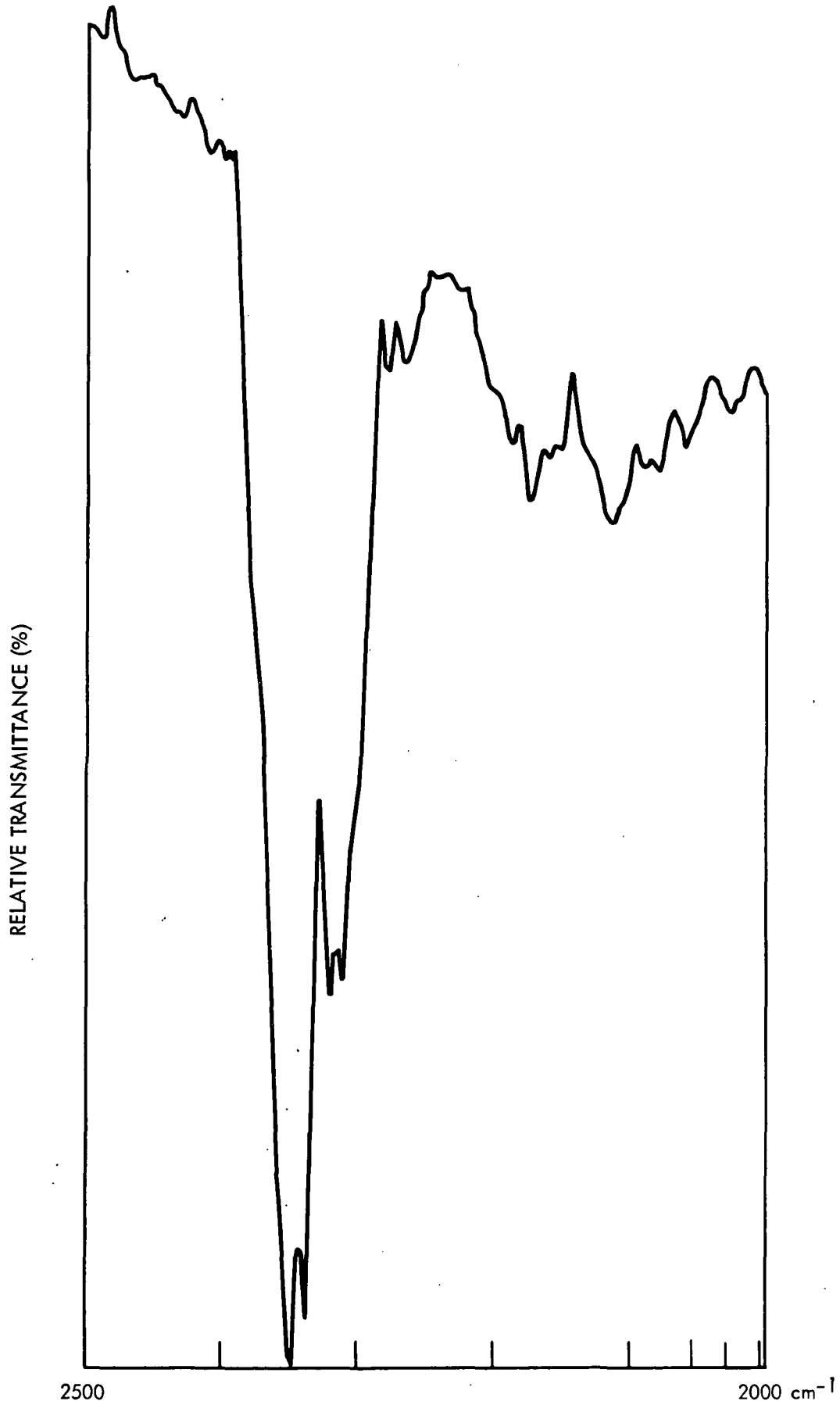

Figure 34. Infrared absorption spectrum of CO_2 and CO (expanded scale).

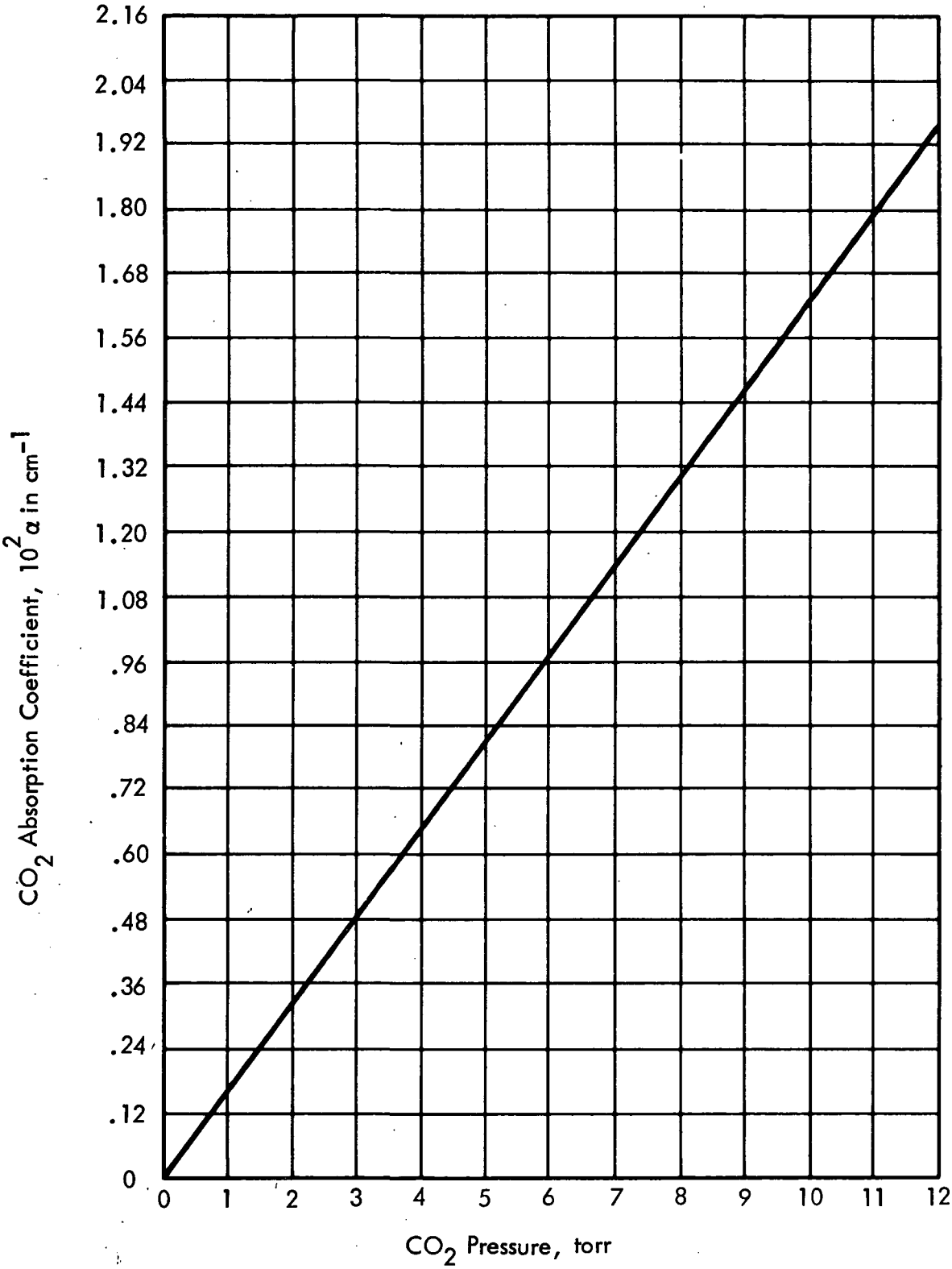

Figure 35. Plot of absorption Coefficient, α, of pure CO_2 versus CO_2 pressure for $\alpha = [\ln(I_o/I)]/x$ measured at $\tilde{\nu} = 2355\ cm^{-1}$, x=8 cm and 75°F temperature, and 8 Cm^{-1} equivalent slit width.

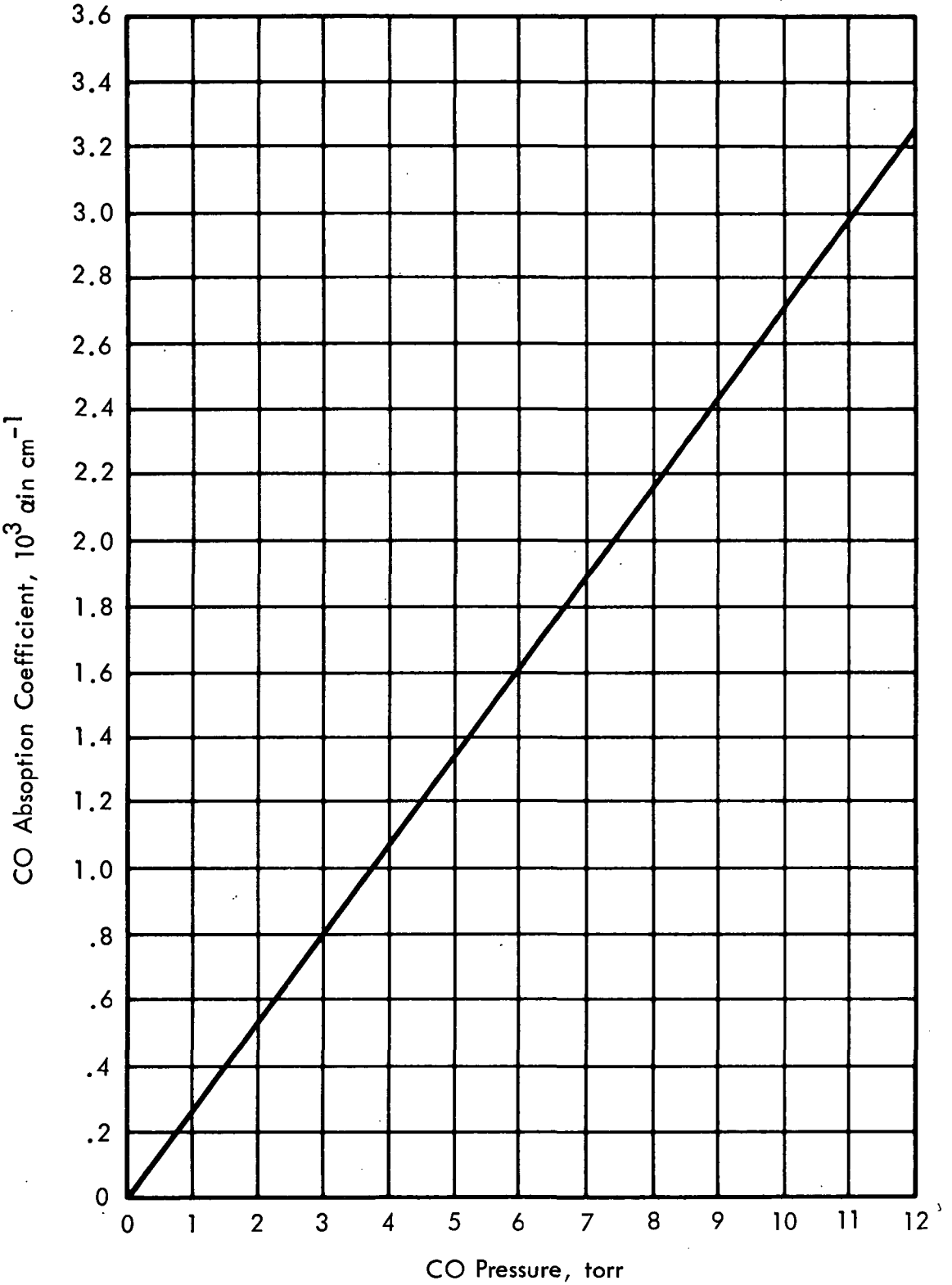

Figure 36. Plot of Absorption Coefficient, α , of pure CO versus CO pressure for $\alpha = [\ln(I_o/I)]/x$ measured at $\tilde{\nu} = 2175\ cm^{-1}$, x=8 cm and 75°F temperature, and 8 Cm^{-1} equivalent slit width.

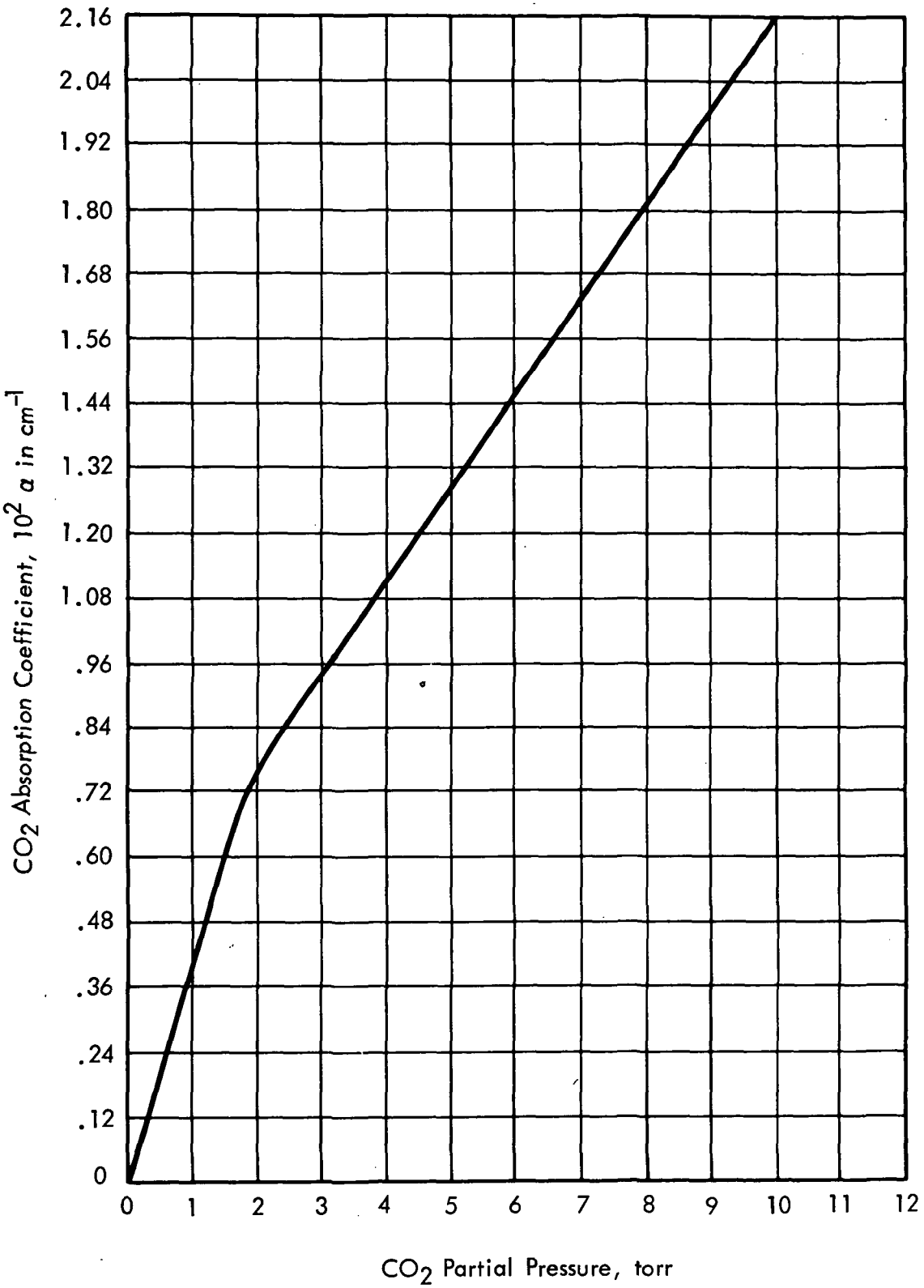

Figure 37. Plot of Absorption Coefficient, α , of CO_2 versus partial pressure, P, for a gas mixture of 20 torr total pressure (P torr CO_2, 10-P torr CO, 9.4 torr He, 0.6 torr Xe) and $\alpha = [\ln(I_o/I)]/x$ measured at $\tilde{\nu}$= 2355 cm^{-1}, x = 8 cm and 75°F, and 8 Cm^{-1} equivalent slit width.

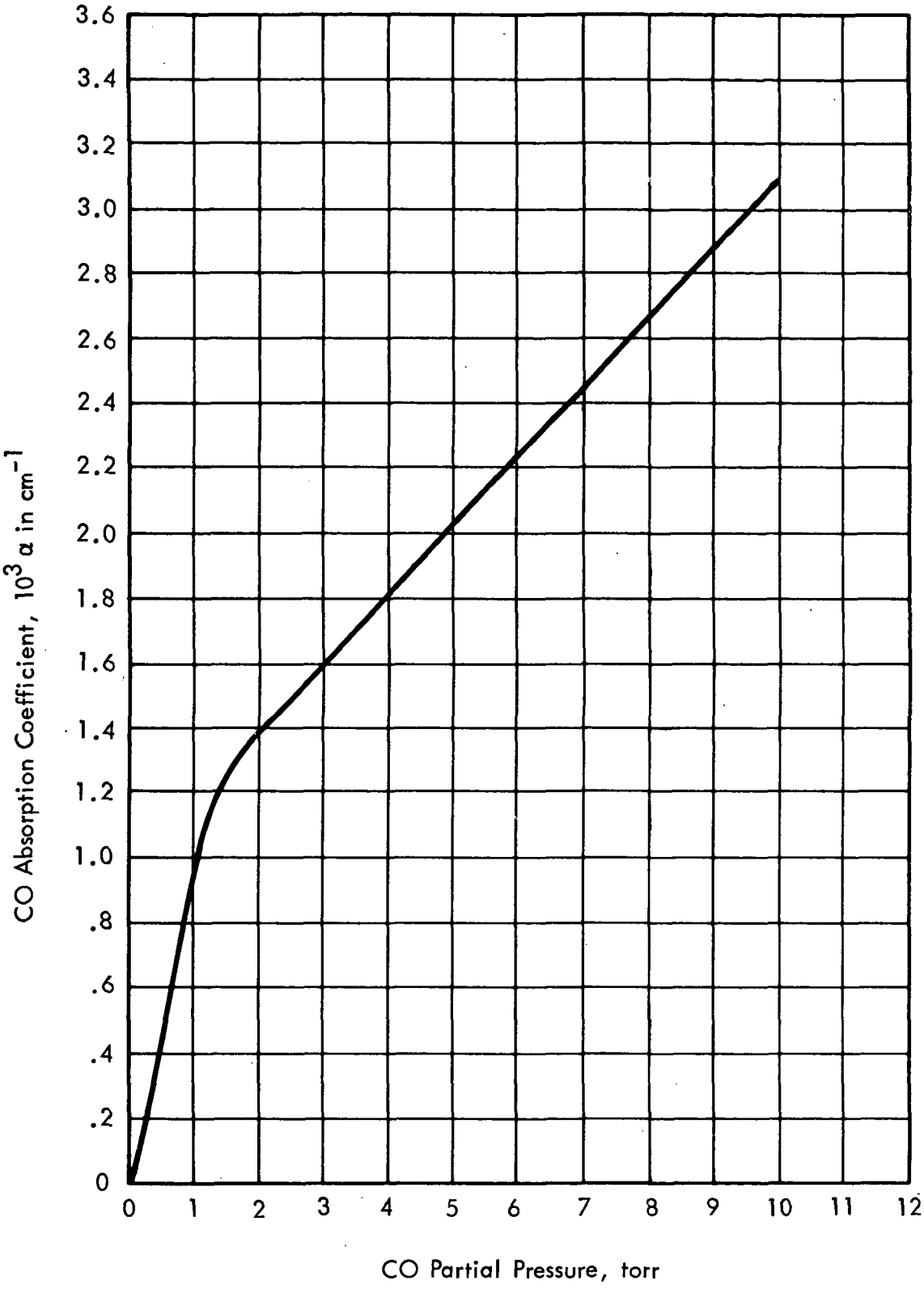

Figure 38. Plot of Absorption Coefficient, α , of CO versus CO partial pressure, P, for a gas mixture of 20 torr total pressure (P torr CO, 10-P torr CO_2, 9.4 torr CO_2, 9.4 torr He, .6 torr Xe) and $\alpha = [\ln(I_o/I)] / x$ measured at $\tilde{\nu} = 2175\ cm^{-1}$, x = 8 cm and 75°F, and 8 Cm^{-1} equivalent slit width.

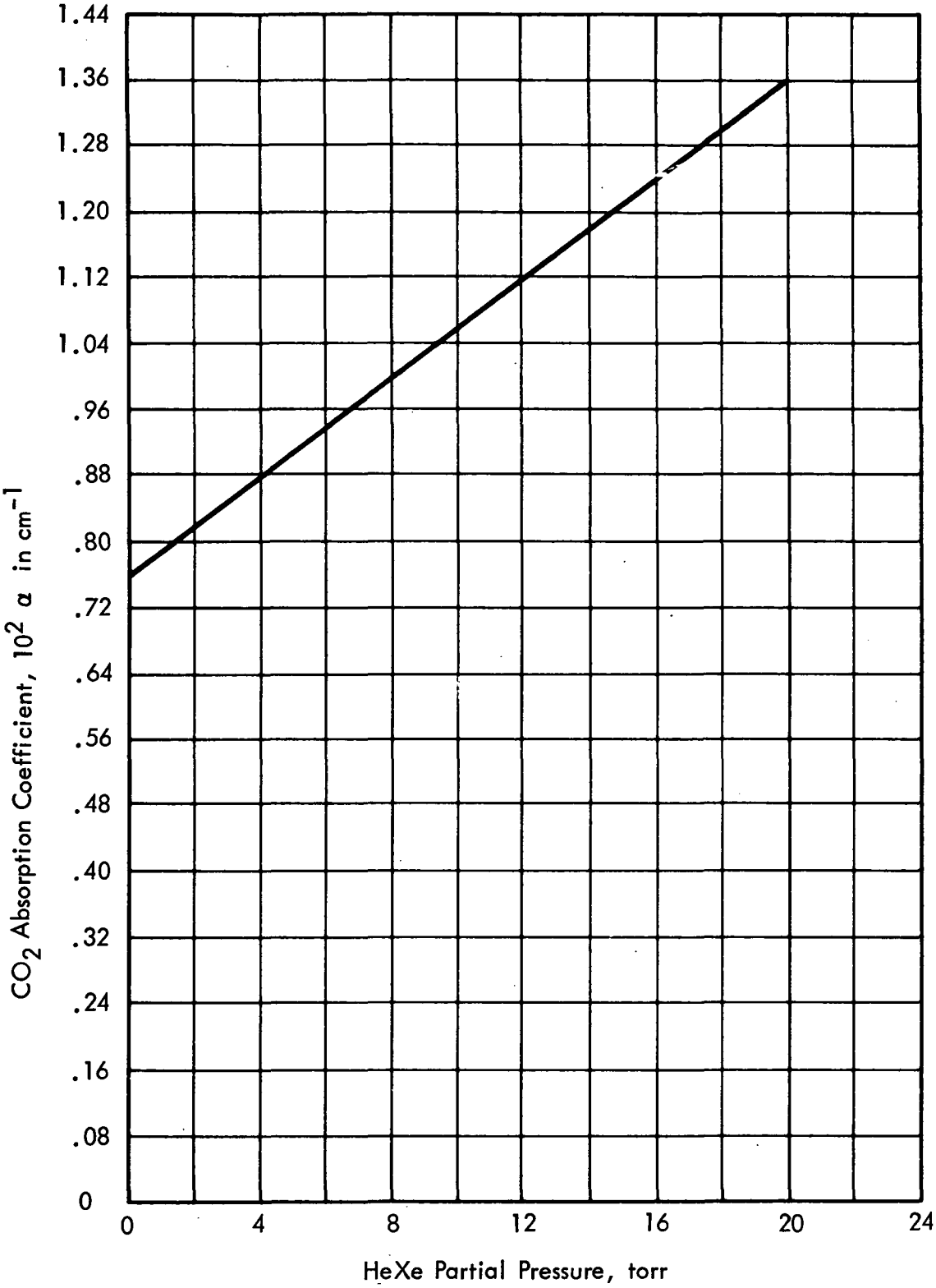

Figure 39. Plot of Absorption Coefficient, α , of 4.65 torr CO_2 versus HeXe partial pressure, P, for a gas mixture of P+4.65 torr total pressure and $\alpha = [\ln(I_o/I)]/x$ measured at $\tilde{\nu} = 2355\ cm^{-1}$, x = 8 cm and 75°F , and 8 Cm^{-1} equivalent slit width.

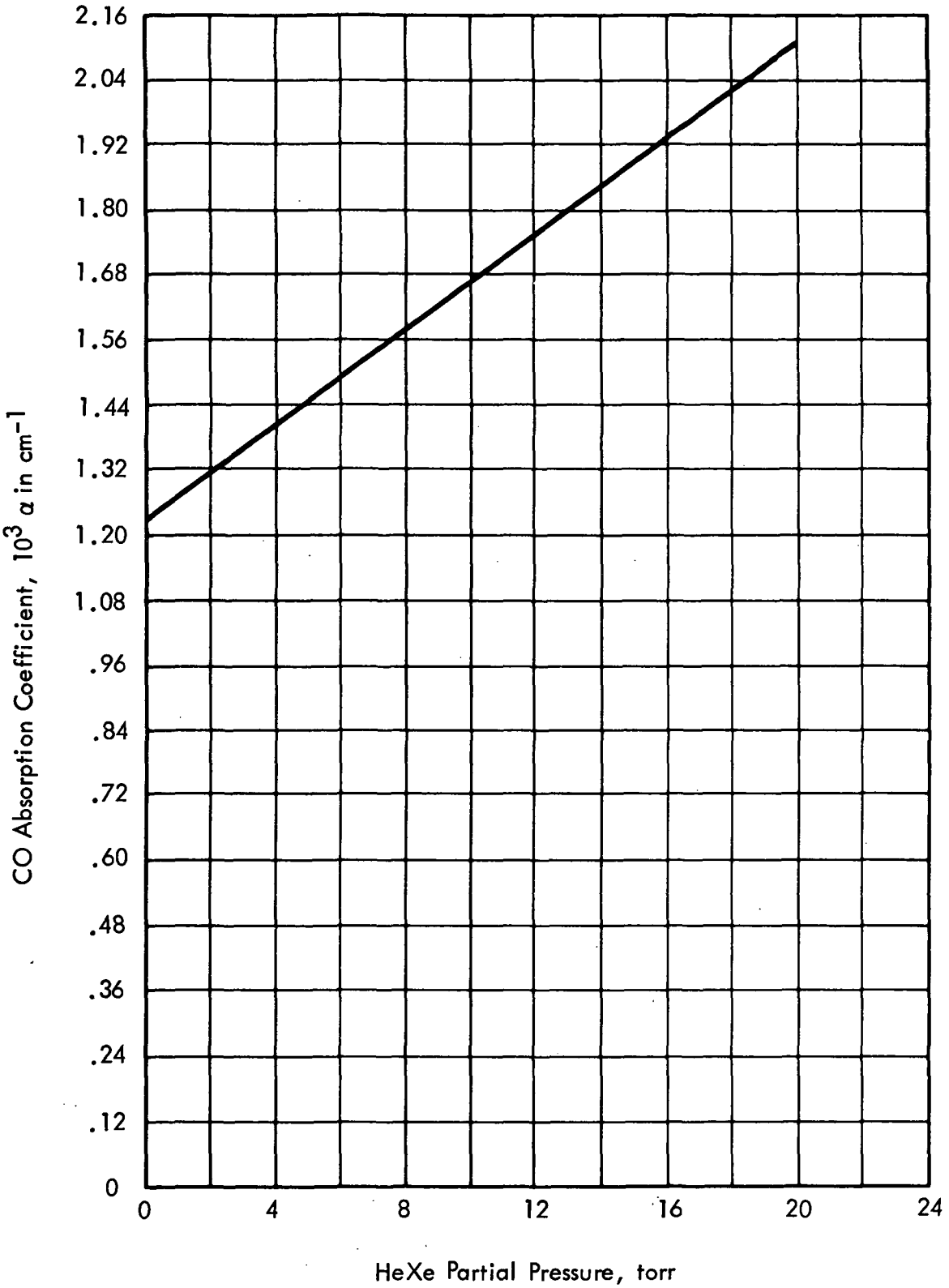

Figure 40. Plot of Absorption Coefficient, α , of 4.65 torr CO versus HeXe partial pressure, P, for a gas mixture of P+4.65 torr total pressure and $\alpha = [\ln(I_o/I)]/x$ measured at $\tilde{\nu} = 2175\ cm^{-1}$, x = 8 cm and 75°F, and 8 Cm^{-1} equivalent slit width.

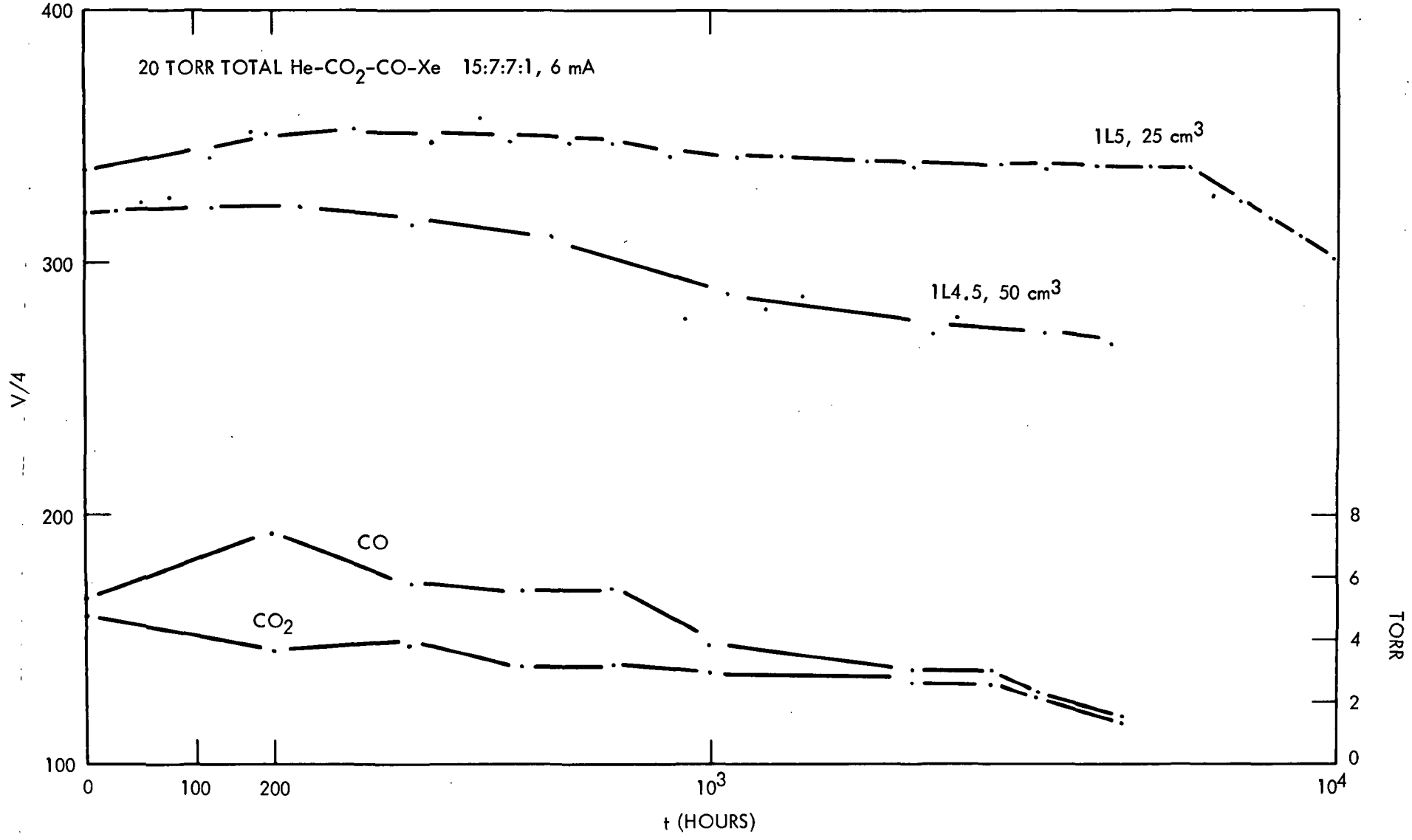

Figure 41. Silver Cathodes: Voltage versus operating time (upper curves) and CO_2 and CO partial pressures versus operatimg time (lower curves).

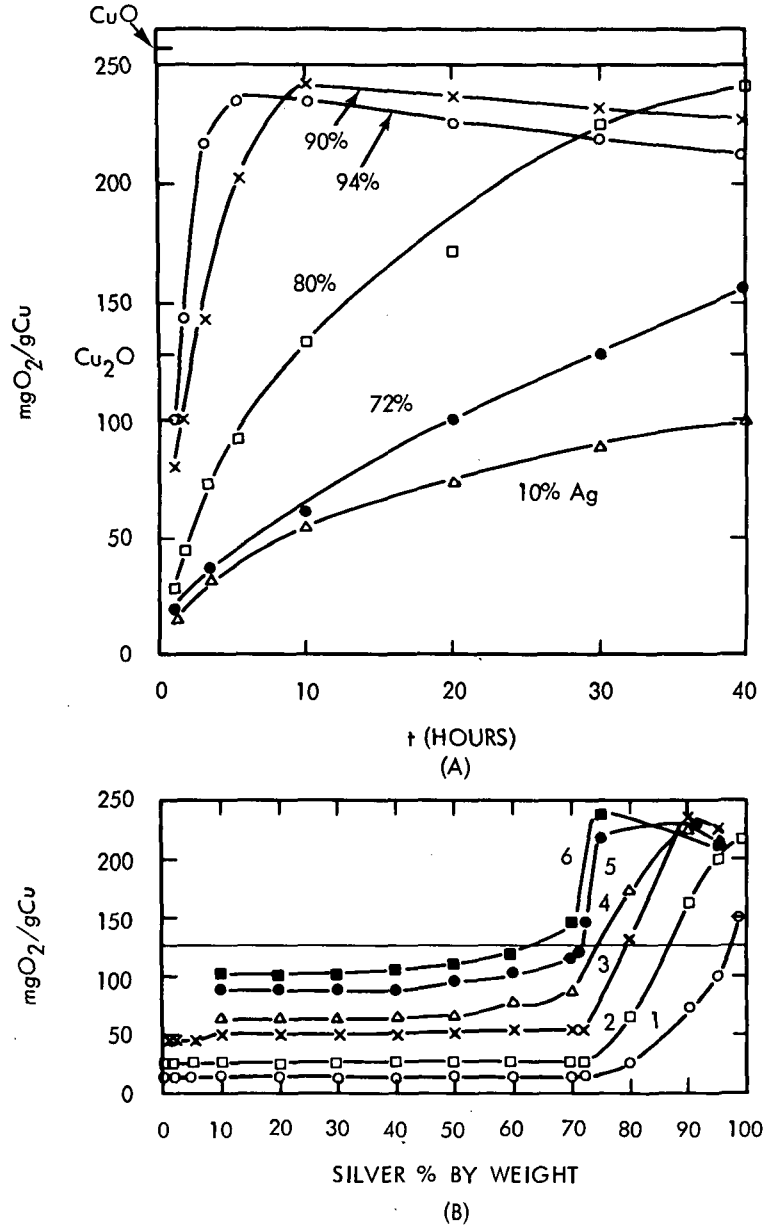

Figure 42. Silver-Copper Alloys: A. Internal oxidation of alloys versus time at 750°C in 1 atm. of oxygen; B. Oxidation of alloys versus percent composition with curves 1 through 6 for oxidation times of 0.5, 3, 10, 20, 30 and 40 hours respectively at 750°C in 1 atm. of oxygen. (From E. Raub and M. Engel, Z.F. Metalkunde 30, 83, 1938)

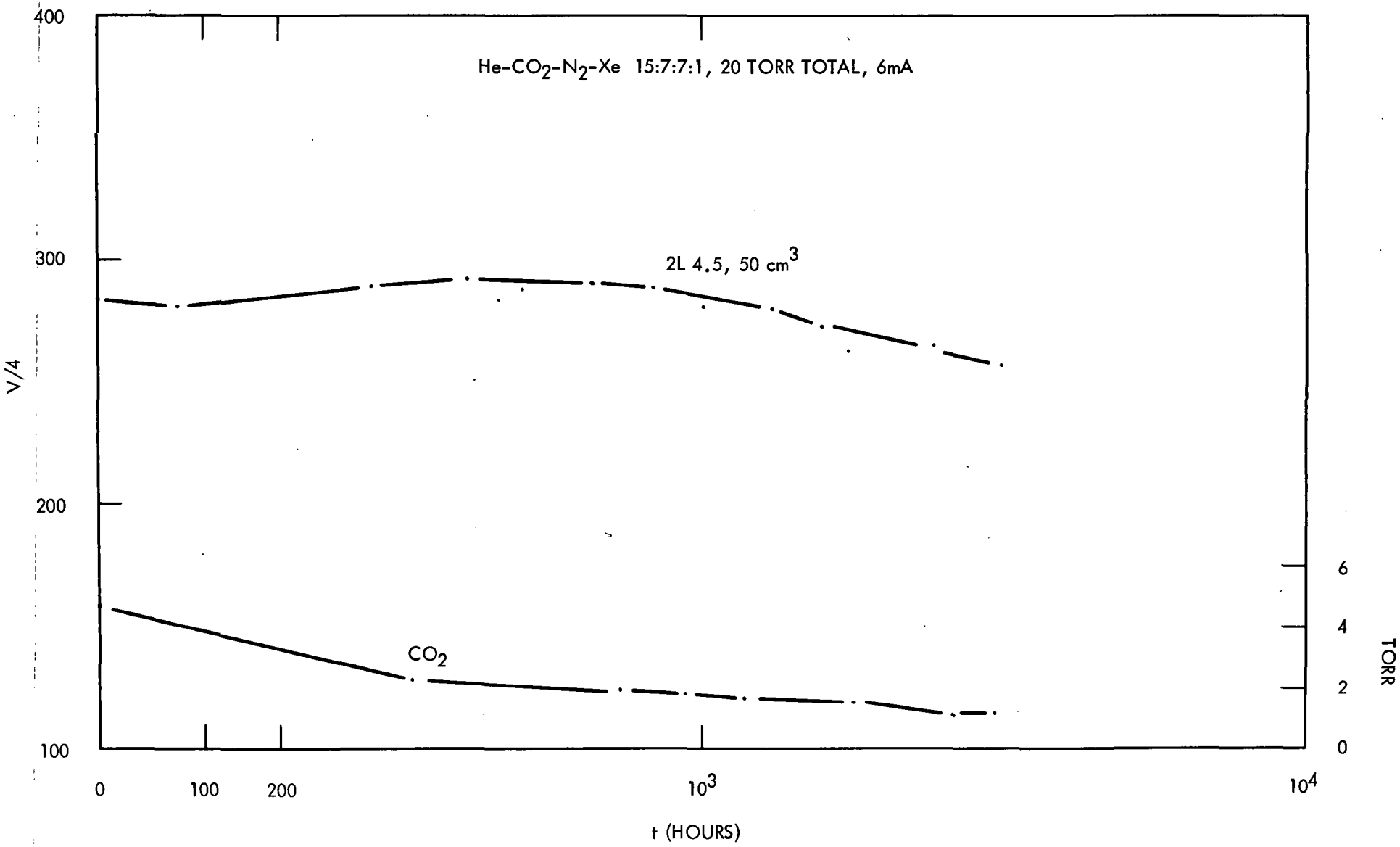

Figure 43. Silver-Cadmium Oxide Cathodes (Ag 0.8 Cd/O): Voltage versus operating time (upper curve); CO_2 partial pressure versus operating time (lower curve).

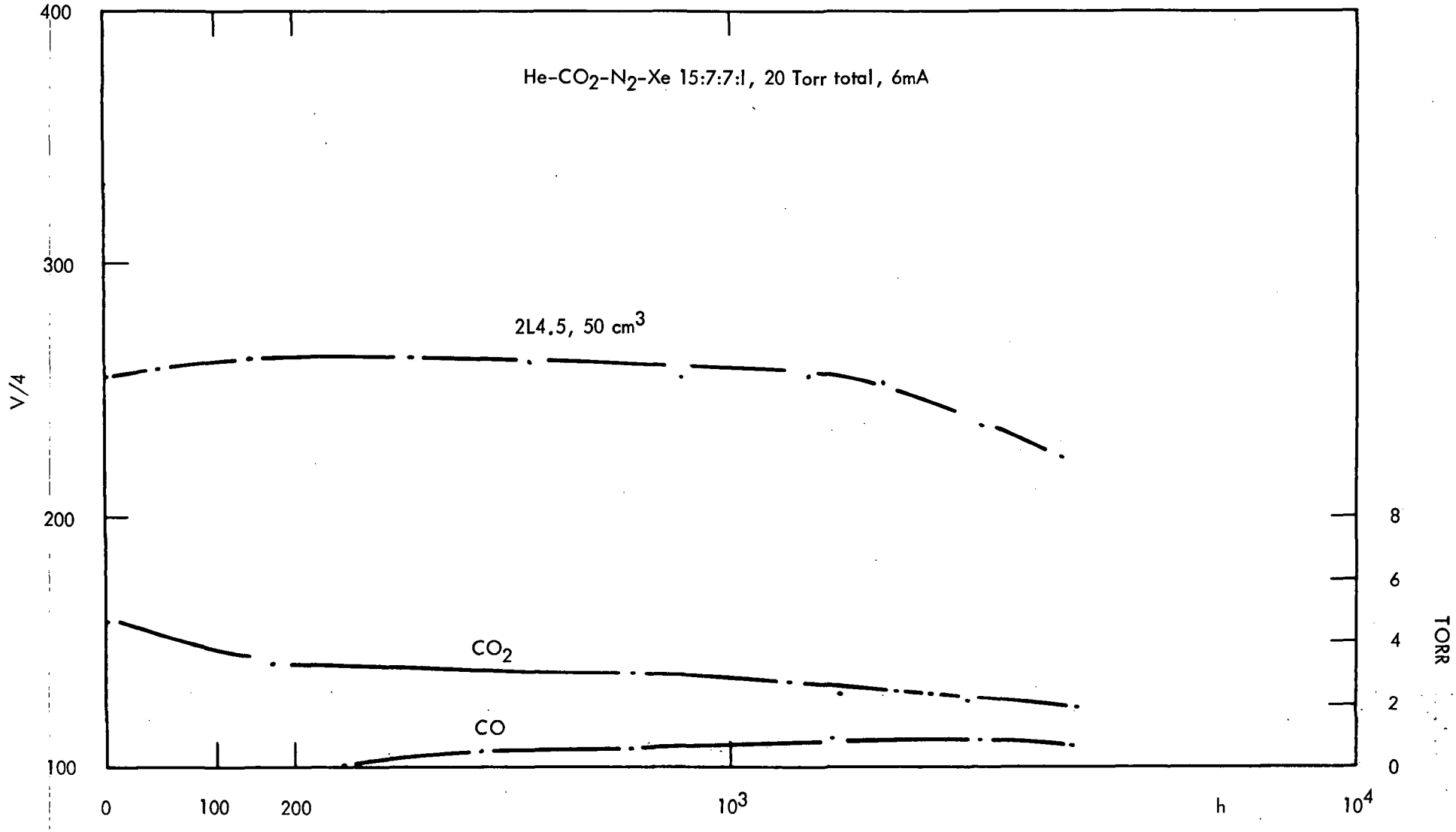

Figure 44. Silver-Cadmium Oxide Cathode (Ag5 Cd/O): Voltage versus operating time (upper curve); CO_2 and CO partial pressures versus operating time (lower curves).

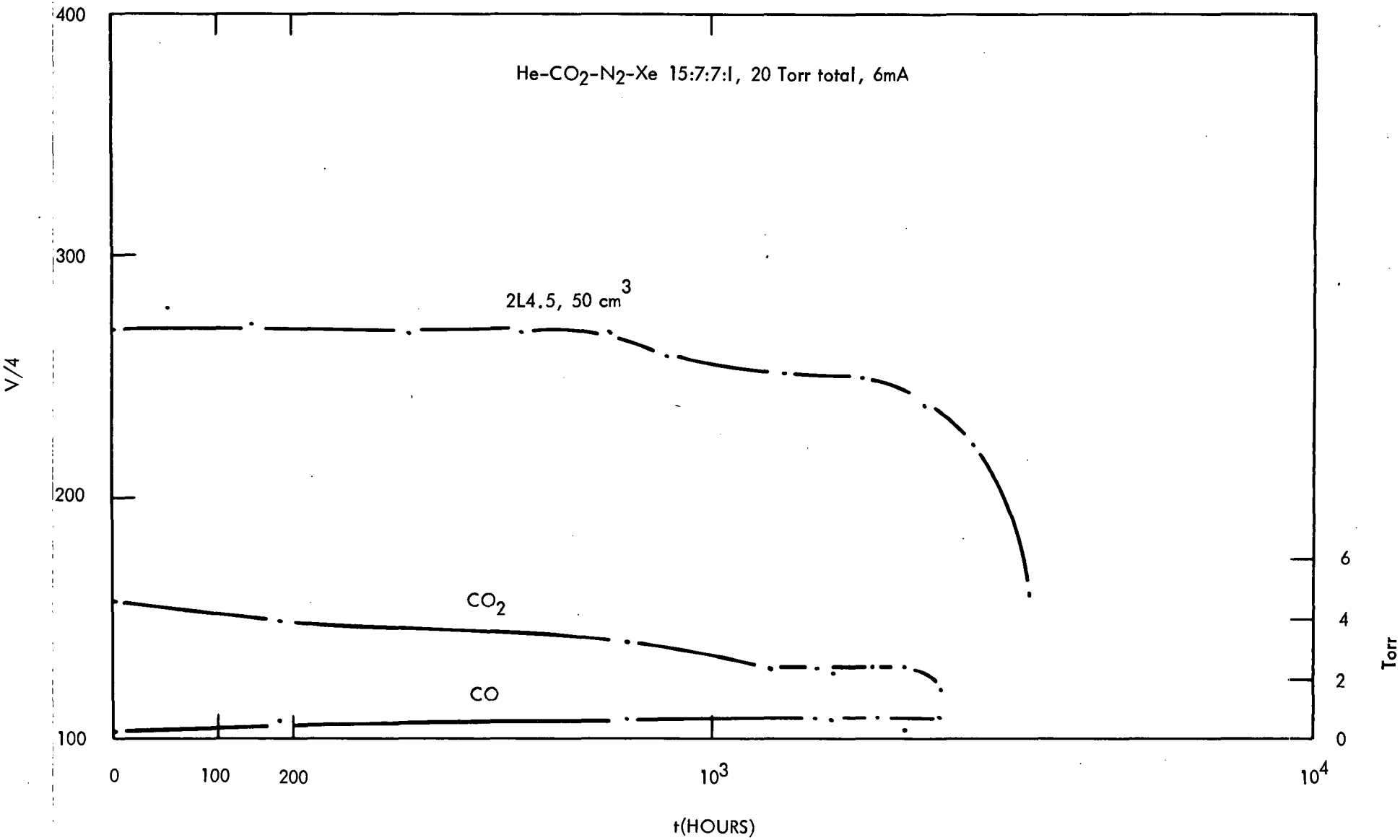

Figure 45. Silver-Cadmium Oxide Cathode (Ag 10 Cd/O): Voltage versus operating time (upper curve); CO_2 and CO partial pressures versus operating time (lower curves).

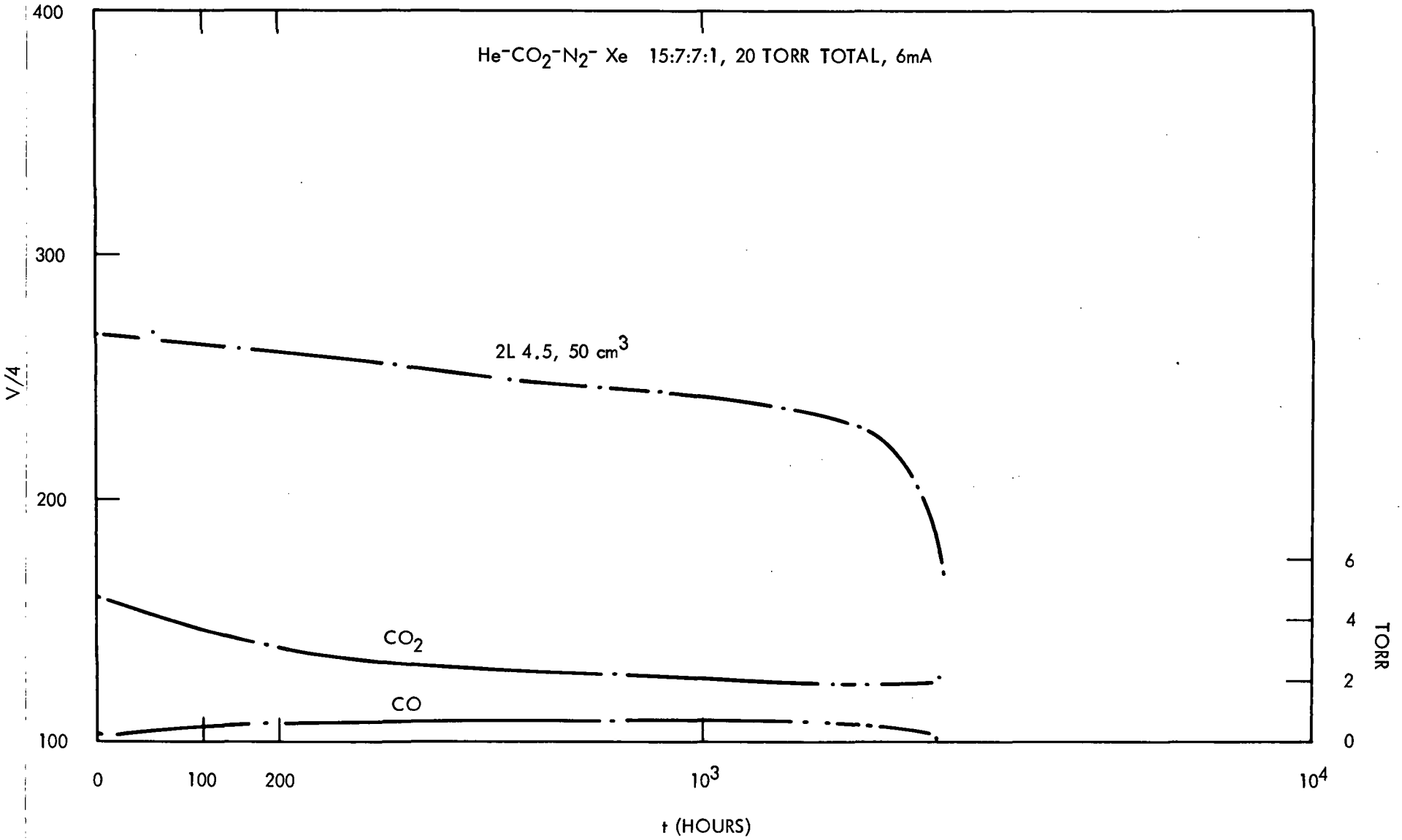

Figure 46. Silver-Cadmium Oxide Cathode (Ag20 Cd/O): Voltage versus operating time (upper curve); CO_2 AND CO Partial pressures versus operating time (lower curves).

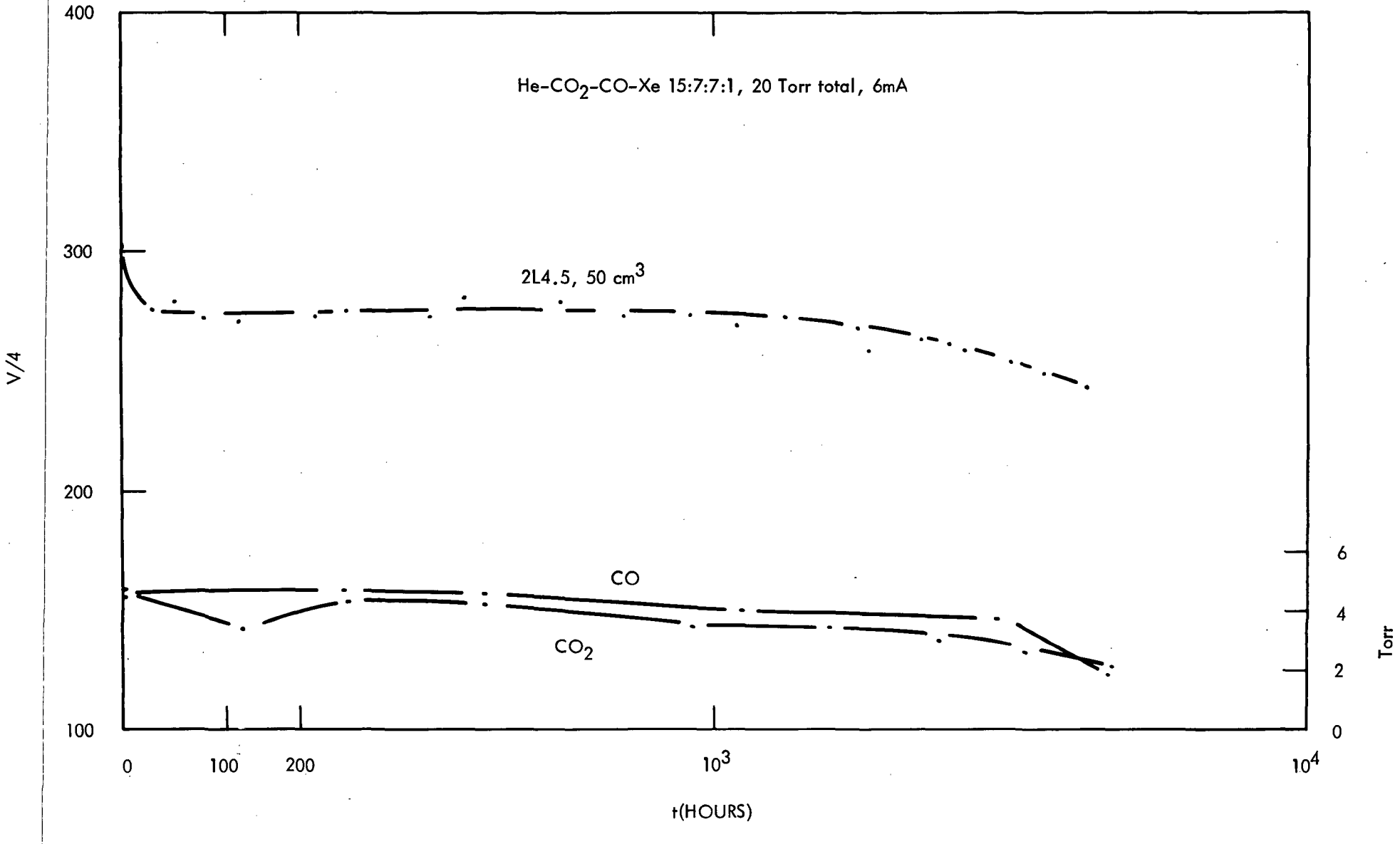

Figure 47. Silver-Copper Oxide Insulated Cathode (Ag 5 Cu/O): Voltage versus operating time (upper curve); CO_2 and CO partial pressures versus operating time (lower curves).

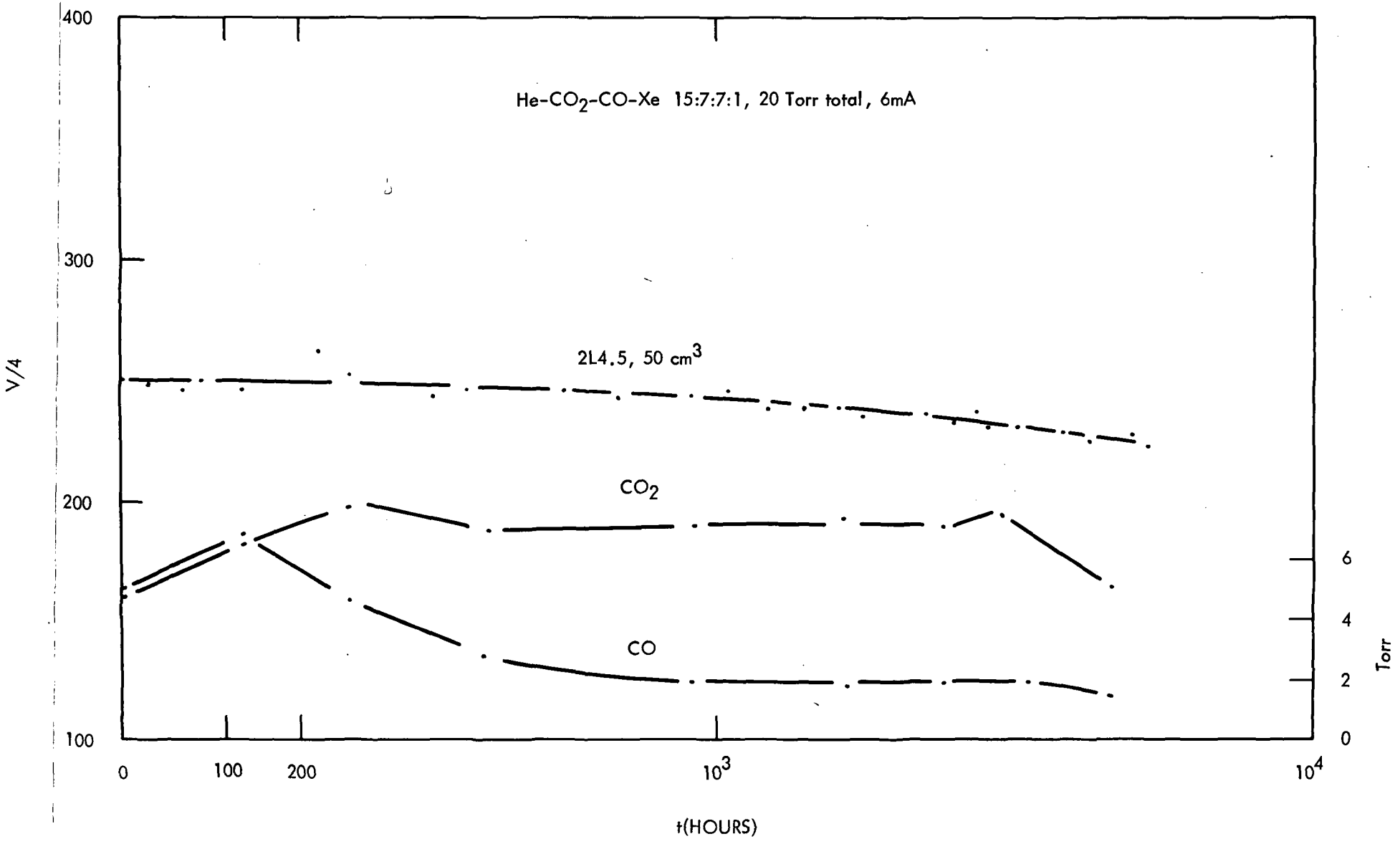

Figure 48. Silver-Copper Oxide Insulated Cathode (Ag 10 Cu/O): Voltage versus operating time (upper curve); CO_2 and CO partial pressures versus operating time (lower curves).

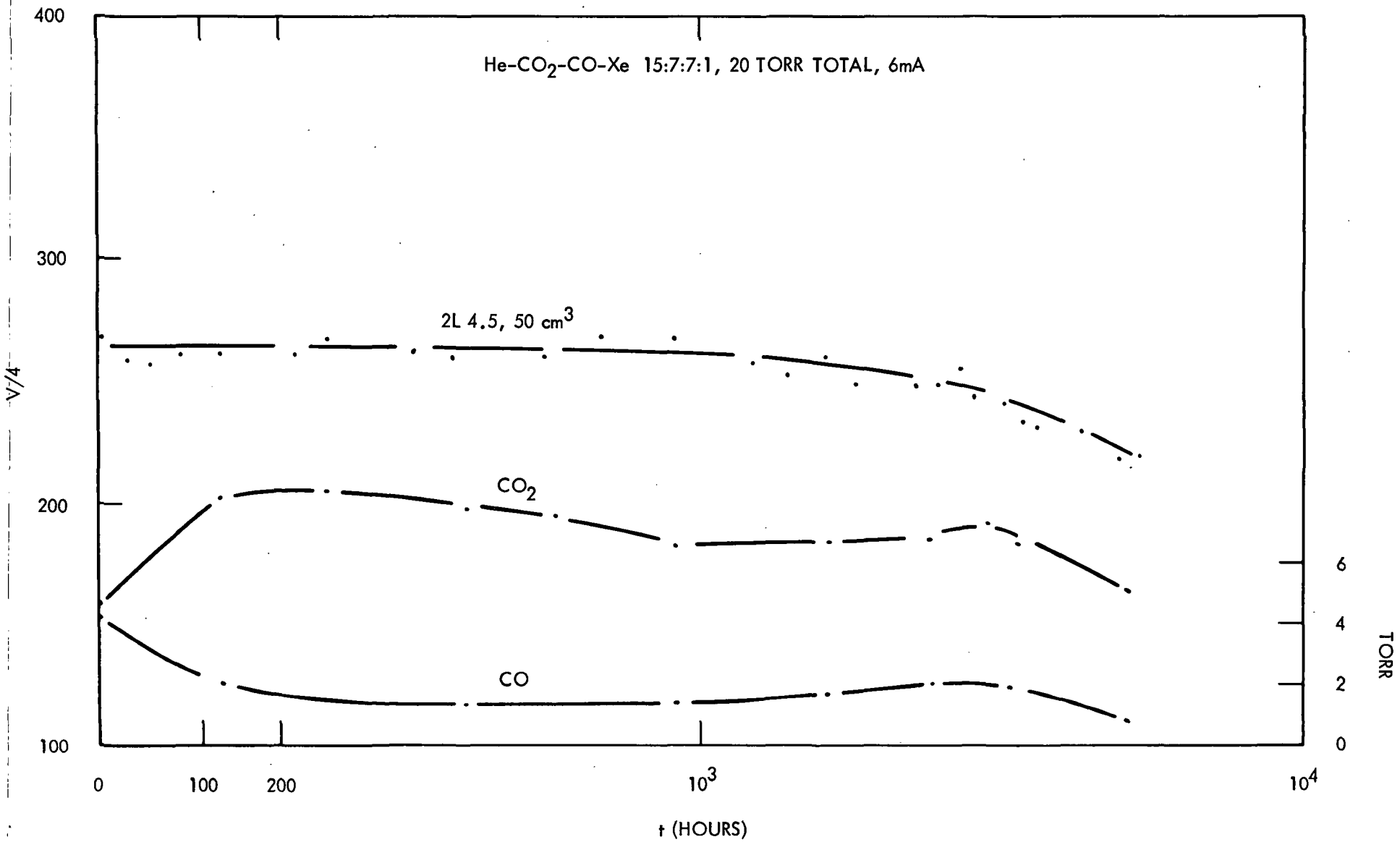

Figure 49. Silver-Copper Oxide Insulated Cathode (Ag 20 Cu/O): Voltage versus operating time (upper curve); CO_2 and CO partial pressures versus operating time (lower curves).

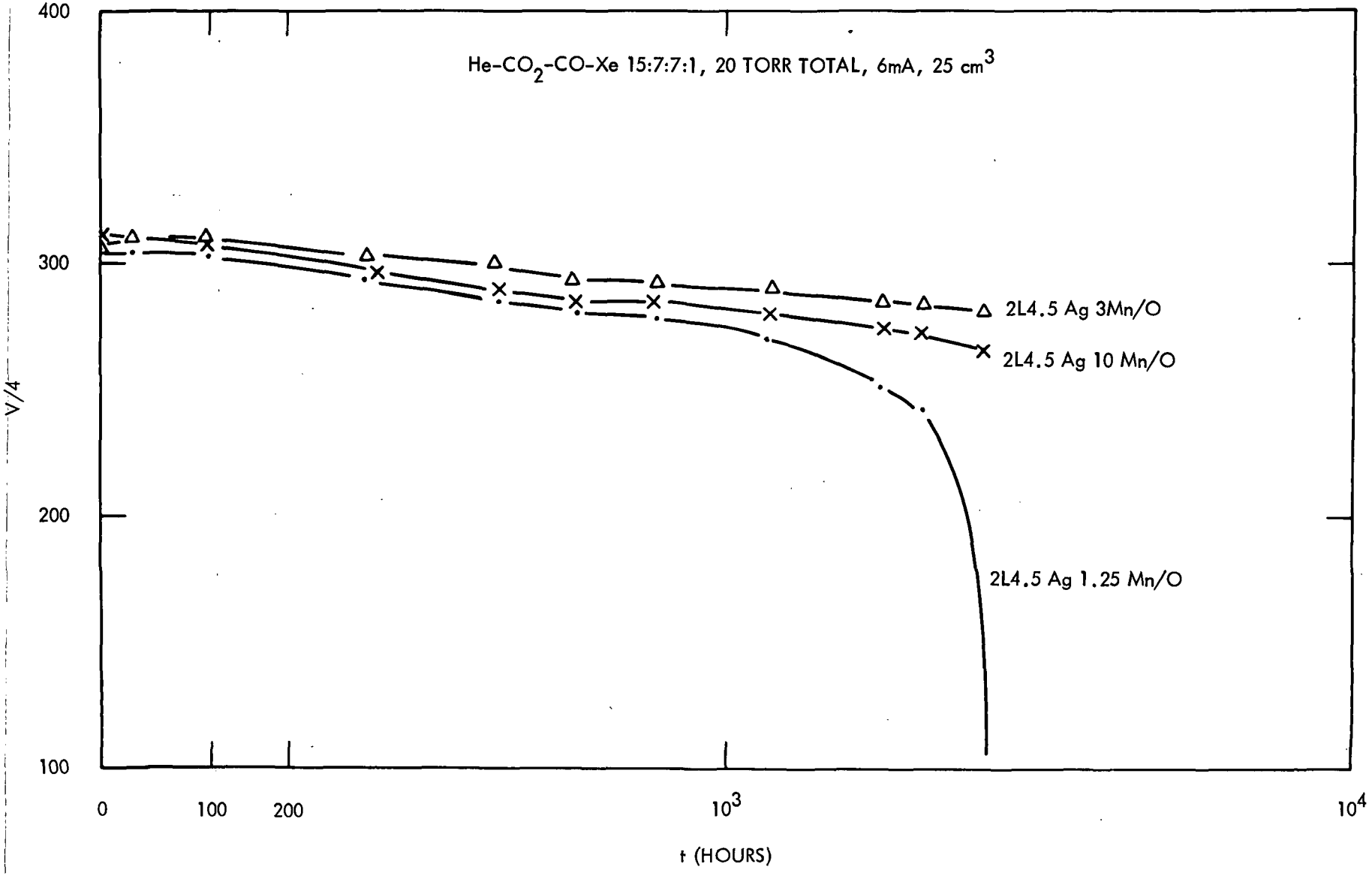

Figure 50. Silver-Manganese Oxide Cathodes (Ag-Mn/O): Voltage versus operating time.

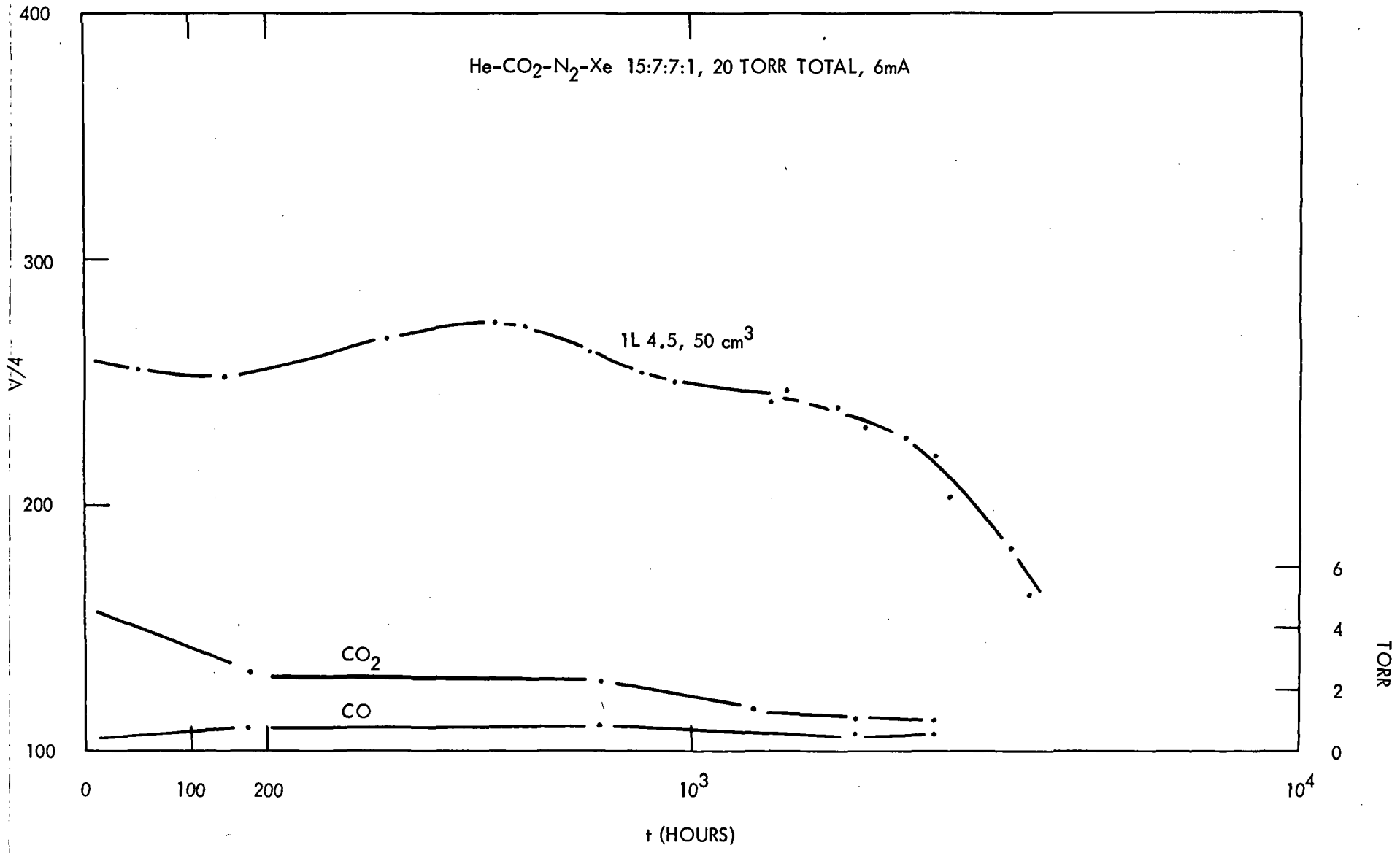

Figure 51. Silver-Nickel Oxide Cathode (Ag 15 Ni/O): Voltage versus operating time (upper curve); CO_2 and CO partial pressures versus operating time (lower curves).

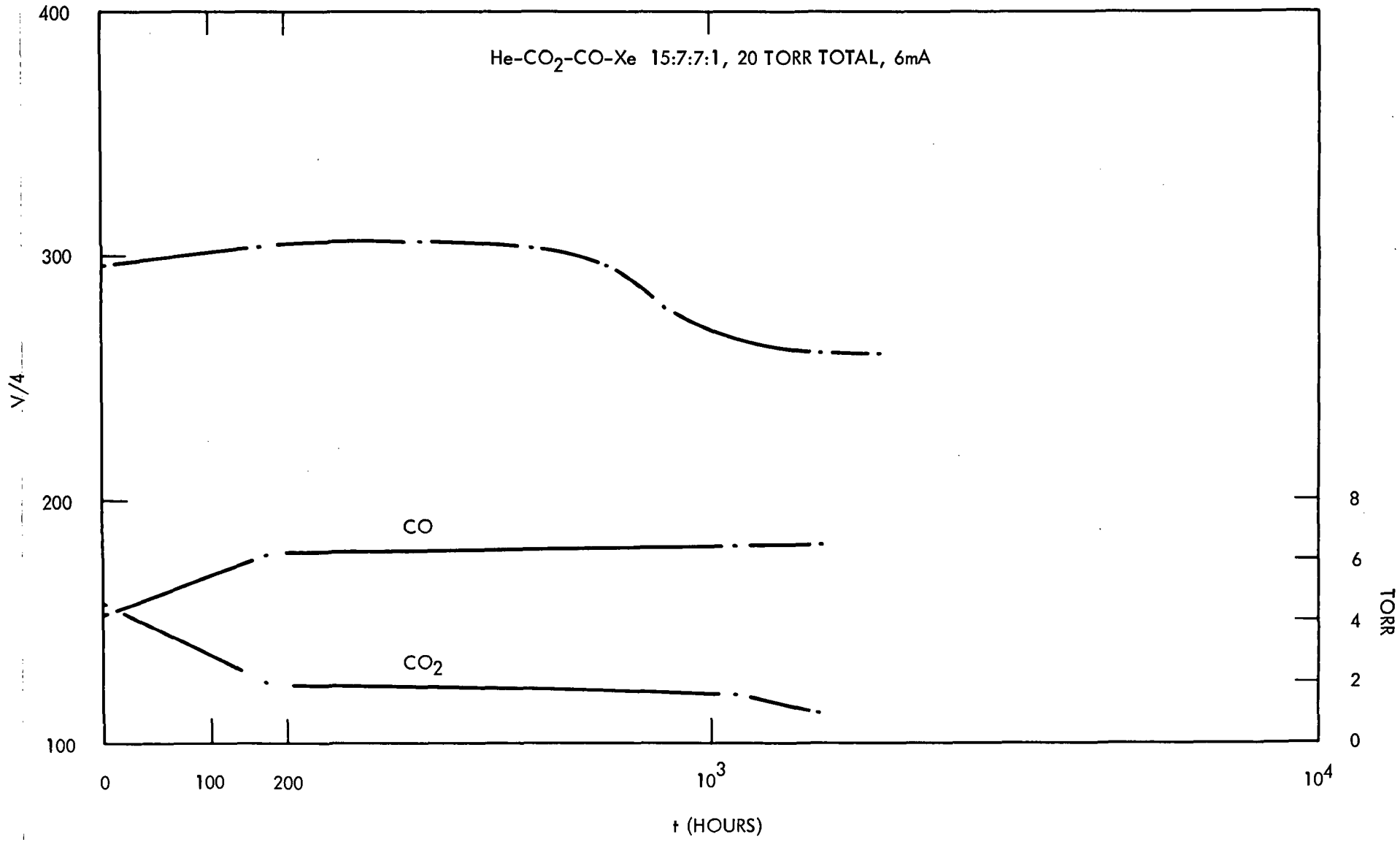

Figure 52. Silver-Zinc Oxide Cathode (Ag 10Zn/O): Voltage versus operating time (upper curve); CO_2 and CO partial pressures versus operating time (lower curves).

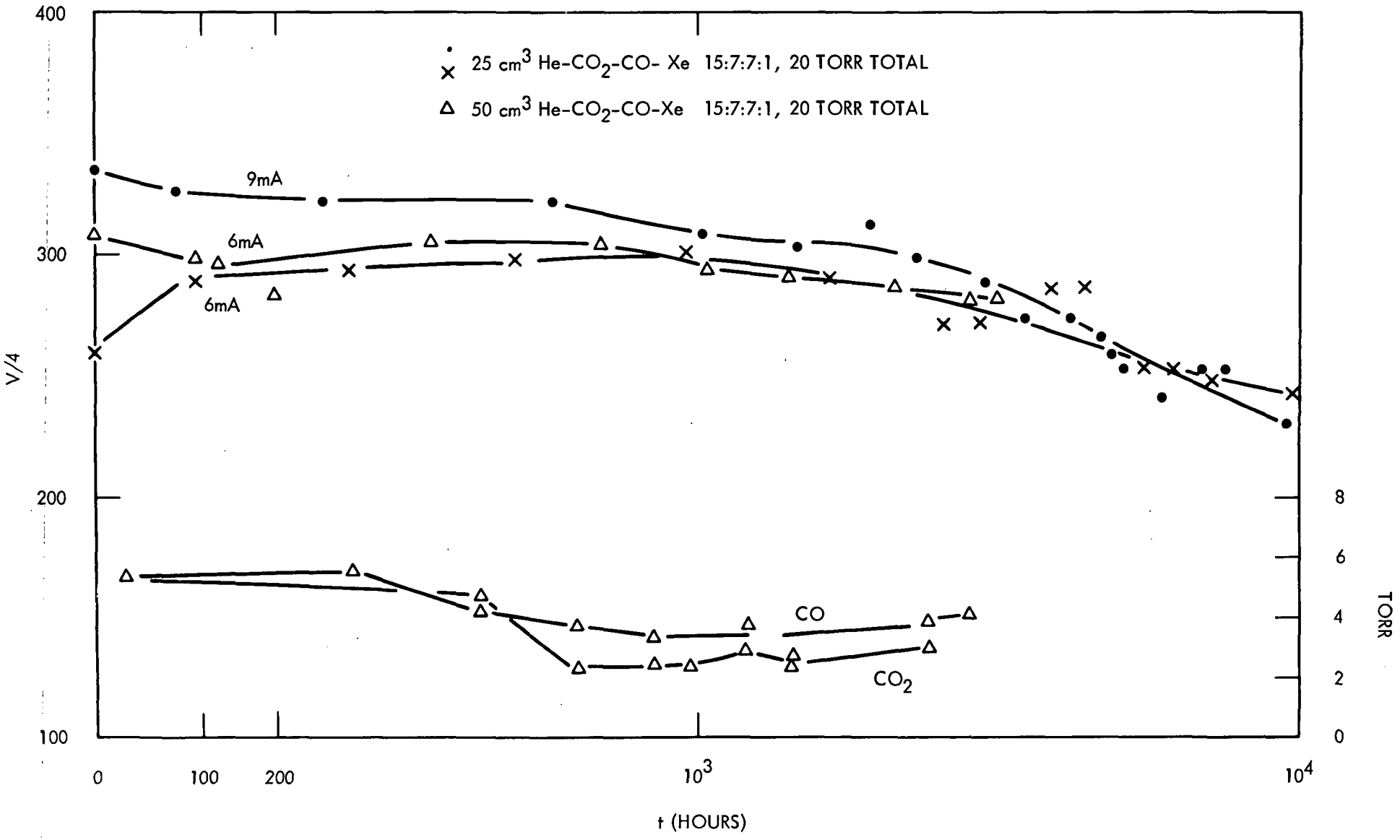

Figure 53. Copper Cathodes (1L 4.5 Cu): Voltage versus operating time (upper curves); CO_2 and CO partial pressures versus operating time (lower curves).

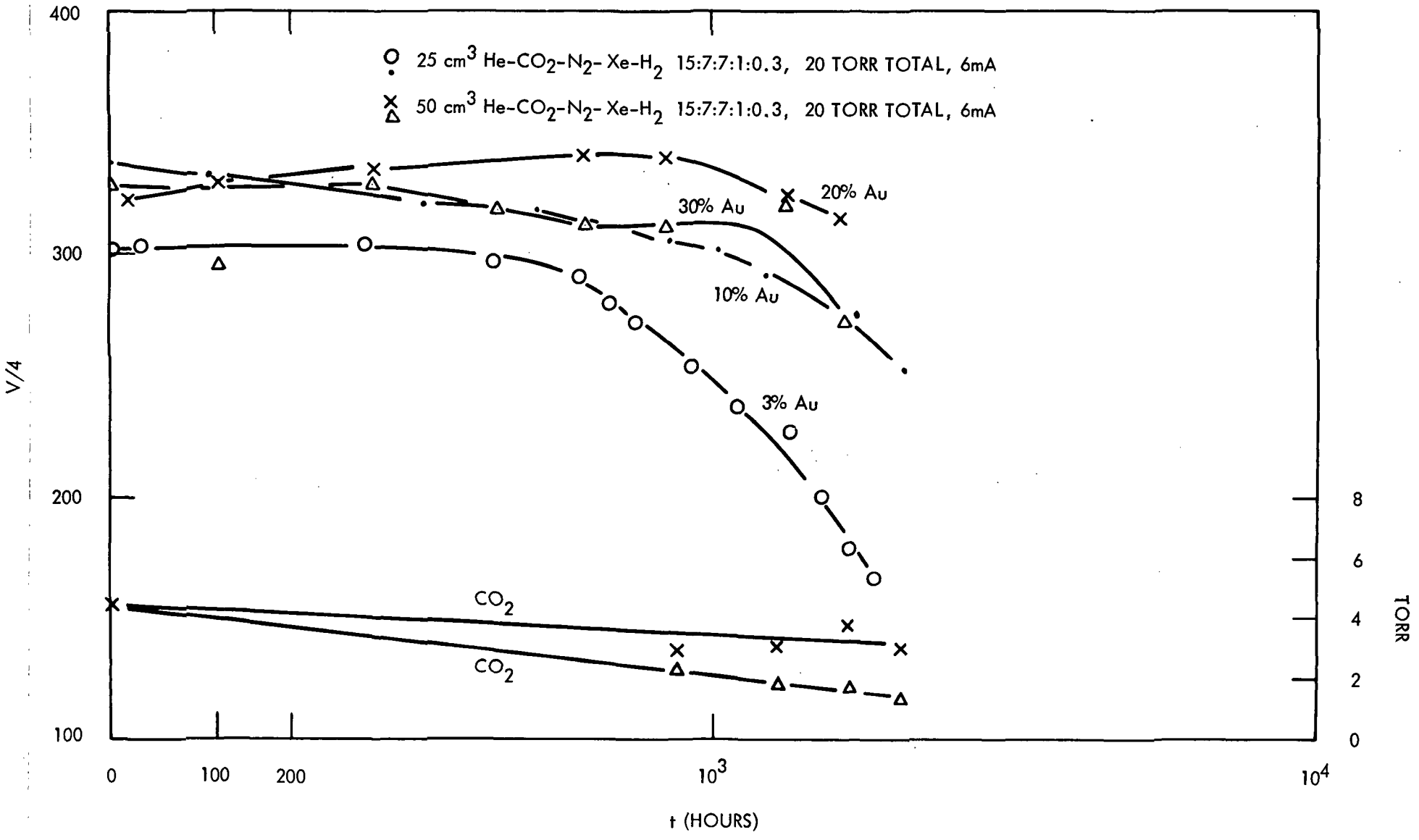

Figure 54. Platinum-Gold Cathodes (3L10 Pt-Au): Voltage versus operating time.

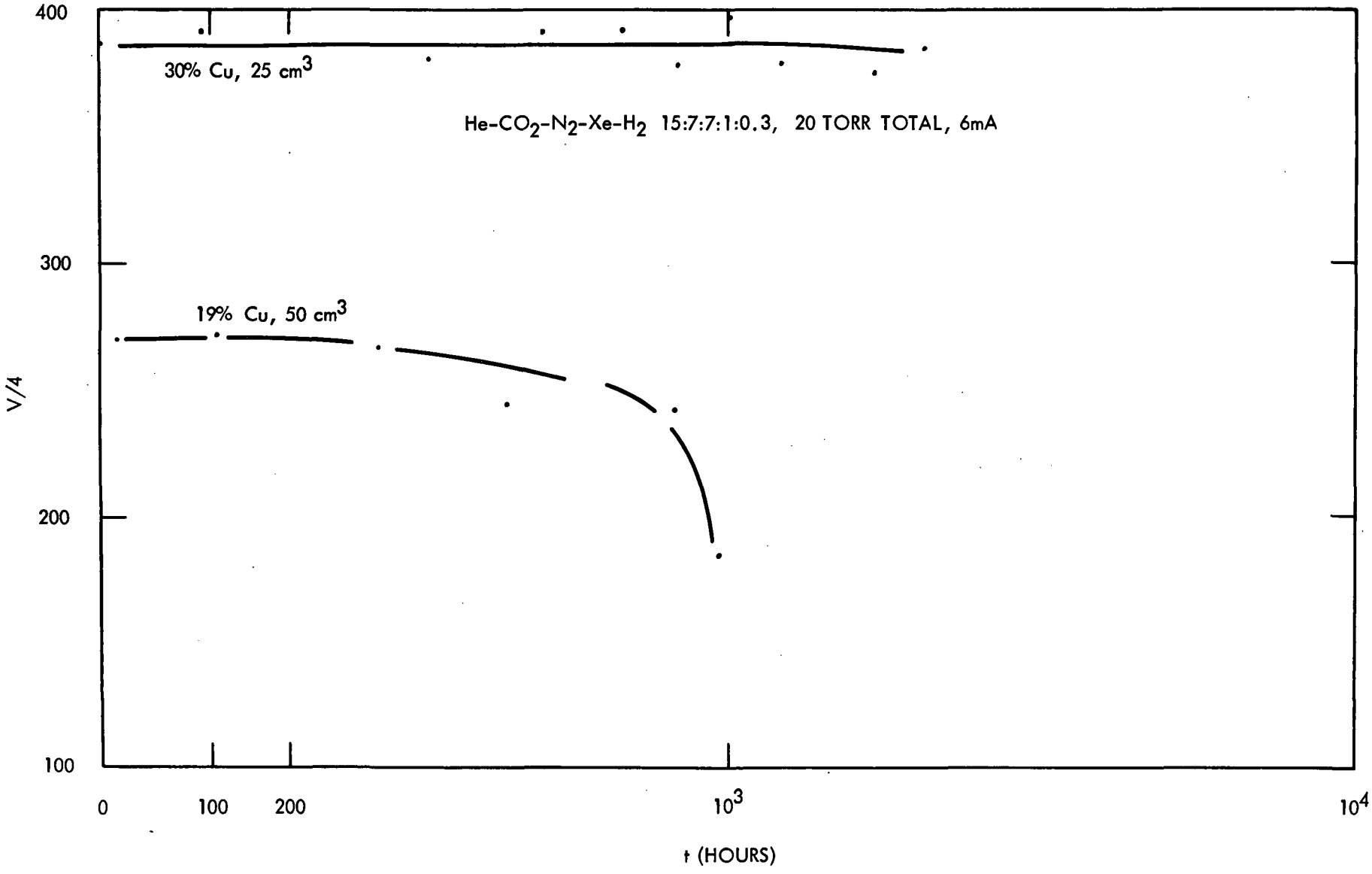

Figure 55. Platin-Copper Cathodes (3L10 Pt-Cu): Voltage versus operating time.

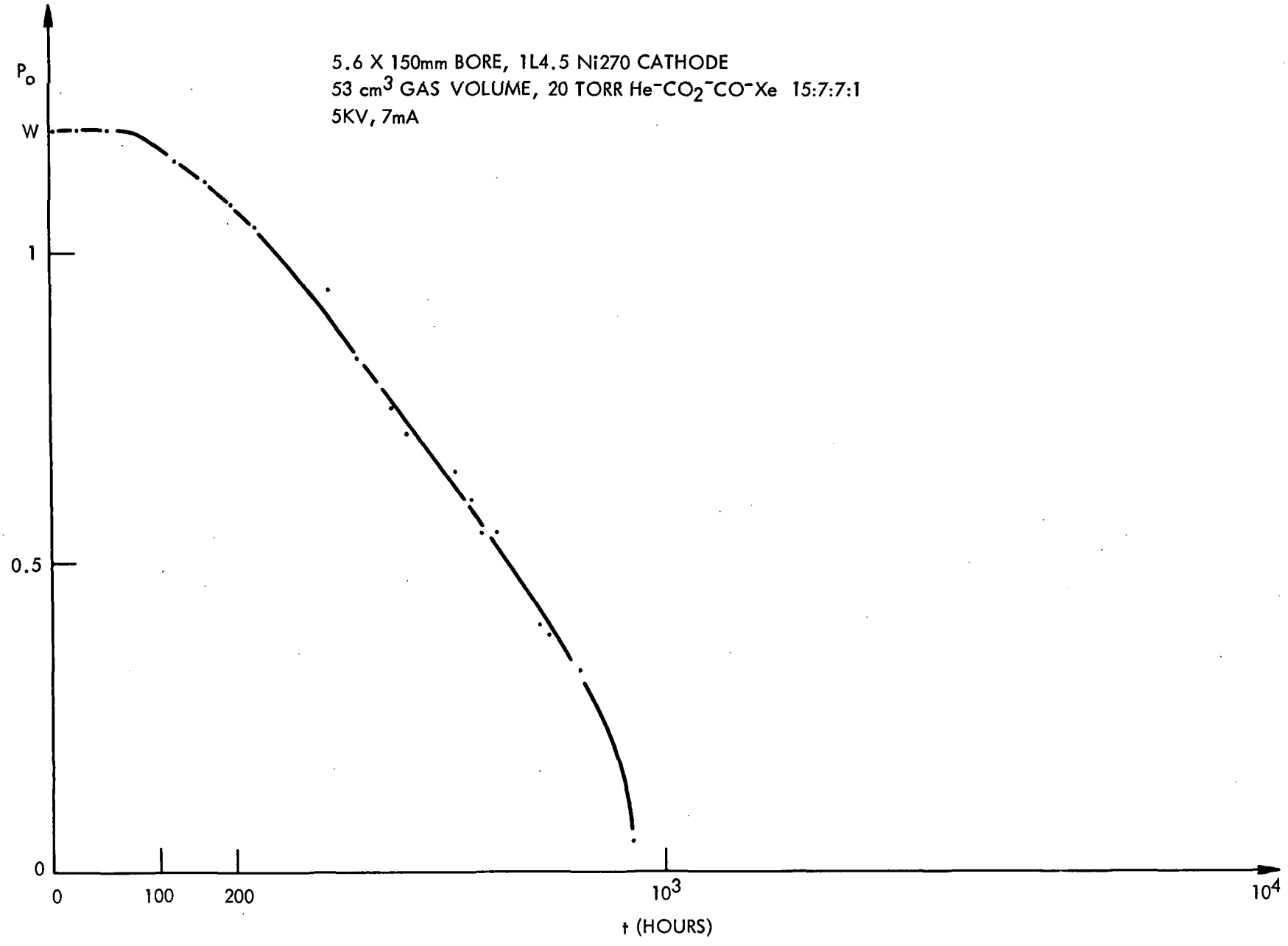

Figure 56. CO_2 Laser power output versus time.

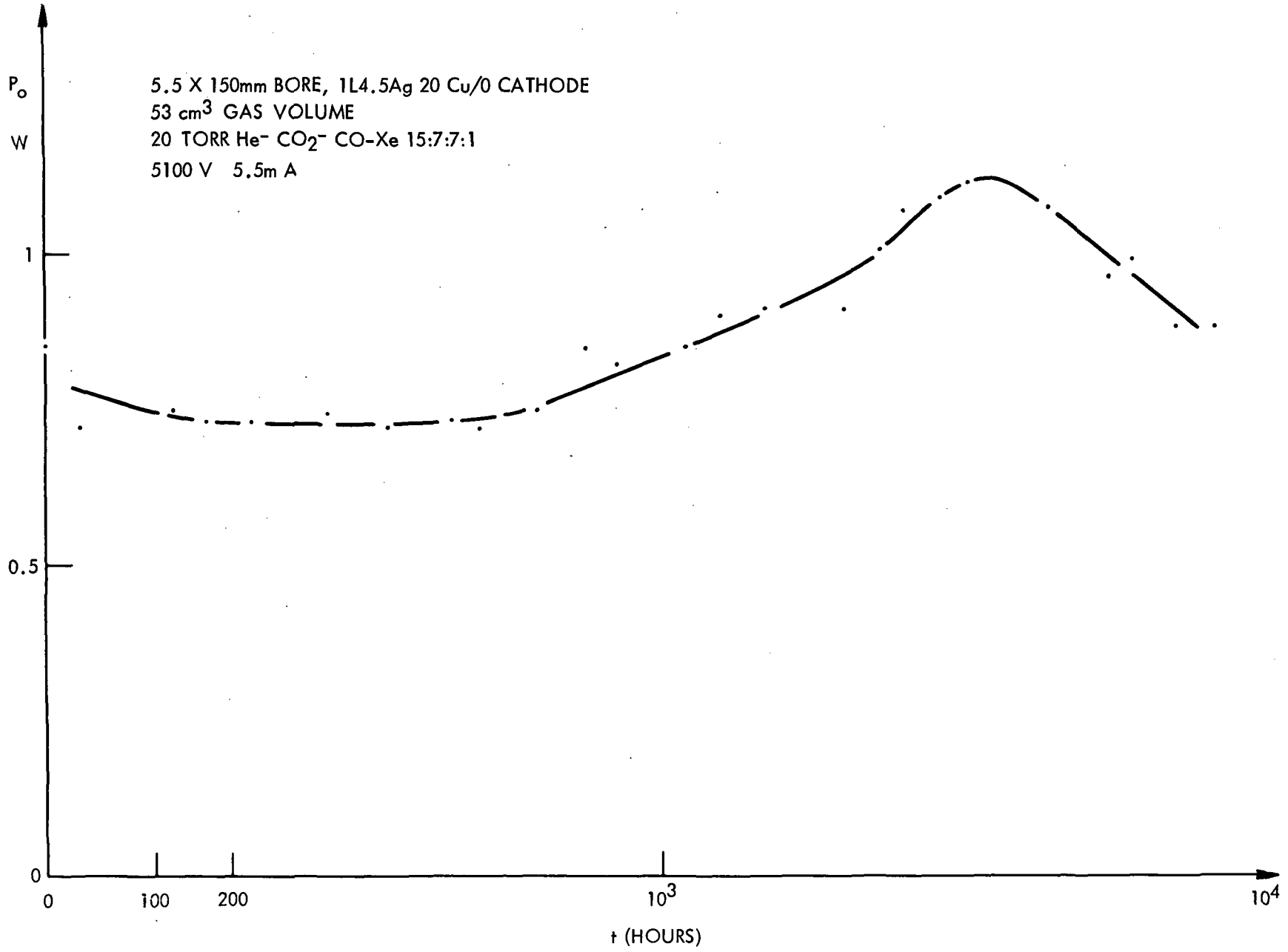

Figure 57. CO_2 Laser power output versus time.

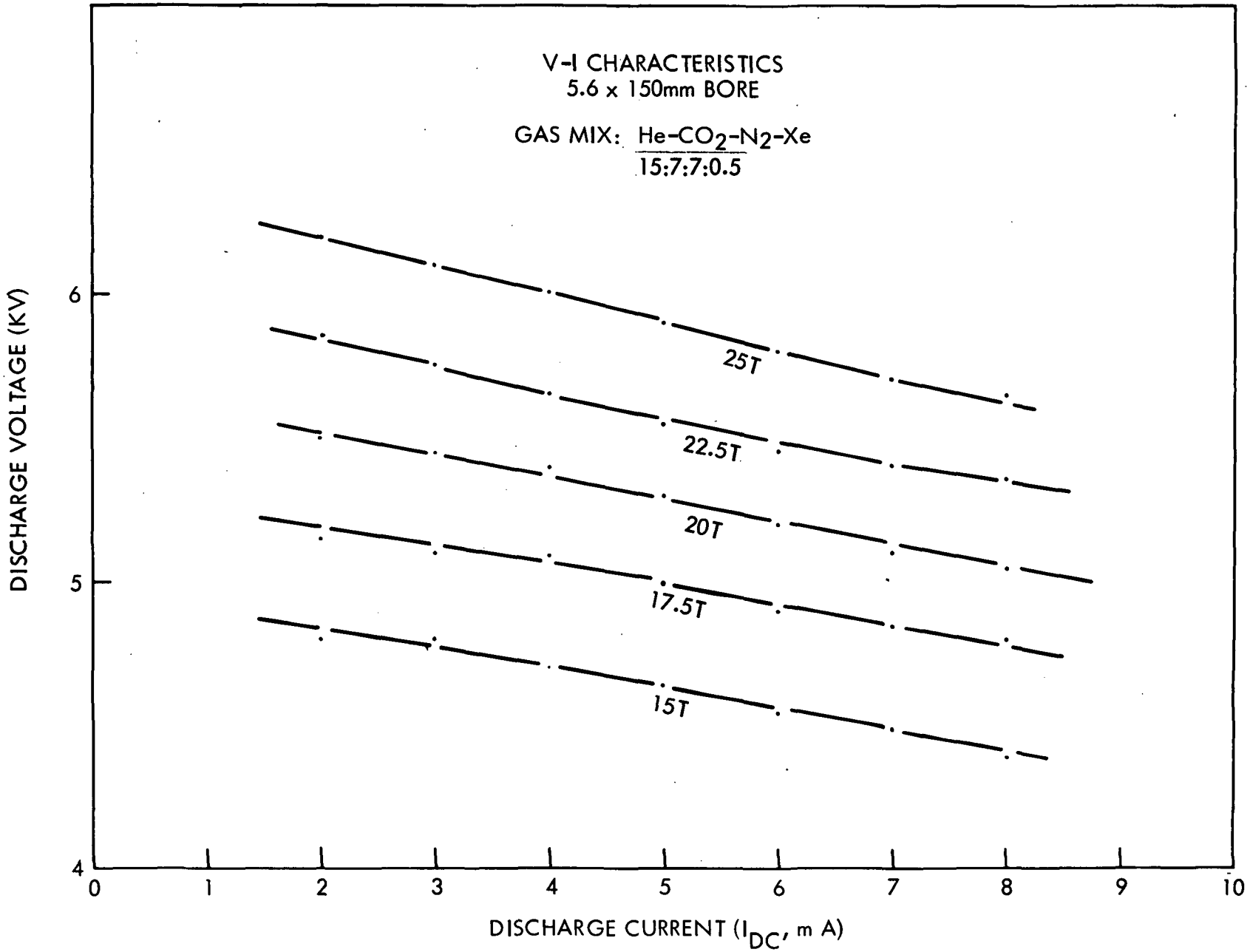
V-I CHARACTERISTICS
5.6 x 150mm BORE
GAS MIX: He-CO2-N2-Xe
15:7:7:0.5
25T
22.5T
20T
17.5T
15T
DISCHARGE VOLTAGE (KV)
6
5
4
0
1
2
3
4
5
6
7
8
9
10
DISCHARGE CURRENT (IDC, m A)

Figure 1a

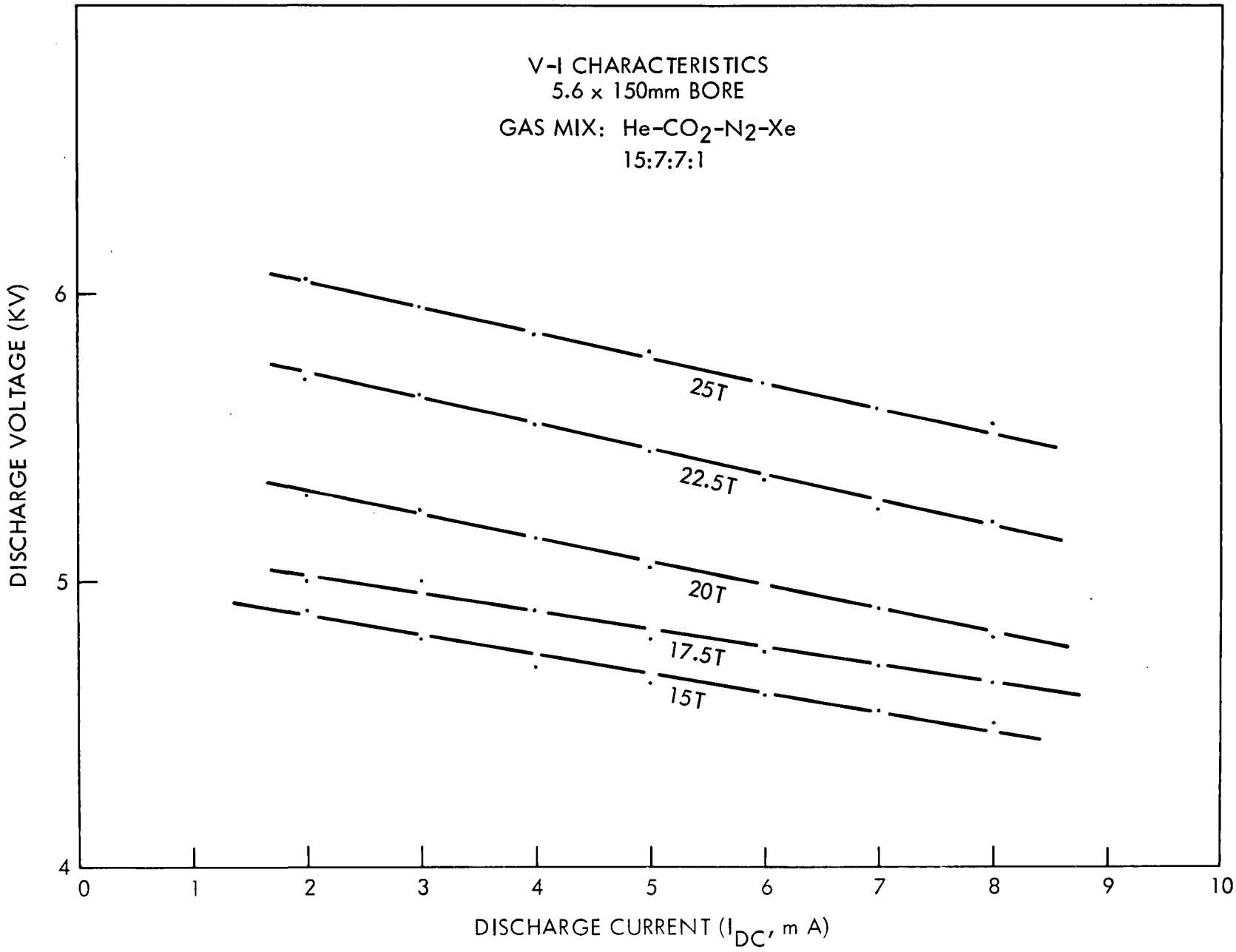
V-I CHARACTERISTICS
5.6 x 150mm BORE
GAS MIX: He-CO_2-N_2-Xe
15:7:7:1
DISCHARGE VOLTAGE (KV)
6
5
4
25T
22.5T
20T
17.5T
15T
0
1
2
3
4
5
6
7
8
9
10
DISCHARGE CURRENT (I_{DC}, m A)

Figure 2a

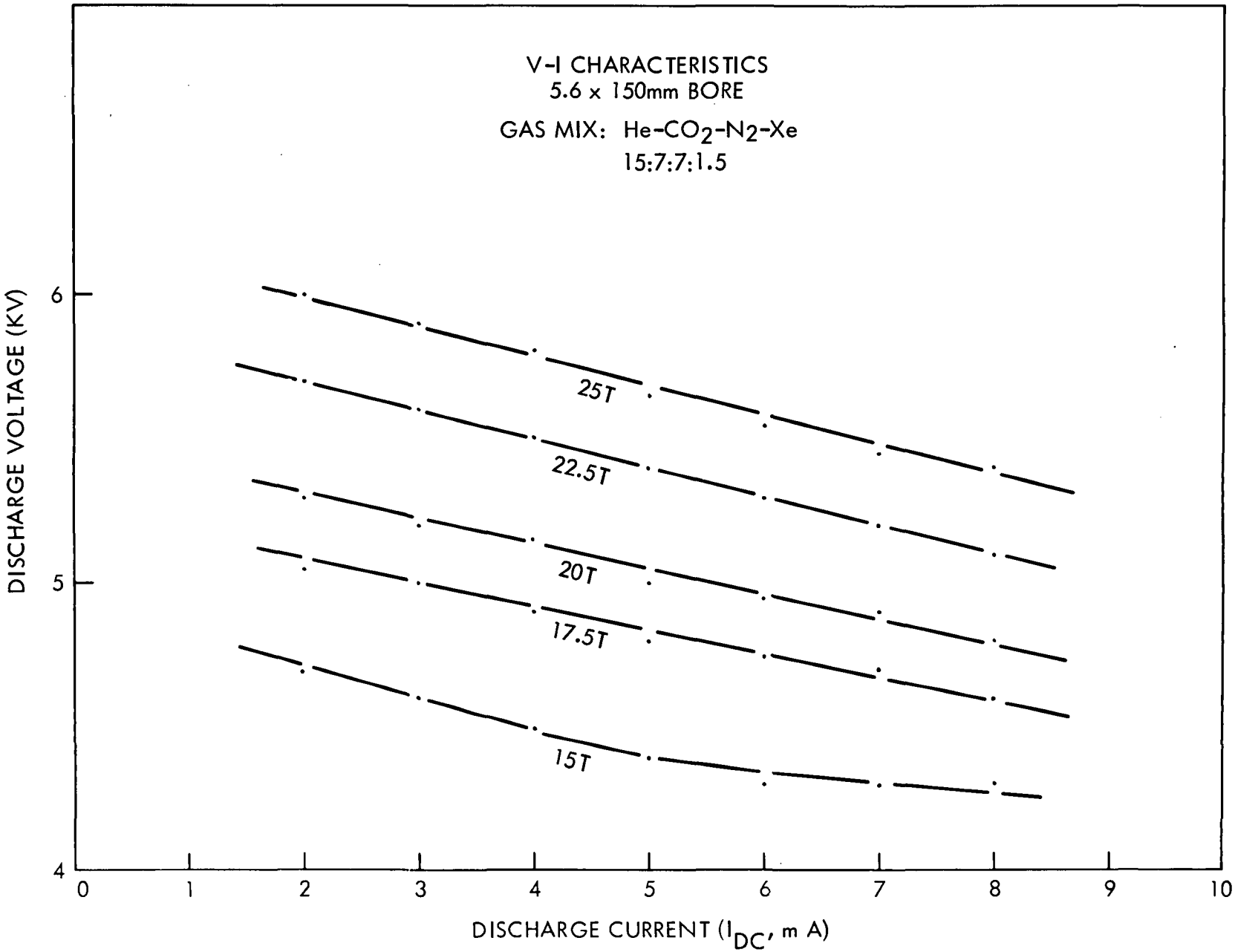
V-I CHARACTERISTICS
5.6 x 150mm BORE
GAS MIX: He-CO_2-N_2-Xe
15:7:7:1.5
25T
22.5T
20T
17.5T
15T
DISCHARGE VOLTAGE (KV)
6
5
4
0
1
2
3
4
5
6
7
8
9
10
DISCHARGE CURRENT (I_{DC}, m A)

Figure 3a

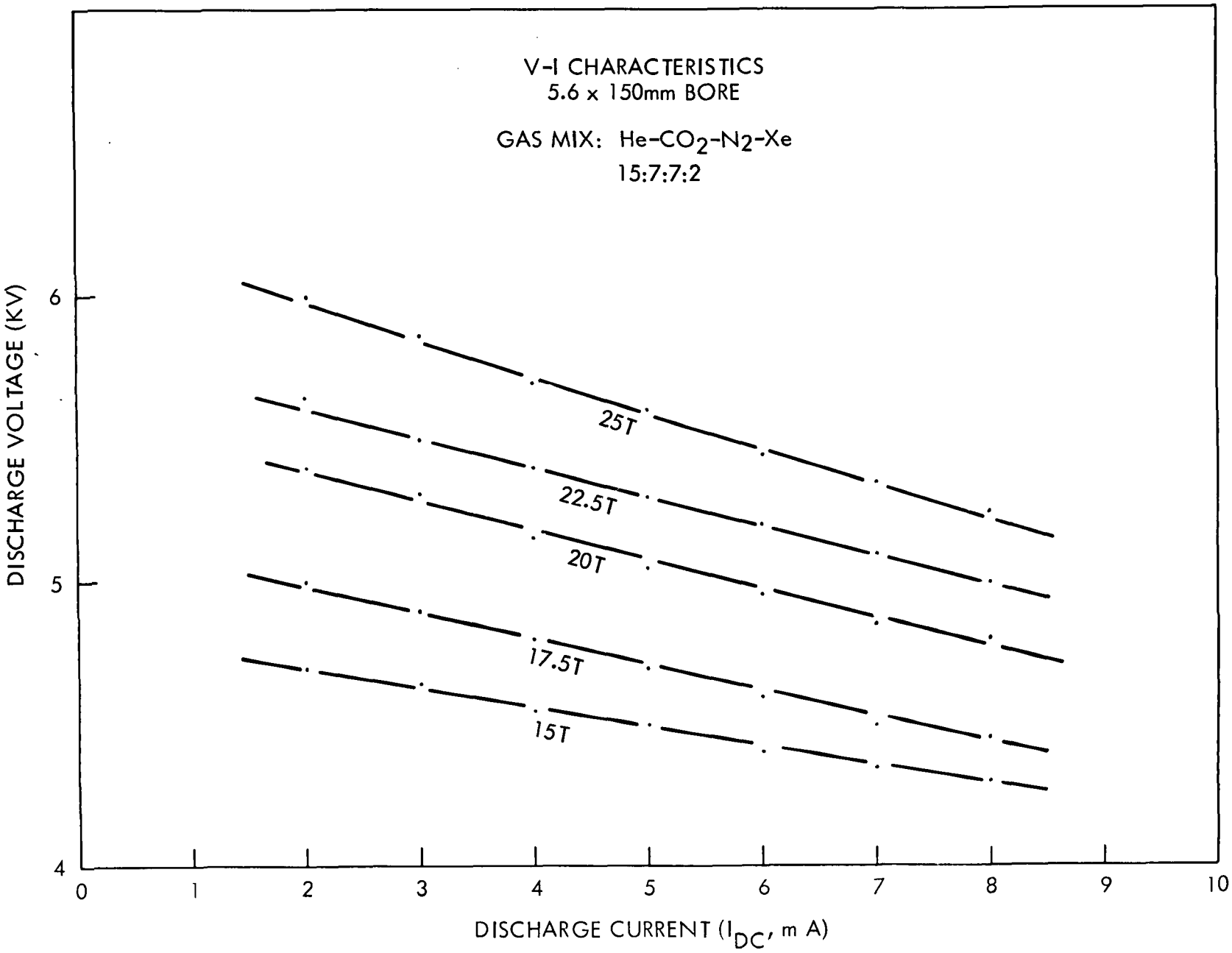
V-I CHARACTERISTICS
5.6 x 150mm BORE
GAS MIX: He-CO_2-N_2-Xe
15:7:7:2
DISCHARGE VOLTAGE (KV)
6
5
4
25T
22.5T
20T
17.5T
15T
0
1
2
3
4
5
6
7
8
9
10
DISCHARGE CURRENT (I_{DC}, m A)

Figure 4a

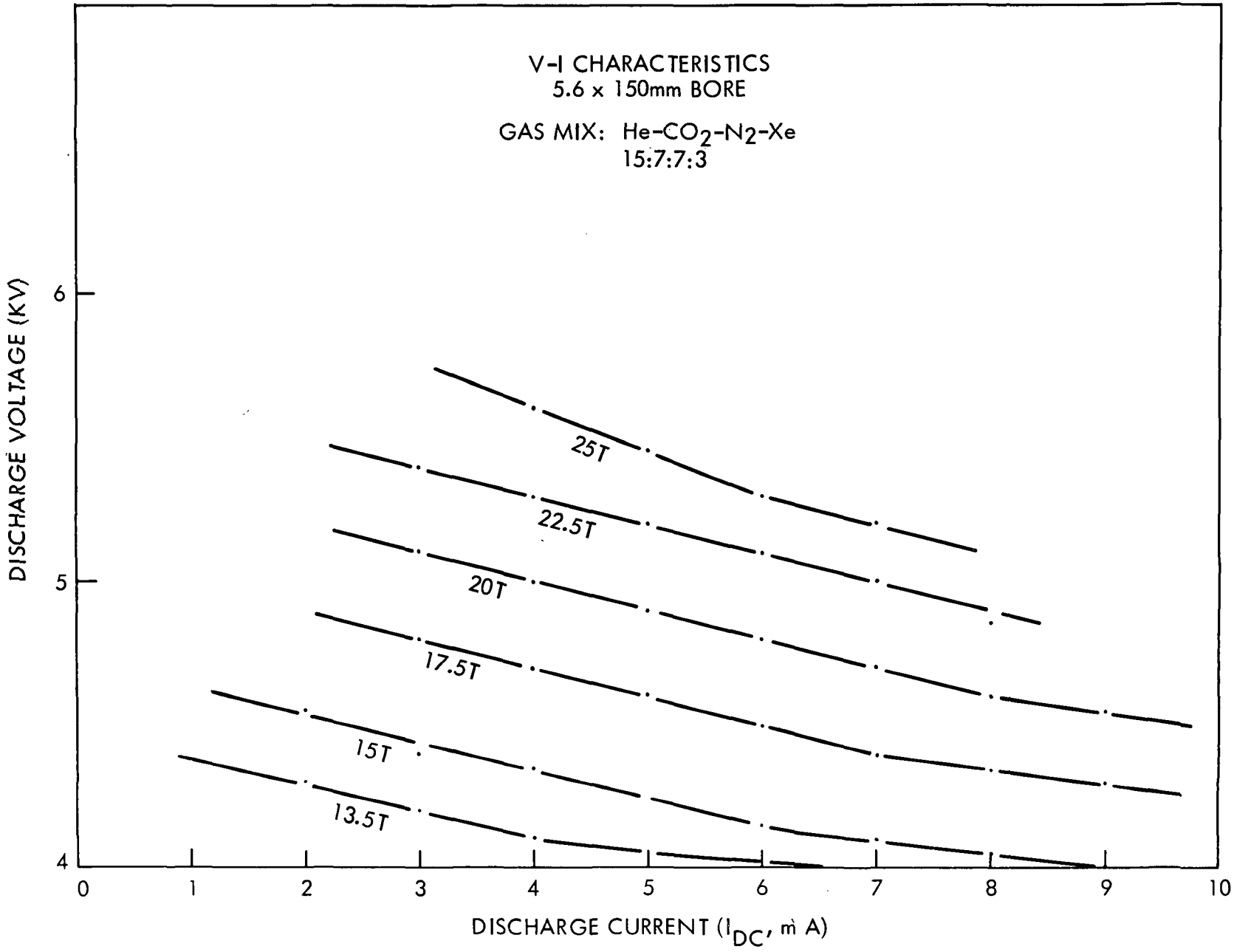
V-I CHARACTERISTICS
5.6 x 150mm BORE
GAS MIX: He-CO_2-N_2-Xe
15:7:7:3
DISCHARGE VOLTAGE (KV)
6
5
4
25T
22.5T
20T
17.5T
15T
13.5T
0
1
2
3
4
5
6
7
8
9
10
DISCHARGE CURRENT (I_{DC}, m A)

Figure 5a

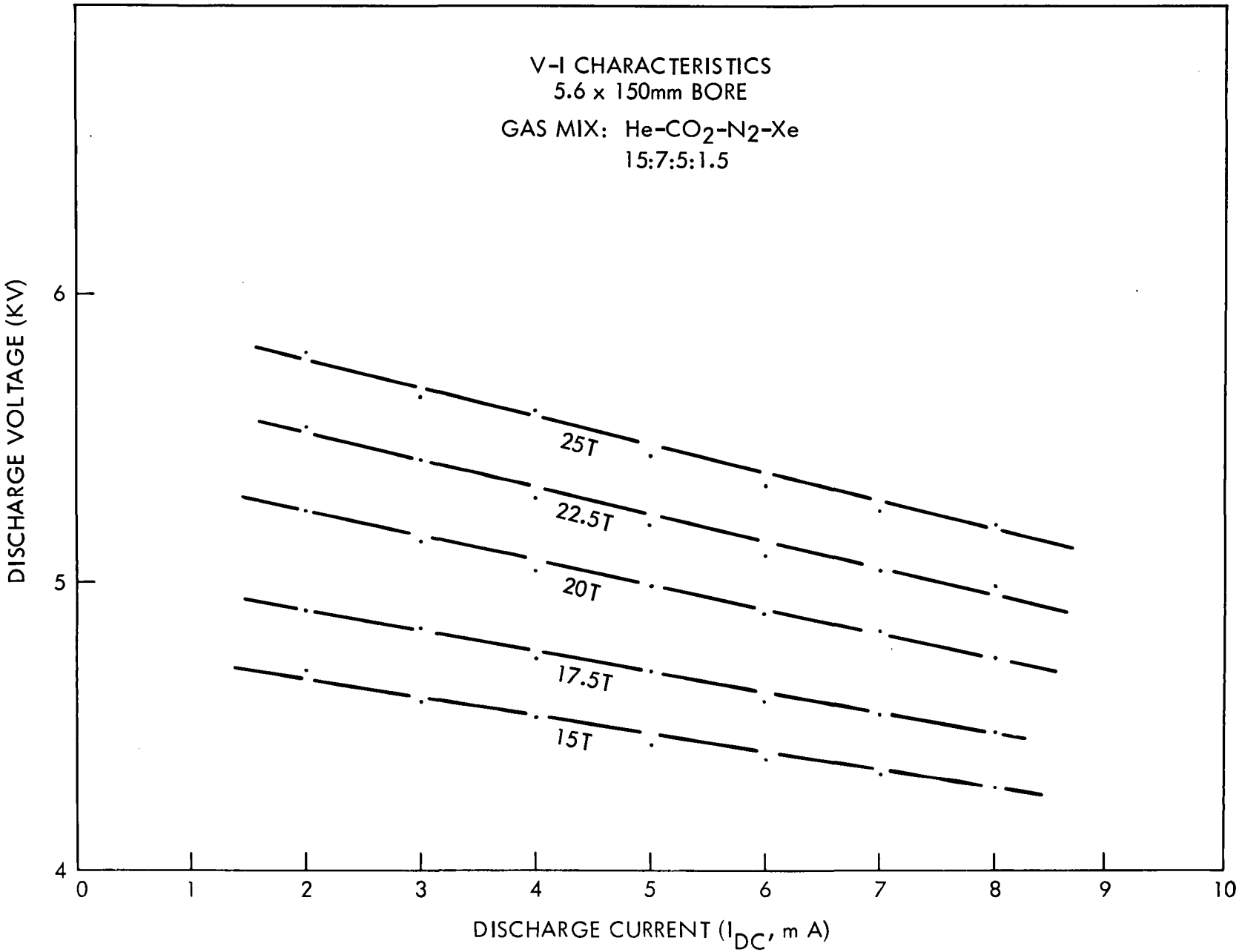
V-I CHARACTERISTICS
5.6 x 150mm BORE
GAS MIX: He-CO_2-N_2-Xe
15:7:5:1.5
25T
22.5T
20T
17.5T
15T
DISCHARGE VOLTAGE (KV)
6
5
4
0
1
2
3
4
5
6
7
8
9
10
DISCHARGE CURRENT (I_{DC}, m A)

Figure 6a

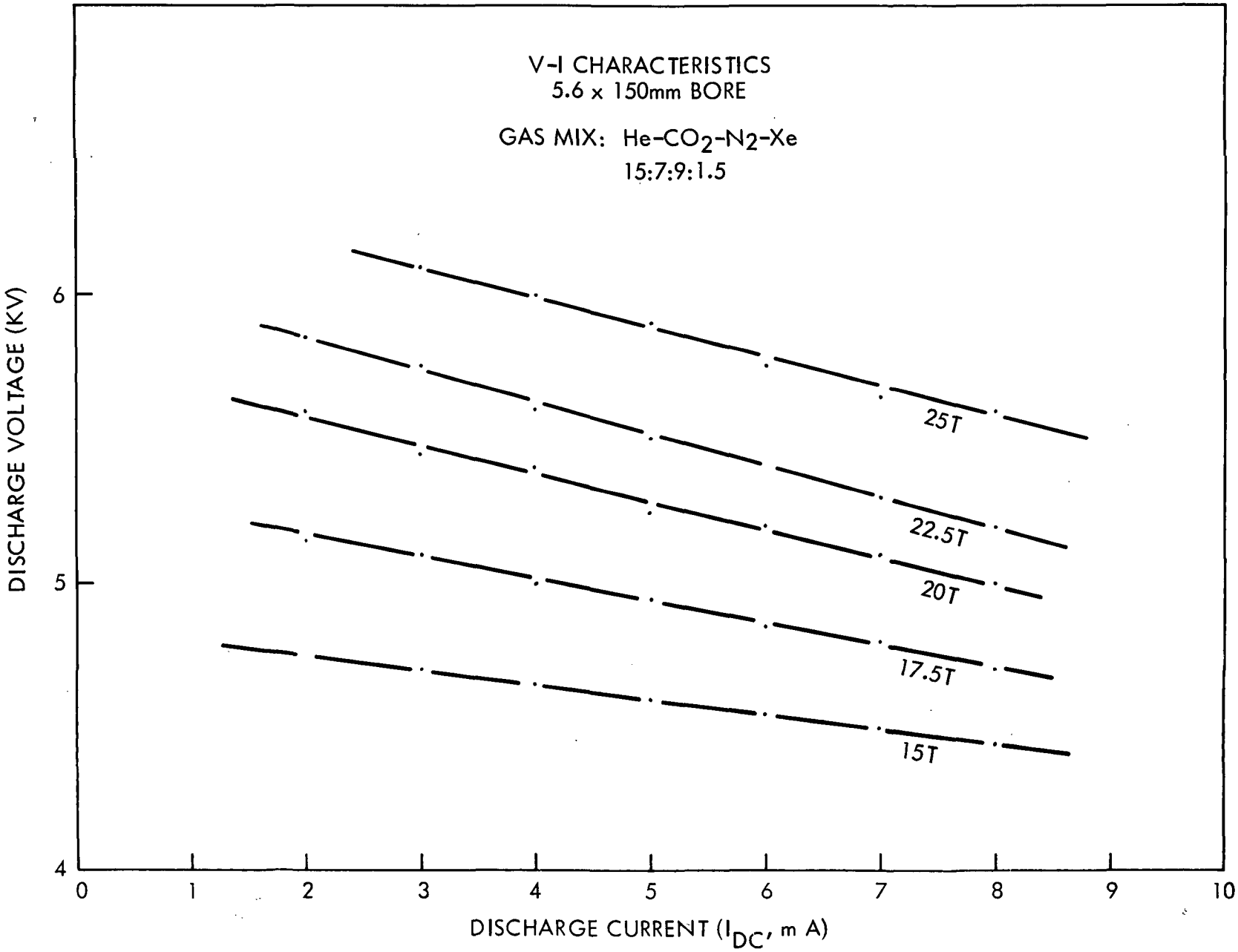
V-I CHARACTERISTICS
5.6 x 150mm BORE
GAS MIX: He-CO_2-N_2-Xe
15:7:9:1.5
DISCHARGE VOLTAGE (KV)
6
5
4
25T
22.5T
20T
17.5T
15T
0
1
2
3
4
5
6
7
8
9
10
DISCHARGE CURRENT (I_{DC}, m A)

Figure 8a

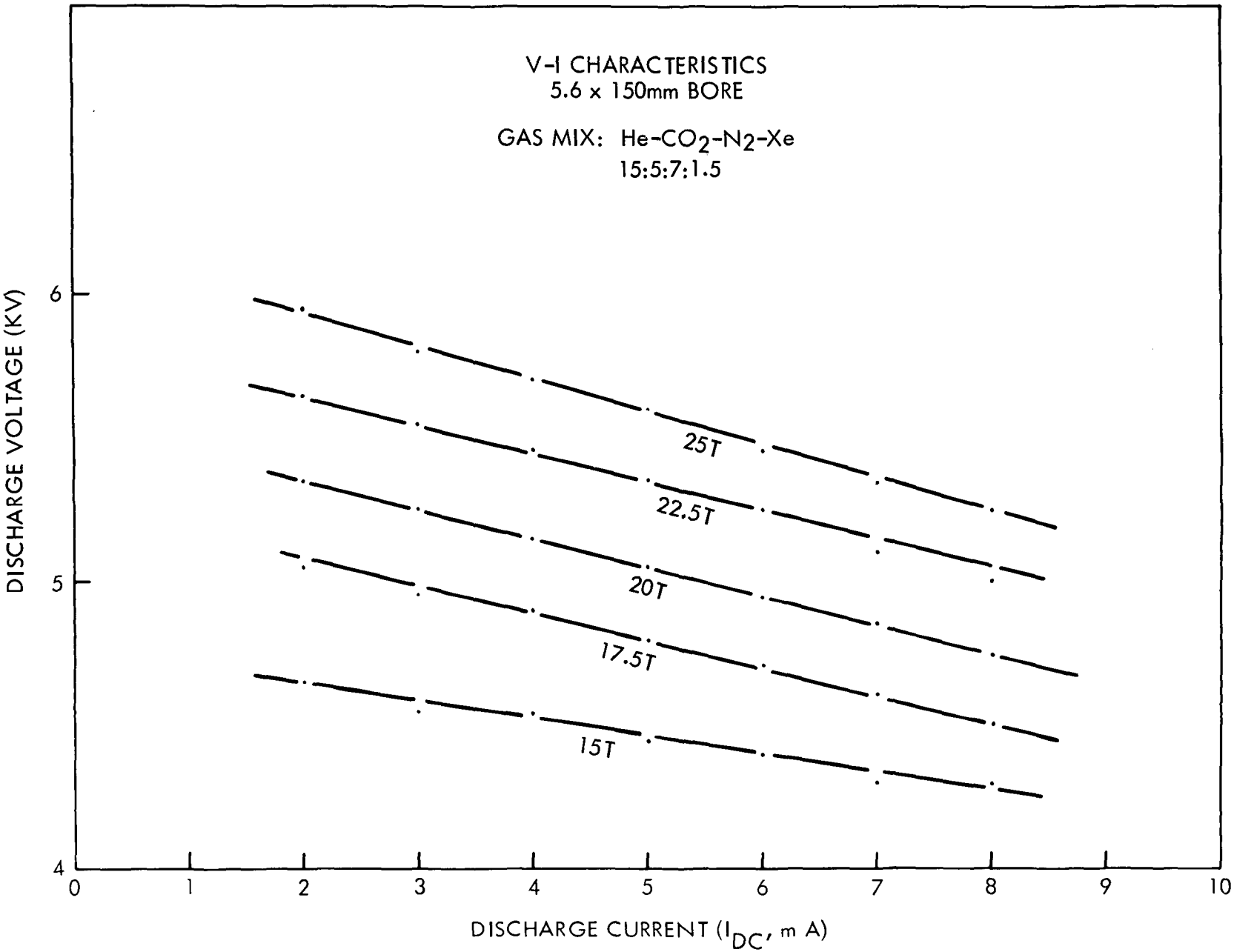
V-I CHARACTERISTICS
5.6 x 150mm BORE
GAS MIX: He-CO_2-N_2-Xe
15:5:7:1.5
25T
22.5T
20T
17.5T
15T
DISCHARGE VOLTAGE (KV)
6
5
4
0
1
2
3
4
5
6
7
8
9
10
DISCHARGE CURRENT (I_{DC}, m A)

Figure 9a

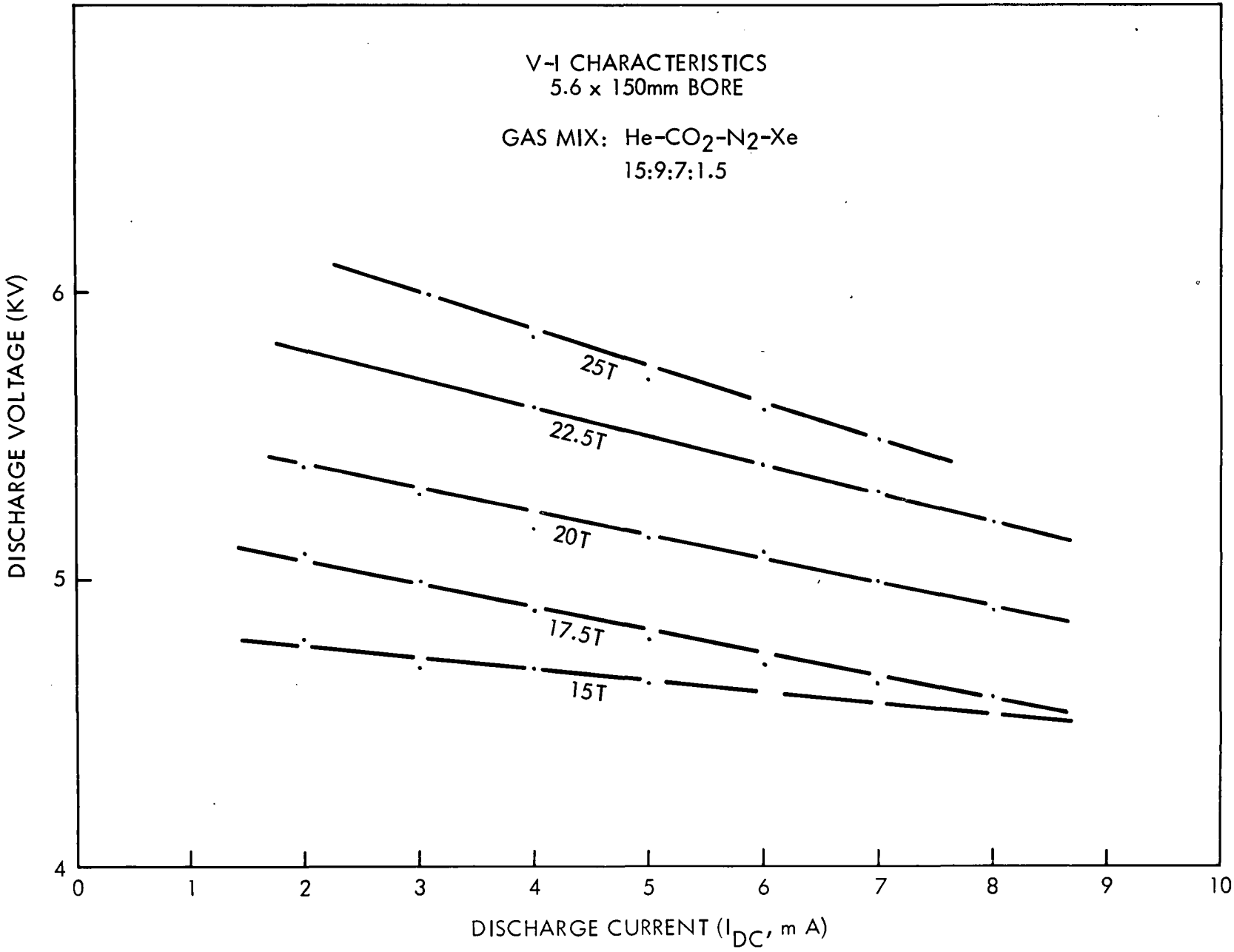
V-I CHARACTERISTICS
5.6 x 150mm BORE
GAS MIX: He-CO_2-N_2-Xe
15:9:7:1.5
25T
22.5T
20T
17.5T
15T
DISCHARGE VOLTAGE (KV)
6
5
4
0
1
2
3
4
5
6
7
8
9
10
DISCHARGE CURRENT (I_{DC}, m A)

Figure 11a

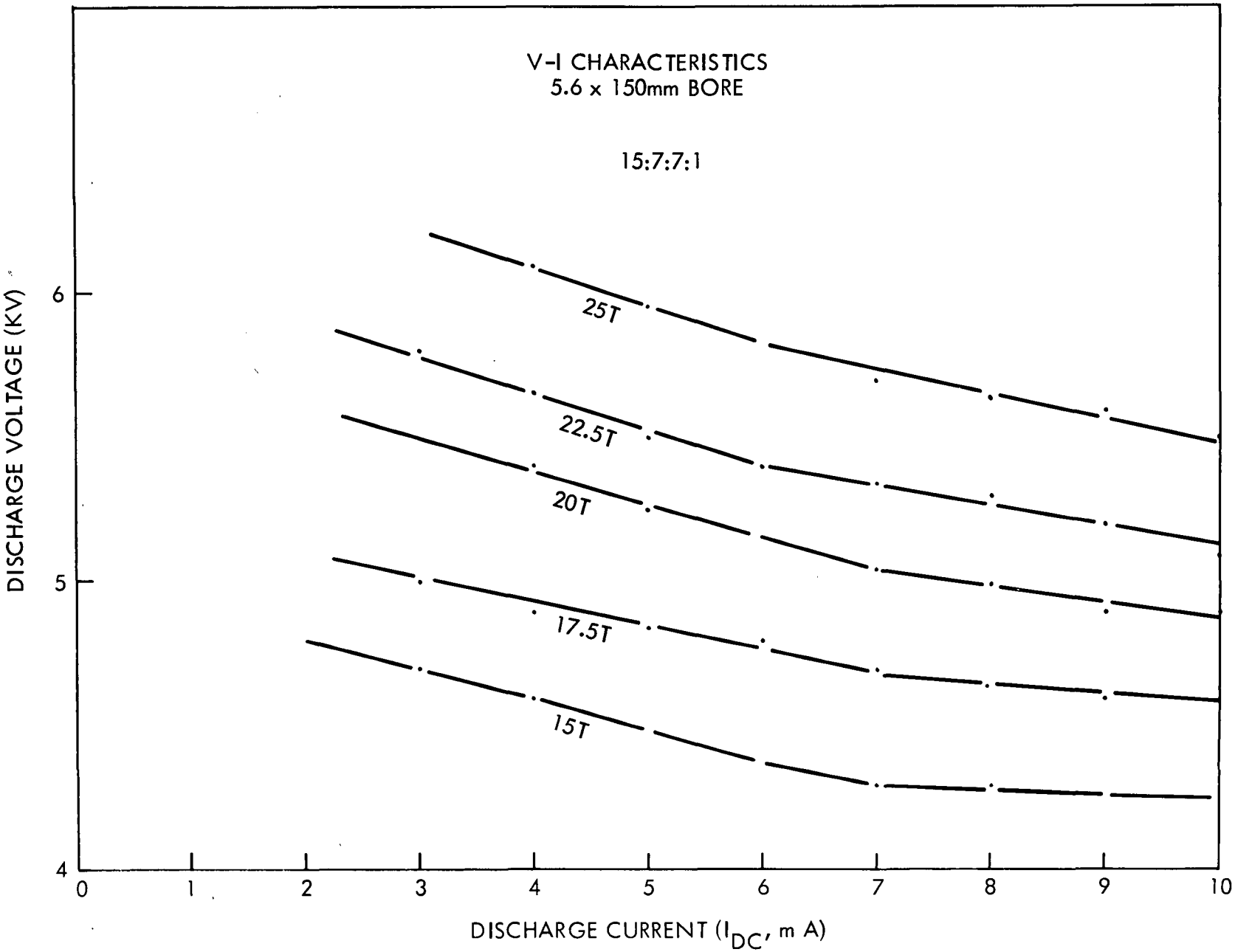
V-I CHARACTERISTICS
5.6 x 150mm BORE
15:7:7:1
25T
22.5T
20T
17.5T
15T
DISCHARGE VOLTAGE (KV)
6
5
4
0
1
2
3
4
5
6
7
8
9
10
DISCHARGE CURRENT (I_{DC}, m A)

Figure 12a

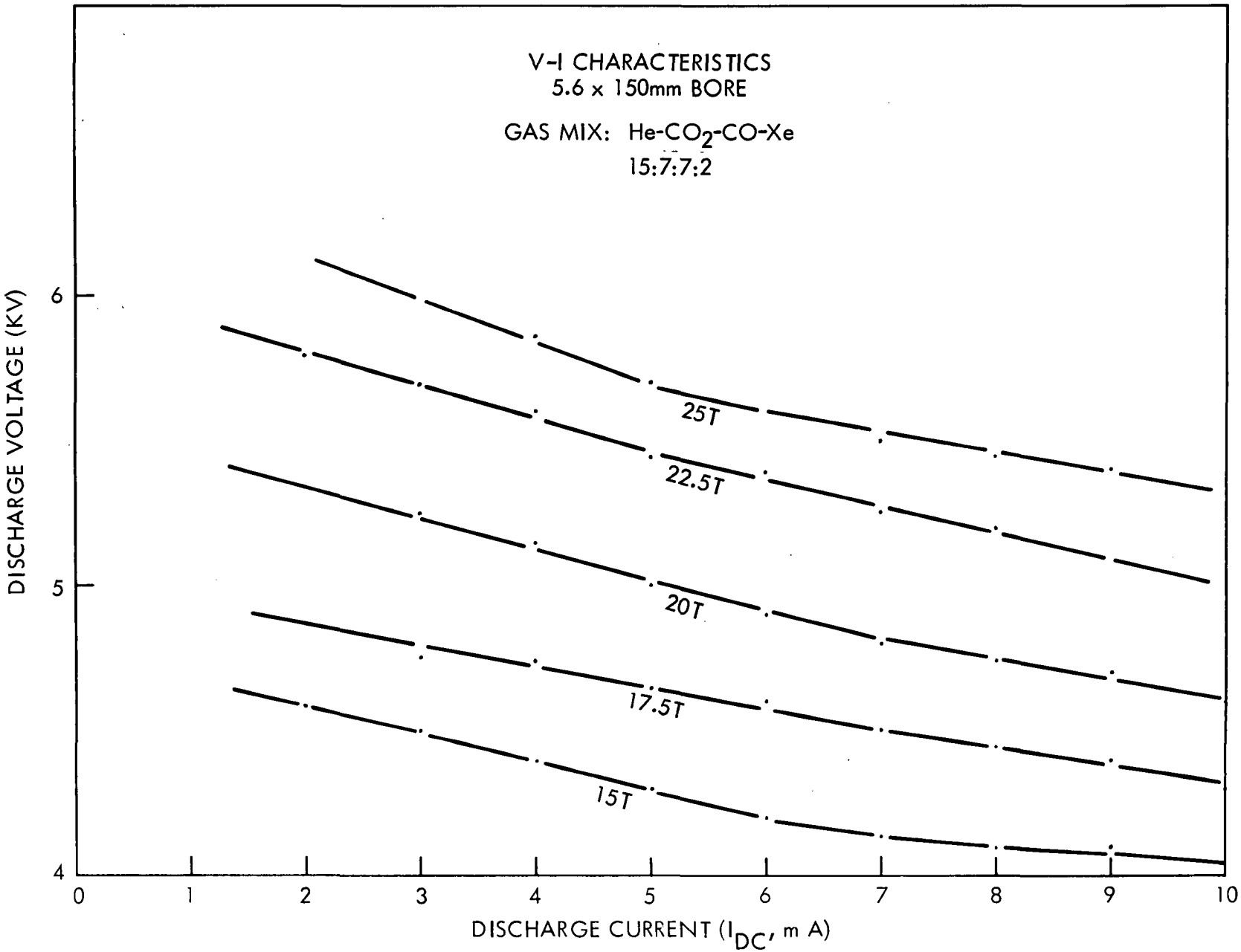
V-I CHARACTERISTICS
5.6 x 150mm BORE
GAS MIX: He-CO_2-CO-Xe
15:7:7:2
25T
22.5T
20T
17.5T
15T
DISCHARGE VOLTAGE (KV)
6
5
4
0
1
2
3
4
5
6
7
8
9
10
DISCHARGE CURRENT (I_{DC}, m A)

Figure 13a

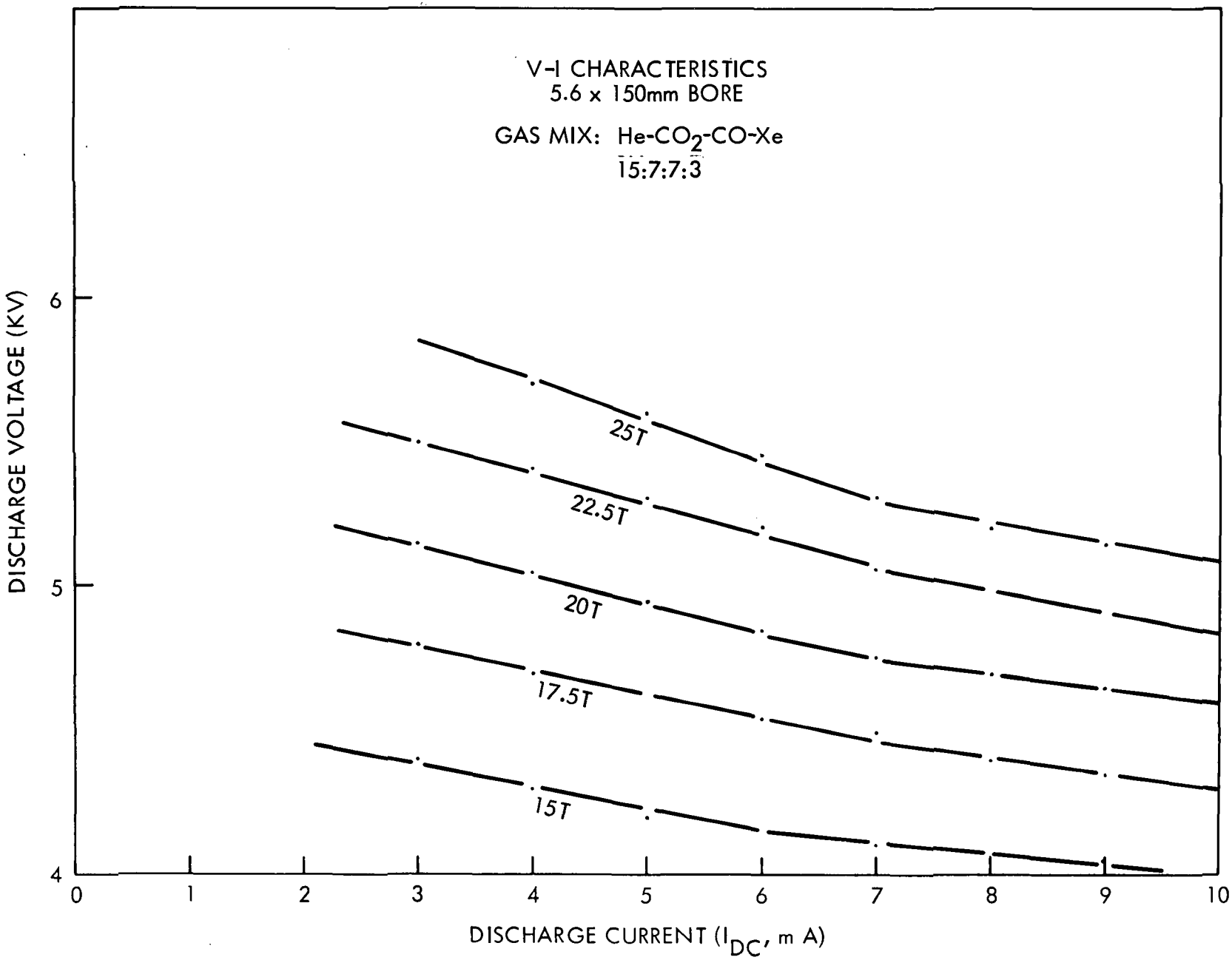
V-I CHARACTERISTICS
5.6 x 150mm BORE
GAS MIX: He-CO_2-CO-Xe
15:7:7:3
DISCHARGE VOLTAGE (KV)
6
5
4
25T
22.5T
20T
17.5T
15T
0
1
2
3
4
5
6
7
8
9
10
DISCHARGE CURRENT (I_{DC}, m A)

Figure 14a

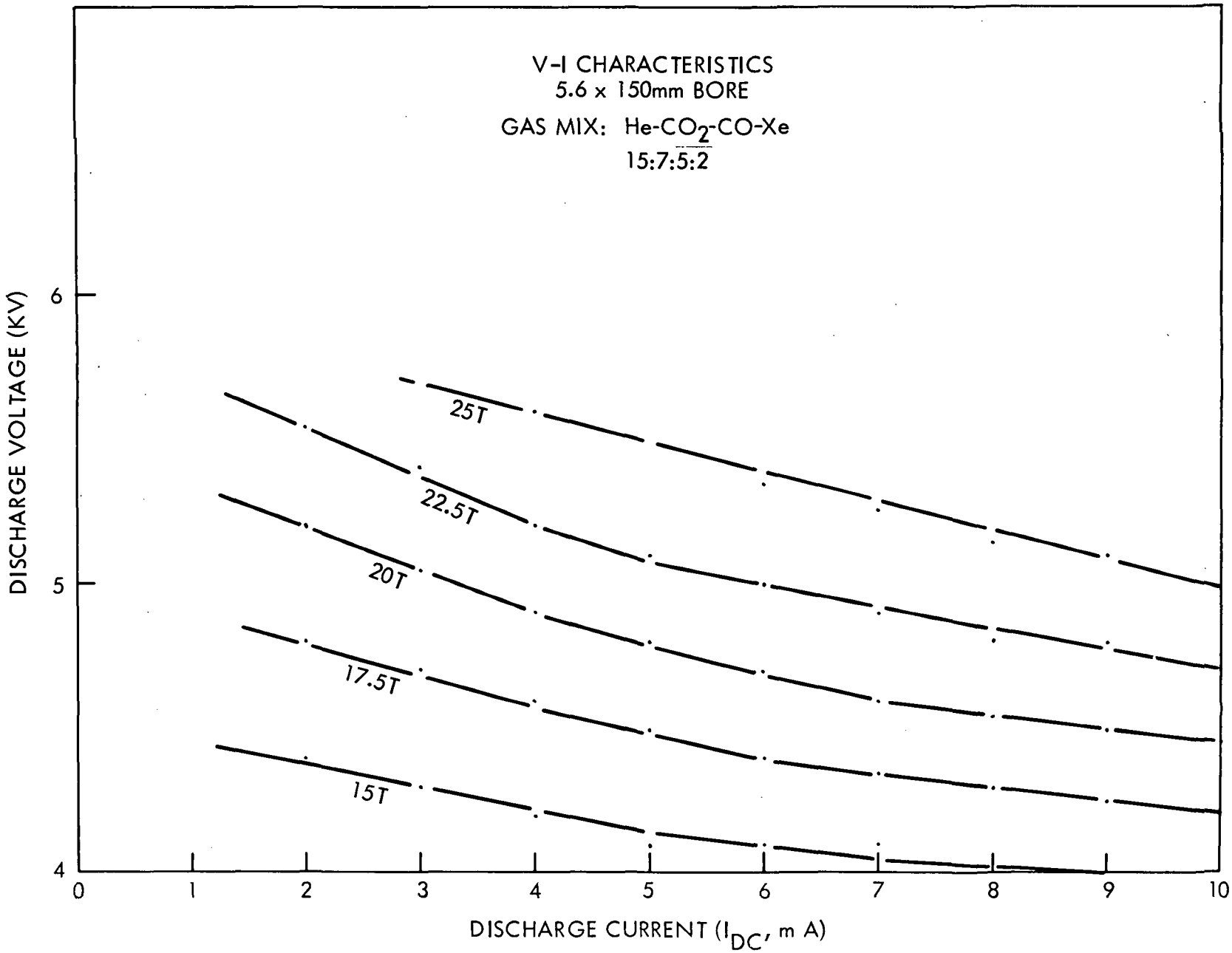
V-I CHARACTERISTICS
5.6 x 150mm BORE
GAS MIX: He-CO_2-CO-Xe
15:7:5:2
DISCHARGE VOLTAGE (KV)
6
5
4
25T
22.5T
20T
17.5T
15T
0
1
2
3
4
5
6
7
8
9
10
DISCHARGE CURRENT (I_{DC}, m A)

Figure 15a

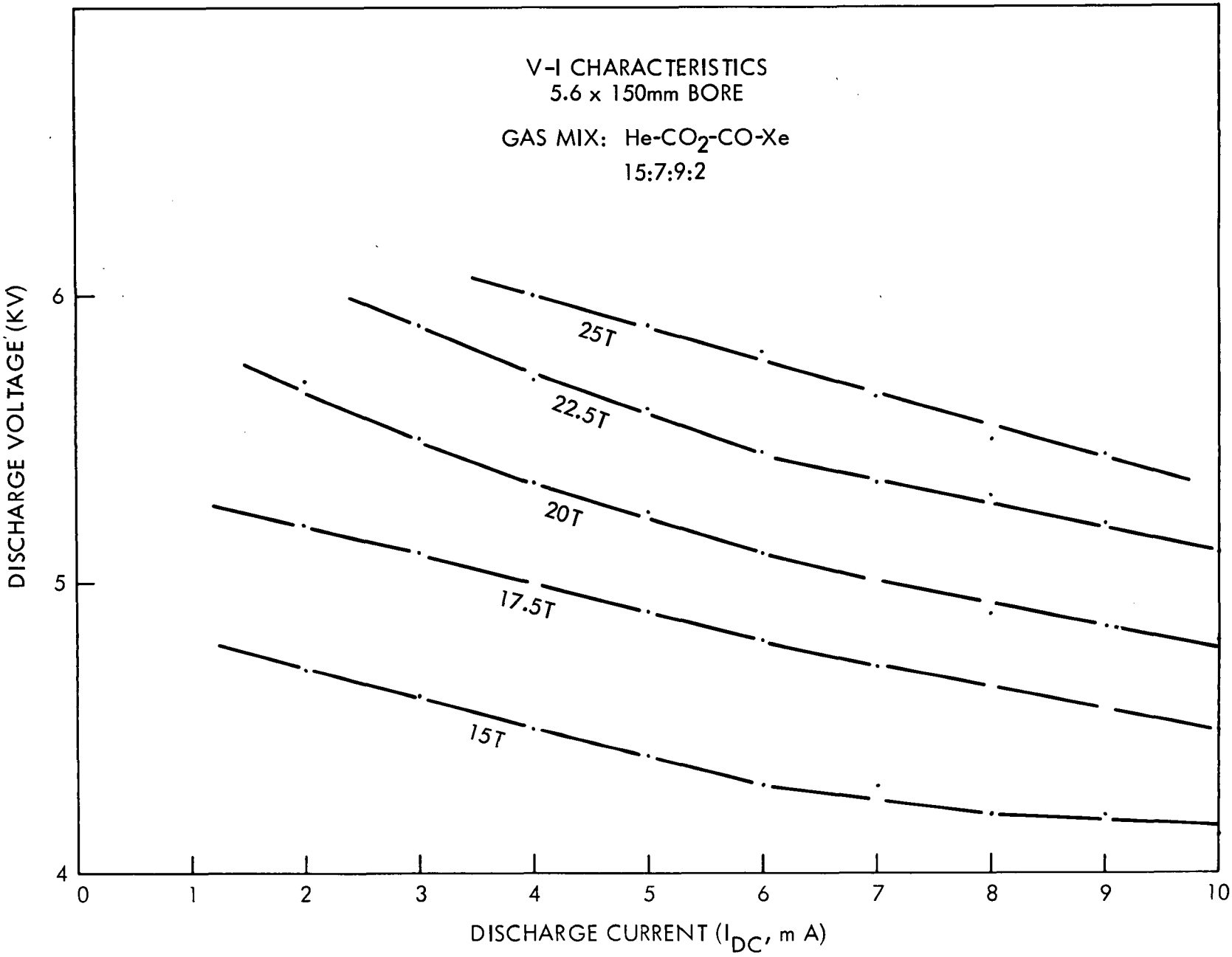
V-I CHARACTERISTICS
5.6 x 150mm BORE
GAS MIX: He-CO_2-CO-Xe
15:7:9:2
25T
22.5T
20T
17.5T
15T
DISCHARGE VOLTAGE (KV)
6
5
4
0
1
2
3
4
5
6
7
8
9
10
DISCHARGE CURRENT (I_{DC}, m A)

Figure 17a

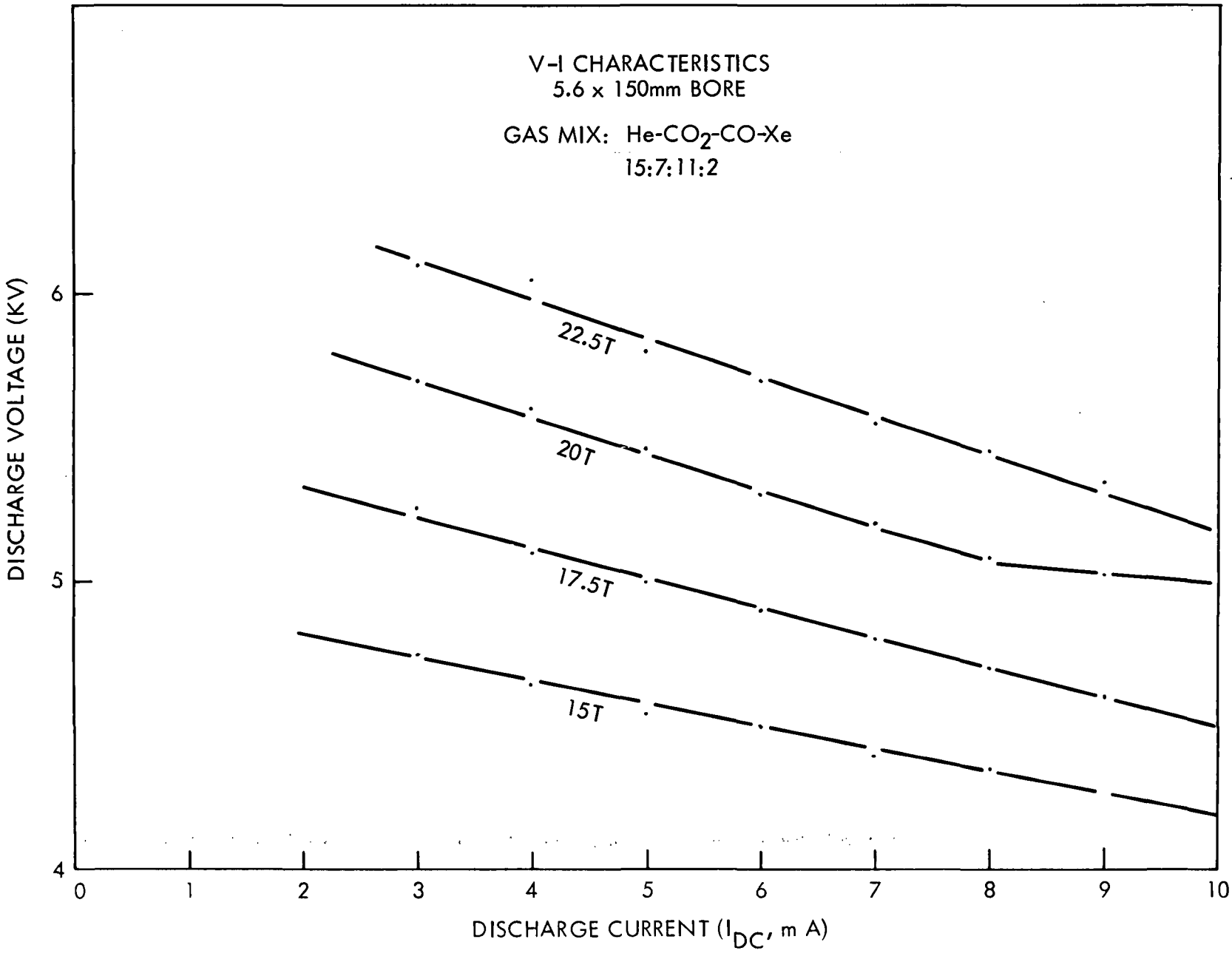
V-I CHARACTERISTICS
5.6 x 150mm BORE
GAS MIX: He-CO_2-CO-Xe
15:7:11:2
22.5T
20T
17.5T
15T
DISCHARGE VOLTAGE (KV)
6
5
4
0
1
2
3
4
5
6
7
8
9
10
DISCHARGE CURRENT (I_{DC}, m A)

Figure 18a

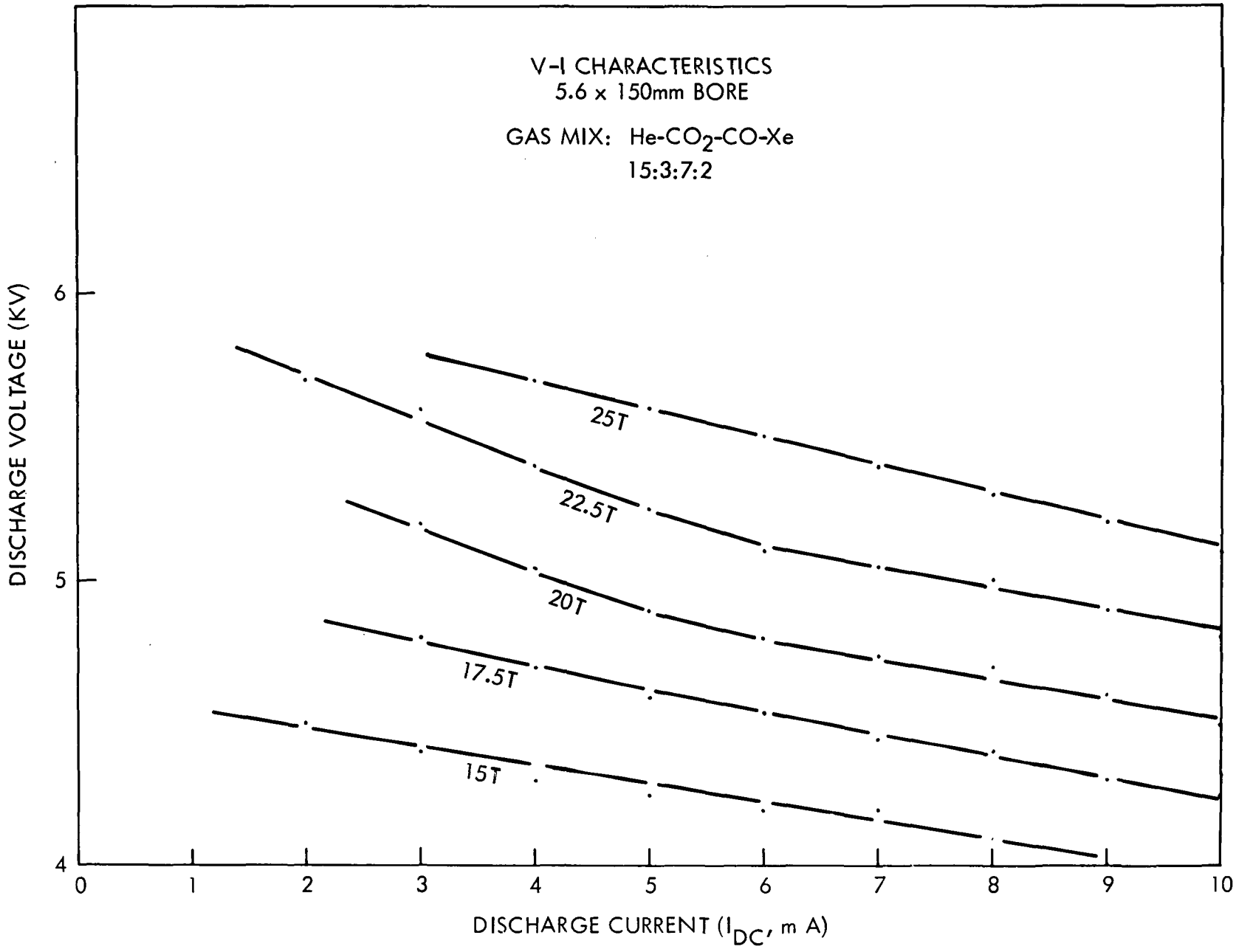
V-I CHARACTERISTICS
5.6 x 150mm BORE
GAS MIX: He-CO_2-CO-Xe
15:3:7:2
DISCHARGE VOLTAGE (KV)
6
5
4
25T
22.5T
20T
17.5T
15T
0
1
2
3
4
5
6
7
8
9
10
DISCHARGE CURRENT (I_{DC}, m A)

Figure 19a

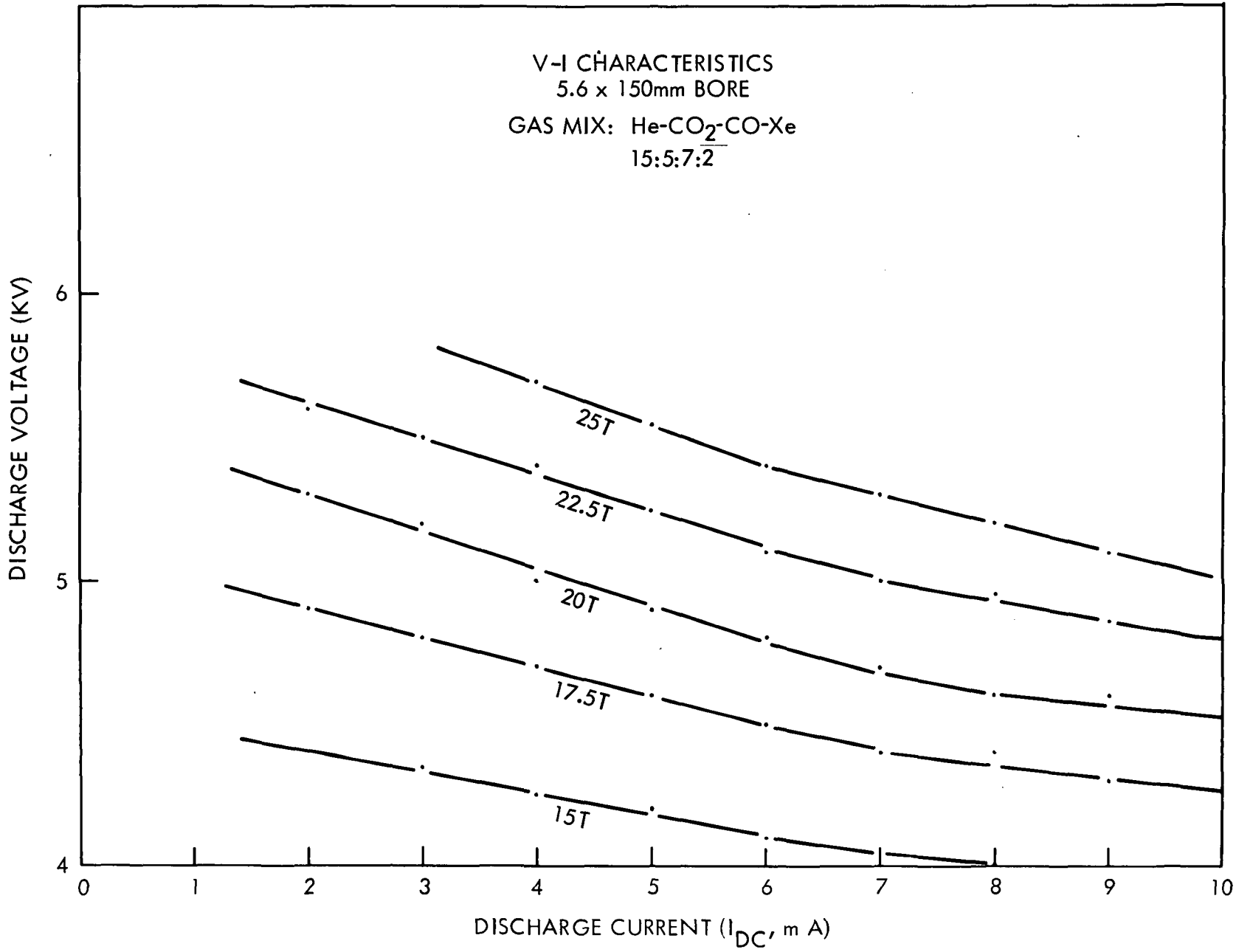
V-I CHARACTERISTICS
5.6 x 150mm BORE
GAS MIX: He-CO_2-CO-Xe
15:5:7:2
DISCHARGE VOLTAGE (KV)
6
5
4
25T
22.5T
20T
17.5T
15T
0
1
2
3
4
5
6
7
8
9
10
DISCHARGE CURRENT (I_{DC}, m A)

Figure 20a

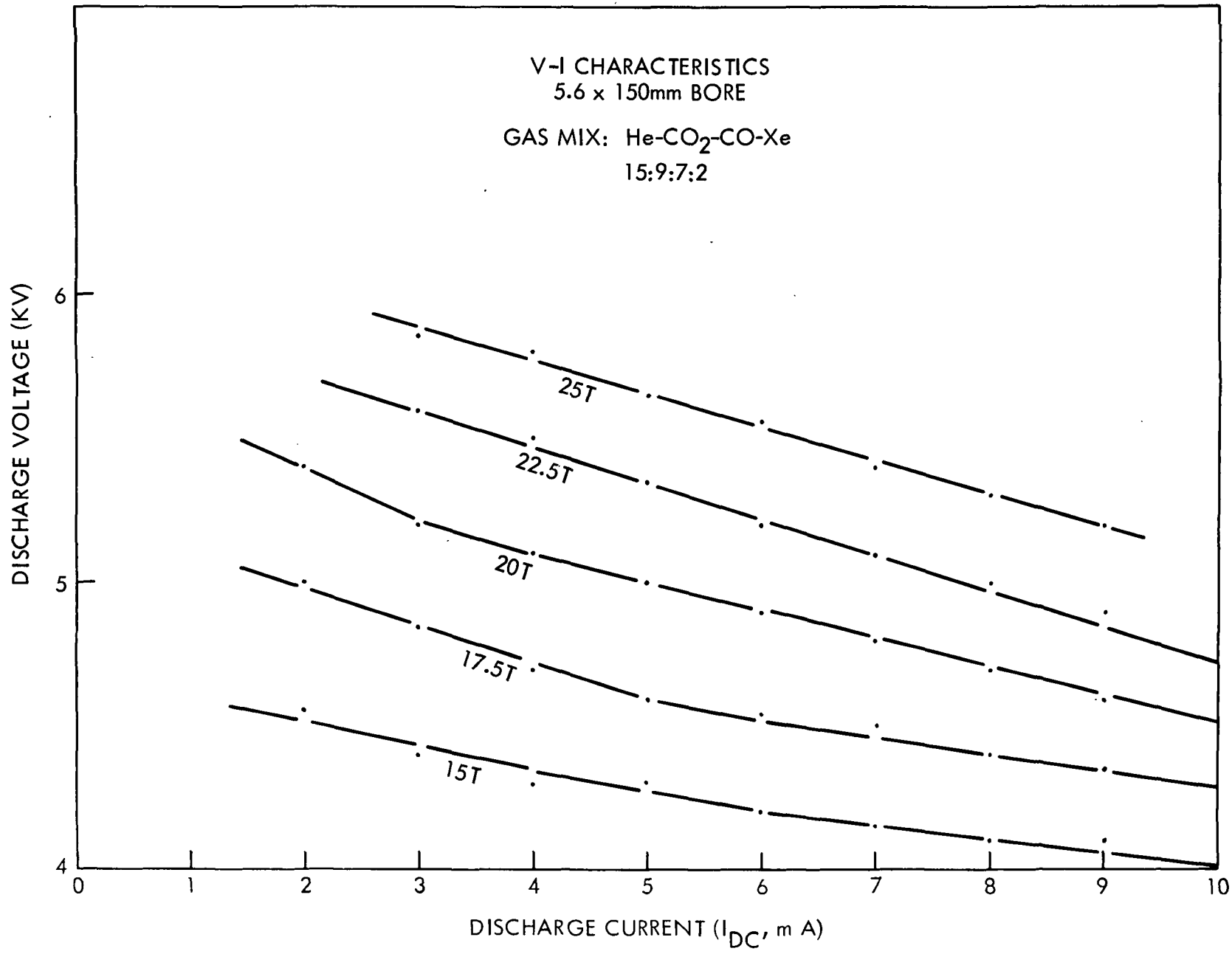
V-I CHARACTERISTICS
5.6 x 150mm BORE
GAS MIX: He-CO_2-CO-Xe
15:9:7:2
25T
22.5T
20T
17.5T
15T
DISCHARGE VOLTAGE (KV)
6
5
4
0
1
2
3
4
5
6
7
8
9
10
DISCHARGE CURRENT (I_{DC}, m A)

Figure 22a

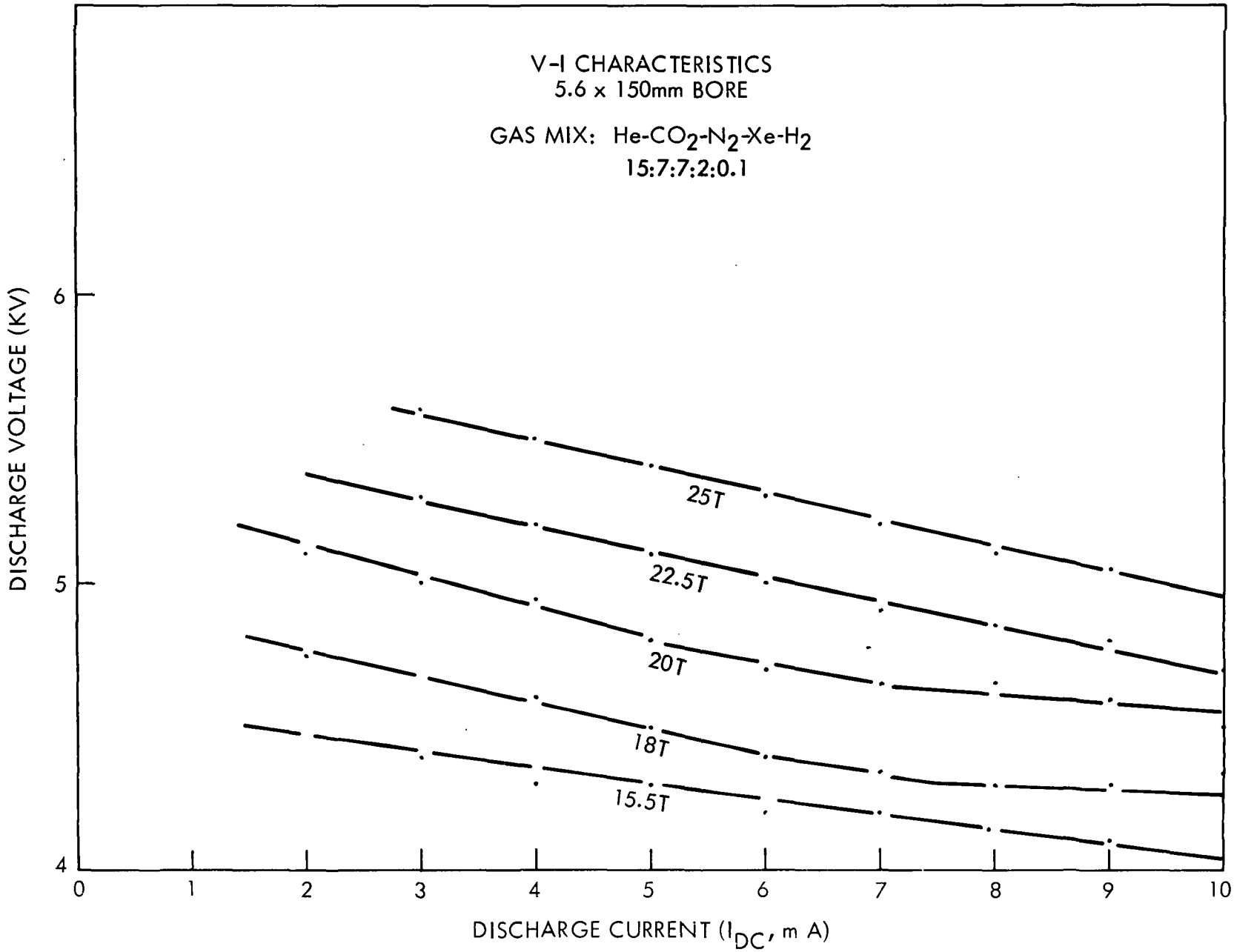
V-I CHARACTERISTICS
5.6 x 150mm BORE
GAS MIX: He-CO_2-N_2-Xe-H_2
15:7:7:2:0.1
DISCHARGE VOLTAGE (KV)
6
5
4
25T
22.5T
20T
18T
15.5T
0
1
2
3
4
5
6
7
8
9
10
DISCHARGE CURRENT (I_{DC}, m A)

Figure 24a

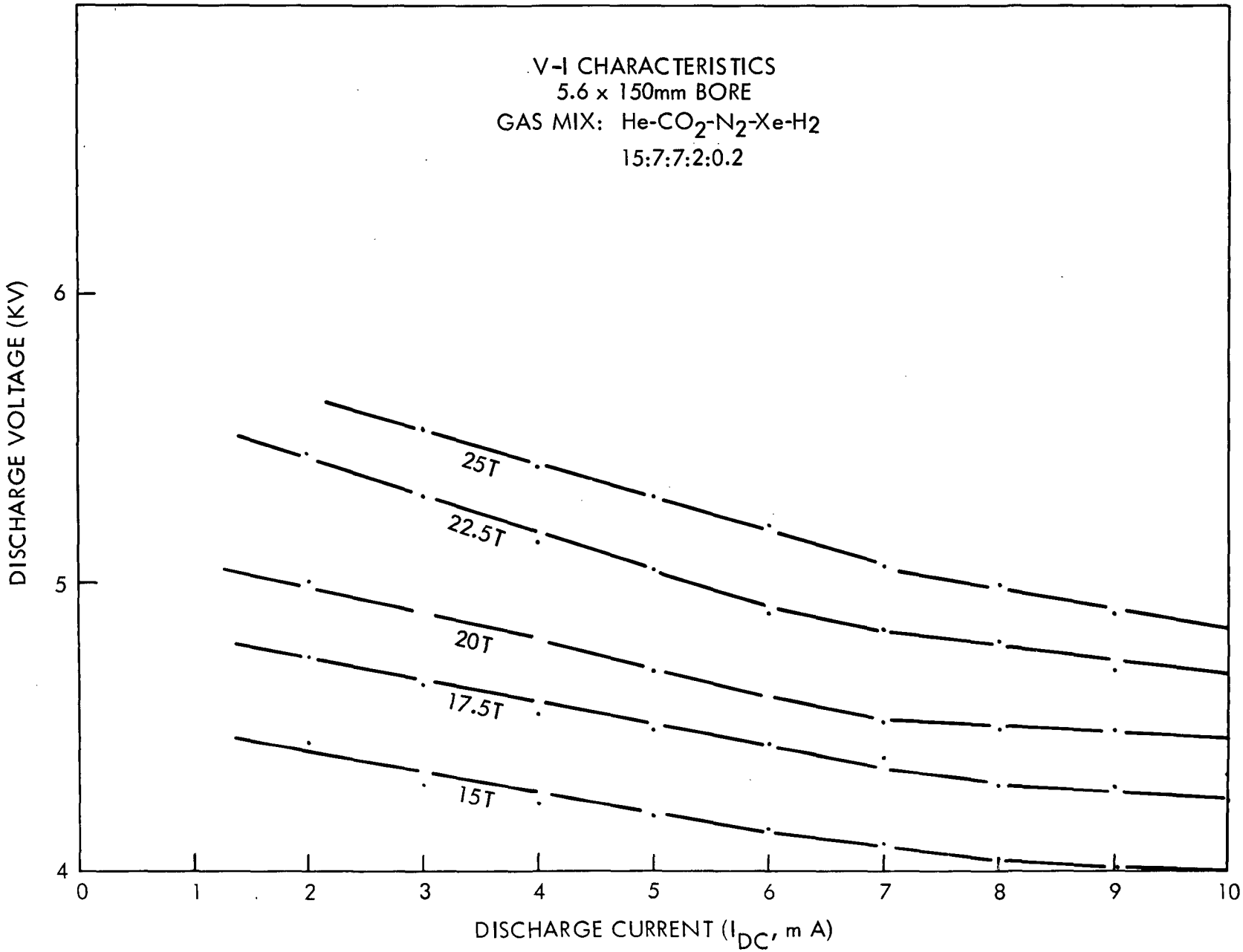
V-I CHARACTERISTICS
5.6 x 150mm BORE
GAS MIX: He-CO_2-N_2-Xe-H_2
15:7:7:2:0.2
DISCHARGE VOLTAGE (KV)
6
5
4
25T
22.5T
20T
17.5T
15T
0
1
2
3
4
5
6
7
8
9
10
DISCHARGE CURRENT (I_{DC}, m A)

Figure 25a

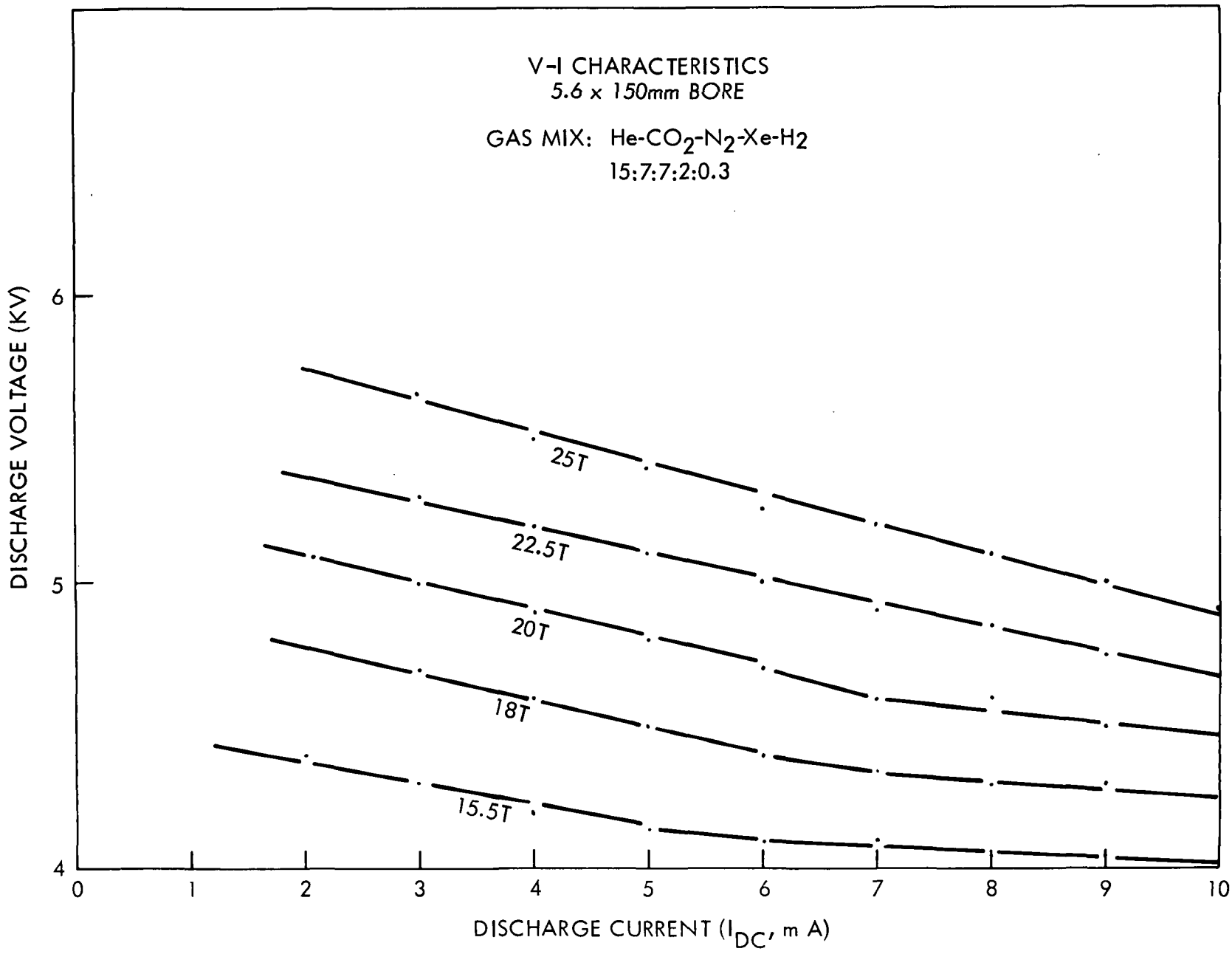
V-I CHARACTERISTICS
5.6 x 150mm BORE
GAS MIX: He-CO_2-N_2-Xe-H_2
15:7:7:2:0.3
DISCHARGE VOLTAGE (KV)
6
5
4
25T
22.5T
20T
18T
15.5T
0
1
2
3
4
5
6
7
8
9
10
DISCHARGE CURRENT (I_{DC}, m A)

Figure 26a

CO_2 LASER

5.6 X 150mm BORE

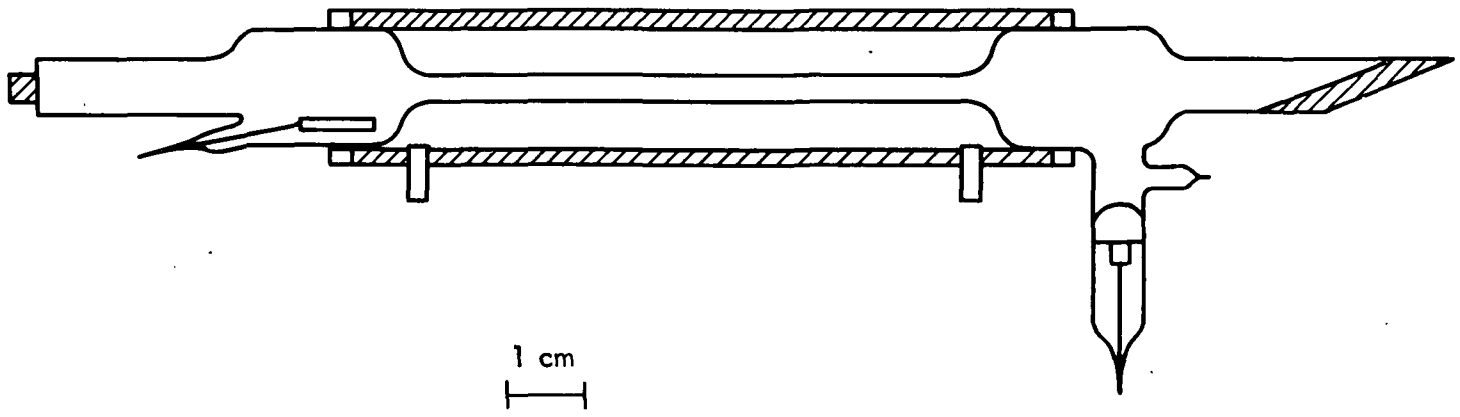

Figure 27a.

Figure 28a. Power Output vs Total Pressure 5.6 x 150mm Bore, 6 MA DC.

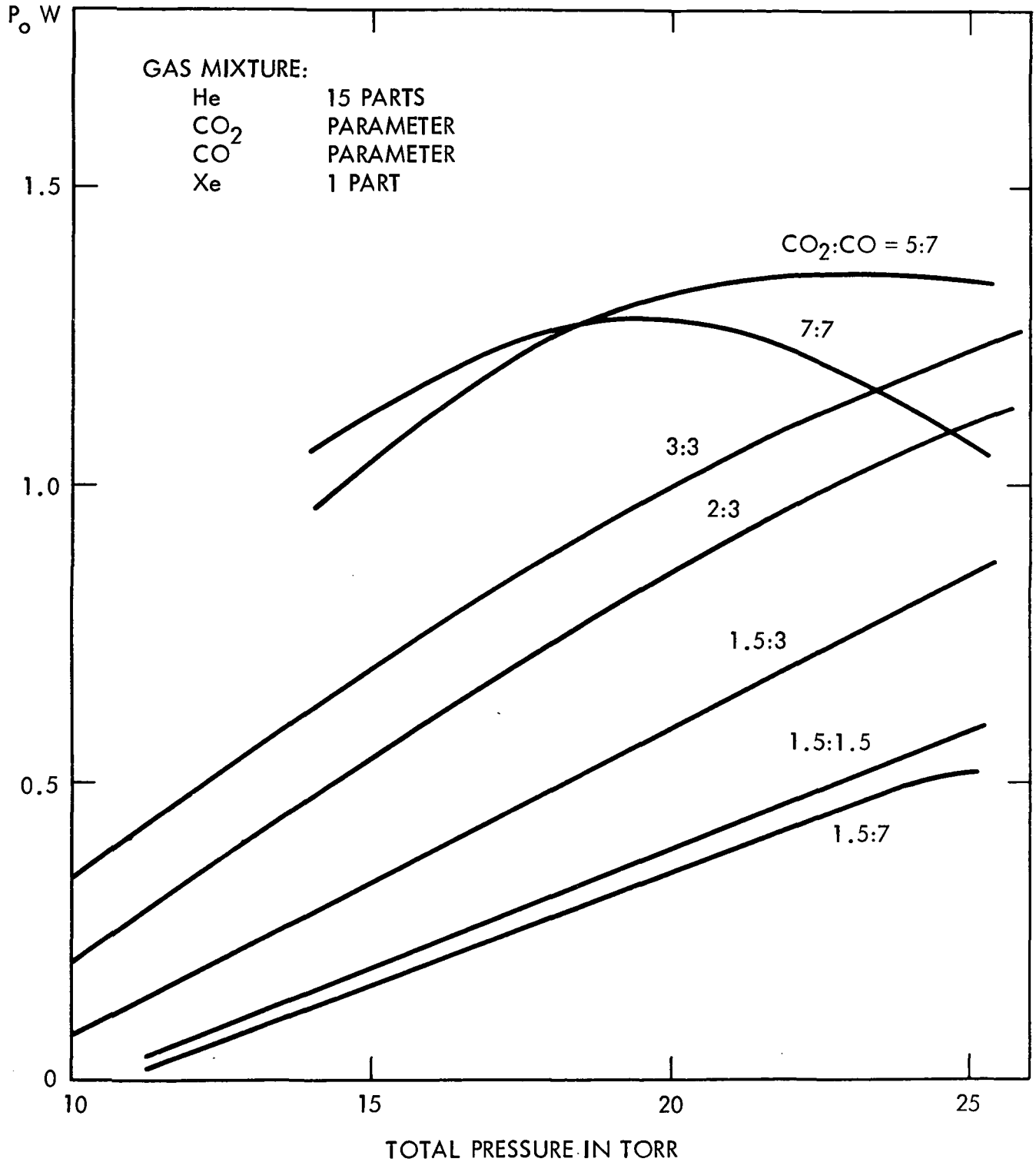

Figure 29a. Power Output vs Total Pressure 5.6 x 150mm Bore, 6m A DC.